IMPROVING FALLOUT CHARACTERIZATION BY USING MULTIVARIATE TECHNIQUES TO DETERMINE COMPOSITION

THESIS

Christopher R. Pitkins, Captain, USAF

AFIT-ENP-MS-18-M-080

DEPARTMENT OF THE AIR FORCE
AIR UNIVERSITY

AIR FORCE INSTITUTE OF TECHNOLOGY

Wright-Patterson Air Force Base, Ohio

AFIT-ENP-MS-18-M-080

IMPROVING FALLOUT CHARACTERIZATION BY USING MULTIVARIATE TECHNIQUES TO DETERMINE COMPOSITION

THESIS

Presented to the Faculty

Department of Engineering Physics

Graduate School of Engineering and Management

Air Force Institute of Technology

Air University

Air Education and Training Command

In Partial Fulfillment of the Requirements for the

Degree of Master of Science

Christopher R. Pitkins, MSA, BS

Captain, USAF

March 2018

AFIT-ENP-MS-18-M-080

IMPROVING FALLOUT CHARACTERIZATION BY USING MULTIVARIATE TECHNIQUES TO DETERMINE COMPOSITION

Christopher R. Pitkins

Captain, USAF

Committee Membership:

Dr. J. W. McClory
Chair

LTC B. E. O'Day, PhD
Member

Dr. J. E. Matzel
Member

AFIT-ENP-MS-18-M-080

Abstract

Multivariate statistical techniques have been applied in order to un-mix nuclear fallout debris chemical data. This information is critical to characterization of fallout particle formation following a nuclear detonation. Understanding the correlation between environmental precursors and actinide concentrations in post-detonation nuclear fallout material aids in understanding the physical and chemical processes that alter nuclear device signatures in the fireball. This research examines 123 nuclear fallout samples from a historical nuclear test. Scanning electron microscopy (SEM) and energy dispersive spectroscopy (EDS) are used to collect chemical compositions of the fallout samples. Principal component analysis (PCA) is applied in order to examine variation in elemental compositions and make estimates of environmental precursor compounds. Geological soil information and prior research are combined to develop a final estimate. Mineral precursor estimates are modeled using multivariate curve resolution-alternating least squares (MCR-ALS). This method was demonstrated as a useful tool in determining composition. The precursors exhibited on polished sample cross-sectional surfaces were spatially correlated with sample radioactivity using autoradiography imaging of the sample set. Results suggest that feldspar is correlated with a moderate level of radioactivity, samples with porous textures have unique compositions with a uniform surface radioactivity, and quartz is anti-correlated with radioactivity. Additionally, size, shape, and morphology each have a relationship with actinide concentration with large, homogeneous and spherical samples exhibiting the highest relative radioactivity.

Dedicated to my family

Acknowledgments

I would like to thank my family and fiancé for their encouragement. Their support led to the success of this research.

I also thank my committee members, and LLNL personnel for their patience and guidance throughout the research project. Sponsor funds provided by the Defense Threat Reduction Agency made the travel and equipment time possible for this research to reach completion.

Christopher R. Pitkins

Table of Contents

Page

Abstract iv
Table of Contents vii
List of Figures ix
List of Tables xiii
I. Introduction 1
1.1. Overview 2
1.2. Problem Statement 5
1.3. Scope of Study 5
1.4. Sponsorship 6
II. Literature Review 7
2.1. Background 7
2.2. Recent Work 16
2.3. Theory 29
III. Methodology 42
3.1. Sample Selection and Preparation 42
3.2. Autoradiography 46
3.3. Scanning Electron Microscopy 48
3.4. Principal Component Analysis 52
3.5. Multivariate Curve Resolution – Alternating Least Squares 59
3.6. Spatially Aligning Precursors and Autoradiography 59
IV. Results 61
4.1. EDS Compositional Data Modeling: PCA 62

4.2. EDS Compositional Data Modeling: MCR-ALS 73

4.3. Precursor Locating and Correlation with Autoradiography.....83

V. Conclusion.....113

5.1. Research Conclusions 113

5.2. Future Research 117

5.3. Summary.....120

Bibliography 121

List of Figures

Page

Figure 1. The double hump curve 10

Figure 2. The nuclear band of stability 11

Figure 3. Bikini atoll fallout sample cross section 13

Figure 4. Nevada tower shot fallout sample cross section 14

Figure 5. Optical images of the 12 samples used by Monroe 17

Figure 6. Autoradiography images of the 12 samples used by Monroe 17

Figure 7. Monroe sample with autoradiography overlayed on SEM elemental map 18

Figure 8. Dierken sample showing SEM elemental map aligned with autoradiography.. 20

Figure 9. Sample image highlighting a calcium rich area with low radioactivity 21

Figure 10. Logarithmic plot of viscosity versus melting temperature 22

Figure 11. PCA results Castro fallout samples 24

Figure 12. Plot of EDS spot scores for PC 1 v. PC 2..... 25

Figure 13. Plot of elemental variable weightings for PC 1 versus PC 2..... 26

Figure 14. Fitzgerald synthetic data set model validation 28

Figure 15. Shell model for electrons 31

Figure 16. BSE image example 33

Figure 17. SE image example 34

Figure 18. PCA score plot example showing clusters near compositional loadings 36

Figure 19. Illustration of the “forward” mixing process 39

Figure 20. Illustration of the un-mixing process shown in equation 1. 40

Figure 21. Examples of fallout particles prior to mounting and polishing. 43

Figure 22. Optical image of all 140 mounted samples 44

Figure 23. 1-DW-25 half-millimeter samples mounted in an aluminum puck..... 45

Figure 24. Typhoon scanner and standard film cassette used for the autoradiography. ... 46

Figure 25. Full autoradiography image of samples for this research..... 47

Figure 26. Sample classification examples..... 49

Figure 27. SEM mosaic image of an irregular sample..... 50

Figure 28. SEM image of a single tile from the same Figure 27 51

Figure 29. Eigenvalue versus Principal Component Number..... 54

Figure 30. Cross-validation plot 55

Figure 31. Zoomed-in Cross-validation plot..... 56

Figure 32. Cumulative variance captured for principal components..... 58

Figure 33. DW sample raster data plotted in PC1 vs PC2 space (sample set)..... 63

Figure 34. DW sample raster data plotted in PC1 vs PC2 space (degree of mixing)..... 64

Figure 35. Comparison of homogeneous, heterogeneous and porous samples 65

Figure 36. DW data plotted in PC1 vs PC2 space (sample size)..... 66

Figure 37. DW data plotted in PC1 vs PC2 space (sample shape) 67

Figure 38. Chemical loadings for each element considered in the DW dataset 68

Figure 39. DW data plotted in PC1 vs PC2 space with chemical loadings 69

Figure 40. DW data plotted in PC1 vs PC2 space with clusters are encircled 70

Figure 41. Six initial cluster compositions 72

Figure 42. Six initial precursors modeled using MCR-ALS 75

Figure 43. Q-residual values are plotted for the model of six initial precursors 77

Figure 44. Four initial precursors are modeled using MCR-ALS 79

Figure 45. Q-residuals are plotted for the four-precursor estimate..... 80

Figure 46. Five initial precursors are modeled using MCR-ALS..... 82

Figure 47. PCA plot displaying precursors in PC space for the PC1 versus PC2 84

Figure 48. PCA plot displaying precursors in PC space for the PC1 versus PC3 85

Figure 49. PCA plot displaying precursors in PC space for the PC1 versus PC4 86

Figure 50. PCA plot displaying precursors in PC space for the PC2 versus PC3 87

Figure 51. PCA plot displaying precursors in PC space for the PC2 versus PC4 88

Figure 52. PCA plot displaying precursors in PC space for the PC3 versus PC4 89

Figure 53. DW-IRR-6 with tile highlighted containing feldspar raster. 91

Figure 54. DW-IRR-6 with raster highlighted containing feldspar composition. 92

Figure 55. Autoradiography of DW-IRR-6 with tile showing no activity..... 93

Figure 56. DW-GG-1 with tile highlighted containing feldspar raster..... 94

Figure 57. Tile containing feldspar raster..... 94

Figure 58. 1-DW-25-37 SEM image with autoradiography 95

Figure 59. DW-SL-1-10 with highlighted tiles containing feldspar rasters..... 96

Figure 60. 1-DW-14-M2-4 SEM image with and autoradiography 97

Figure 61. 1-DW-25-5 SEM image with autoradiography 98

Figure 62. DW-IRR-10 SEM image with autoradiography..... 99

Figure 63. Tile 17 on DW-IRR-10 SEM with autoradiography 100

Figure 64. DW-IRR-4 SEM image with autoradiography..... 100

Figure 65. Tile 6 on DW-IRR-4 SEM image with autoradiography 101

Figure 66. 1-DW-14-M1-14 SEM image with autoradiography 101

Figure 67. DW-IRR-10 SEM image with autoradiography..... 103

Figure 68. Tile 14 on DW-IRR-10 SEM image with autoradiography 104

Figure 69. DW-Bullets-7 SEM image with autoradiography 104

Figure 70. DW-SL-1-10 with highlighted calcite raster 105

Figure 71. 1-DW-25-22 with highlighted rasters containing calcite composition..... 105

Figure 72. 1-DW-25-42 with highlighted raster containing amphibole composition..... 106

Figure 73. DW-SL-1-5 with highlighted tile containing amphibole raster..... 107

Figure 74. 1-DW-25-5 with highlighted raster containing amphibole composition..... 107

Figure 75. 1-DW-14-M1-20 with highlighted raster containing amphibole..... 108

Figure 76. DW-SL-1-11 with highlighted amphibole raster..... 108

Figure 77. DW-IRR-6 with highlighted area containing monticellite raster. 110

Figure 78. Autoradiography of sample DW-IRR-6 110

Figure 79. 1-DW-14-M2-4 with highlighted raster containing monticellite 111

Figure 80. 1-DW-25-3 with highlighted rasters containing monticellite..... 111

Figure 81. Images of samples: 1-DW-25-3,9,18,27,34 and 1-DW-14-M1-23. 117

List of Tables

Page

Table 1. Fallout sample breakdown for this research 42

Table 2. Typhoon FLA 7000 digital scanner settings 47

Table 4. Captured variance by each principal component in this model. 57

Table 4. Six initial precursor compositions based on PCA clusters 73

Table 5. Four initial precursor compositions provided by LLNL scientists 78

Table 6. Five initial precursor compositions derived from previous modeling 81

Table 7. Five initial precursor guesses percentage of fit to the model 83

Table 8. Feldspar precursors raster information 97

Table 9. Quartz precursor raster information 102

Table 10. Calcite precursor raster information 106

Table 11. Amphibole precursor raster information 109

Table 12. Monticellite precursor raster information 112

IMPROVING FALLOUT CHARACTERIZATION BY USING MCR-ALS AND PCA TO DETERMINE COMPOSITION

I. Introduction

This research focused on the use statistical methods of analysis in order to better characterize how fallout particles form following a surface-interacting nuclear explosion. The tools and statistical techniques have been applied to previously uninvestigated irregular shaped fallout samples as well as spherical samples from the same nuclear test analyzed in previous research. The research methods consisted of using scanning electron microscopy with energy-dispersive x-ray spectroscopy (SEM/EDS) in order to gather compositional oxide data from the sample cross-section surfaces. Autoradiography was used in conjunction to create 2-D radiation intensity maps of the fallout particle cross-sections. Principal component analysis (PCA) was then applied to extract elemental composition variation as well as environmental precursor estimates. Additionally, multivariate curve resolution-alternating least squares (MCR-ALS) was used to model and refine the precursor estimates. The precursors were then spatially correlated with radioactivity on sample surfaces. Specific precursors were found to be co-located with higher degrees of radioactivity than others, suggesting that specific compositions condense with actinides in the fallout formation process. The analysis provided an improved understanding of fallout formation and provided insight into how particle morphology and composition relate to actinide concentration. This information and methods can potentially lead to improvements in understanding how nuclear fuel mixes with environmental material in a nuclear detonation.

1.1. Overview

The current state of international policies and tensions surrounding the use and proliferation of nuclear weapons is at an all-time high since the end of the Cold War. Specifically, tensions with North Korea have sparked international interest and have many questioning what the future of nuclear weapons looks like for the world. The increasing interest in nuclear proliferation from rogue nations and/or violent non-state actors brings questions of how these weapons would be used in not only a conventional way, such as ICBMs, but also unconventional methods such as nuclear terrorism [1]. These questions highlight the need to better understand fallout formation as these materials preserve signatures of the device that have been altered by the physical and chemical processes of fallout formation. In the event of a nuclear detonation, decision makers in charge of post-detonation response will require information quickly. Our ability to quickly provide information to decision makers can enhance national security by deterring the deliberate use of nuclear weapons, especially via terrorism [2]. However, interpreting device signatures after they have been altered in the nuclear fireball is complicated, time-consuming, and requires an understanding of the chemical processes (e.g. fractionation) that occurred post-detonation. Inaccurate assumptions about these chemical processes could impede the attribution process. Examining the chemical variation observed in fallout glasses with respect to different morphologies or other visual characteristics can improve the information provided for analysis, especially in the event of a nuclear explosion in an untested environment such as an urban detonation [3].

The goal of this study is to improve the understanding of the physical and chemical processes through which device material and environmental debris mix to form fallout

glass and utilize multivariate statistical methods to un-mix fallout compositional data to better predict how device materials incorporate into fallout. Previous research, described in Chapter 2, mostly utilized principal component analysis to characterize fallout. This research uses PCA as well as MCR-ALS in order to un-mix fallout particle element/compounds and identify those of highest correlation with actinides. PCA is useful when there is no prior information about the precursors. Elemental correlations are made as those compositions of each element are not linearly independent. Solely using PCA to determine sample composition, the user can have difficulties defining particle compositions which encompass the dataset as a whole. The addition of MCR-ALS allows for the use of *a priori* information such as common rock forming mineral compositions at the location the particles were formed. This allows for analysis of particles originating from a nuclear detonation of unknown origin or those originating from a detonation in an unfamiliar environment [4]. The samples used for this study were collected from a historical nuclear weapon test and prepared as described in Chapter 3. The samples were put through various non-destructive tests in order to characterize the samples by visual characteristics, radioactivity, and elemental composition. The areas within each sample which exhibit high levels of radioactivity (akin to the location of unspent fuel and actinides) are used in conjunction with elemental compositions following the un-mixing process. The information gathered was used to demonstrate the use of MCR-ALS as well as finding actinides co-located with specific elements and/or mineral compounds. This research incorporates the efforts of previous AFIT Master's students as well as work done at the National Labs during the last decade [5].

The samples selected for this research consisted of a collection of 123 spherical particles of varying diameter as well as irregularly shaped particles. Lawrence Livermore National Lab (LLNL) scientists prepared the particles for analysis which were gathered from bulk samples of fallout and soil collected from a single historical nuclear test. The samples were mounted using epoxy and various specimen holders. Each sample set was polished to expose a smooth cross-section of each particle on the mountings.

Elemental composition data was gathered for each sample set using SEM/EDS. PCA was applied to determine the elemental compositions in the samples which account for the majority of the variation in the sample set [6]. PCA for the spherical samples has been previously conducted by various AFIT and LLNL researchers in the past decade as described in Chapter 2 [7] [8] [9] [10]. In this research, PCA was used to determine precursor composition estimates in conjunction with geological soil research. Following PCA, MCR-ALS was applied to the chemical data to model and refine precursor estimations. Solving for precursor abundances using known chemical composition is known as un-mixing [11]. With a refined model of which mineral precursors exist in the sample set, the precursors can be identified on sample surfaces using the compositional data. When compared with the autoradiography results, the radioactivity is then visually and spatially correlated with precursors on sample surfaces. Previous application of PCA on fallout samples demonstrated that the PCA is effective in identifying element compositions that have a correlation with actinide concentration [12]. This research will expand on previous research in un-mixing nuclear fallout compositions and correlating specific compounds to actinide concentration. This is in conjunction with PCA on samples

with unknown elemental abundances and will further improve the quality of information extracted from fallout samples.

1.2. Problem Statement

This research examines the use of MCR-ALS in addition to PCA in order to identify correlations between mineral precursors and actinide concentration as well as identifying unrecognized precursor components in fallout particles. The correlations potentially reflect the nature and behavior of matter in the process of fallout formation. By using the various spectroscopy techniques discussed, as well as statistical analyses, the research provides insight into how environmental debris as well as unspent nuclear fuel behave during formation, as well as following the condensation of matter in a nuclear explosion. Major questions include:

1. What precursors or mineral compounds in fallout particles are spatially correlated with high concentrations of actinides?
2. Is MCR-ALS an effective method of identifying unknown precursor components when the investigator has incomplete knowledge of starting mixture compositions?
3. Does fallout particle morphology, size, or degree of mixing impact the precursor composition or the actinide concentration in samples as well as the correlation between the two?

1.3. Scope of Study

This research focuses on 123 fallout samples. Some are previously examined spherical samples, but this set also includes irregular shaped samples from the same

historical test referred to as “DW” in this research. The samples were prepared by LLNL. Autoradiography and SEM/EDS measurements were performed at LLNL. The data was analyzed using PCA and MCR-ALS. MCR-ALS was a method introduced by LLNL scientists in order to identify mineral precursors without prior knowledge of the sample composition [4]. This analysis culminates the final phase of the three-year MIDAS program as outlined in the 2017 quarterly performance report [5].

1.4. Sponsorship

This work is supported under the MIDAS program, Defense Threat Reduction Agency (DTRA), as part of a three-year joint effort by LLNL and AFIT.

II. Literature Review

The mechanisms and nature of fallout formation have been studied since the first nuclear tests. Most of the research was conducted in the 1950s and 60s and consolidated in reports concerning the bulk properties and characteristics of fallout samples. This study focuses on non-destructive spectroscopy techniques along with statistical models in order to better understand fallout formation and how actinides mix with environmental precursors. The following chapter will discuss a brief background of fallout formation, recent work conducted in this area of study, and theoretical background of the research methods.

2.1. Background

To understand the formation of fallout particles, the fundamentals of nuclear weapon design and effects must be understood. A nuclear weapon consists of multiple interworking parts. The basic setup includes the fuel used to generate and sustain a chain reaction, typically U-235 or Pu-239. Surrounding the fuel is a trigger mechanism, high explosives, and a surrounding case. The explosives either compress or geometrically form a critical mass of nuclear fuel. A critical mass means that there is sufficient fuel to sustain a chain reaction of atomic fissions. At a minimum, when one atom fissions, a daughter neutron resulting from that fission induces the fission of another atom [13]. The science and technology behind the design of modern nuclear weapons is considered sensitive information, and it is highly sophisticated and more detailed than the simple description given. While the details of the components are not necessarily relevant for the purposes of this research, it is important to note that all of these materials, including the surrounding

environmental debris, will potentially be included in the fallout particles as the material is heated and cooled throughout the formation process inside the resulting explosion. The resulting release of energy from the fission chain reaction will create a fireball engulfing surrounding material [14].

Nuclear Event Description

When the chain reaction is triggered, and atoms begin undergoing the fission process, in a matter of microseconds the energy released heats up the fuel and the immediate surrounding environment to roughly 100 million Kelvin. As this happens, a fireball is formed, and it begins to expand diffusively around the explosion center. Initially, the fireball growth rate exceeds the speed of sound, thus, the shockwave from the massive increase in pressure due to temperature increase and energy release does not surpass the fireball radius. Depending on the proximity of the detonation to the surface, environmental material will be vaporized immediately by the extreme temperatures. This material is mixed into the fireball with other case and fuel debris. When the fireball expansion slows below the speed of sound, the shockwave separates from the fireball in a process known as hydrodynamic separation. As expansion continues, following separation from the fireball, the shockwave contacts the ground in the case of a near surface burst. When this occurs, a reflected shockwave sends ground and surrounding debris into the fireball. This is in addition to the previously vaporized weapon debris. The fireball rises due to its temperature and the shockwave reflection. This reflected shockwave causes a toroidal motion of gas and debris, creating the signature “mushroom” cloud shape commonly associated with nuclear explosions. As the fireball cools, the vaporized debris will solidify, remain gaseous, or become a liquid, depending on compositional properties. Throughout this process

particles “fall out” of the cloud and onto the ground below [13]. This applies to the particles examined in this research, as they were collected form areas in the immediate vicinity of detonation.

The composition of glassy fallout particles examined in this research depends on many factors throughout the particle formation. This will be discussed in further detail in the following paragraphs. Some particles enter the stratosphere, while other larger or heavier particles fall to the ground at an earlier point in time. As mentioned, the composition of individual particles plays a part in the time at which the particles quench in the atmosphere. This is also impacted by the temperature. The yield of the weapon will have an effect on the height of stabilization and the amount of raw material consumed, but condensation is dependent upon temperature and composition. That is to say the components or minerals contained in the particle itself were engulfed into the fireball and mixed to form the particle. If the detonation occurs high enough in altitude, the particles which form will consist mostly of unspent fuel and weapon debris. This is due to the fact that the fireball did not interact with the surface to draw in soil and other debris. For near surface bursts, the fallout particles will be a combination of unspent fuel, weapon debris, and environmental material due to the fireball location as well as the shockwave interaction with the ground [13].

When the detonation occurs, the fissionable atoms generally result in two or possibly three fission fragments. These fragments are typically radioactive atoms and consist of a broad array of different isotopes. The amount of any isotope resulting from a detonation is referred to as the yield fraction. The yield fraction depends on what type of fuel is used for the weapon as well as the energy spectrum of the neutrons generating the

fission [13]. This yield fraction is commonly described using the double hump curve shown in Figure 1.

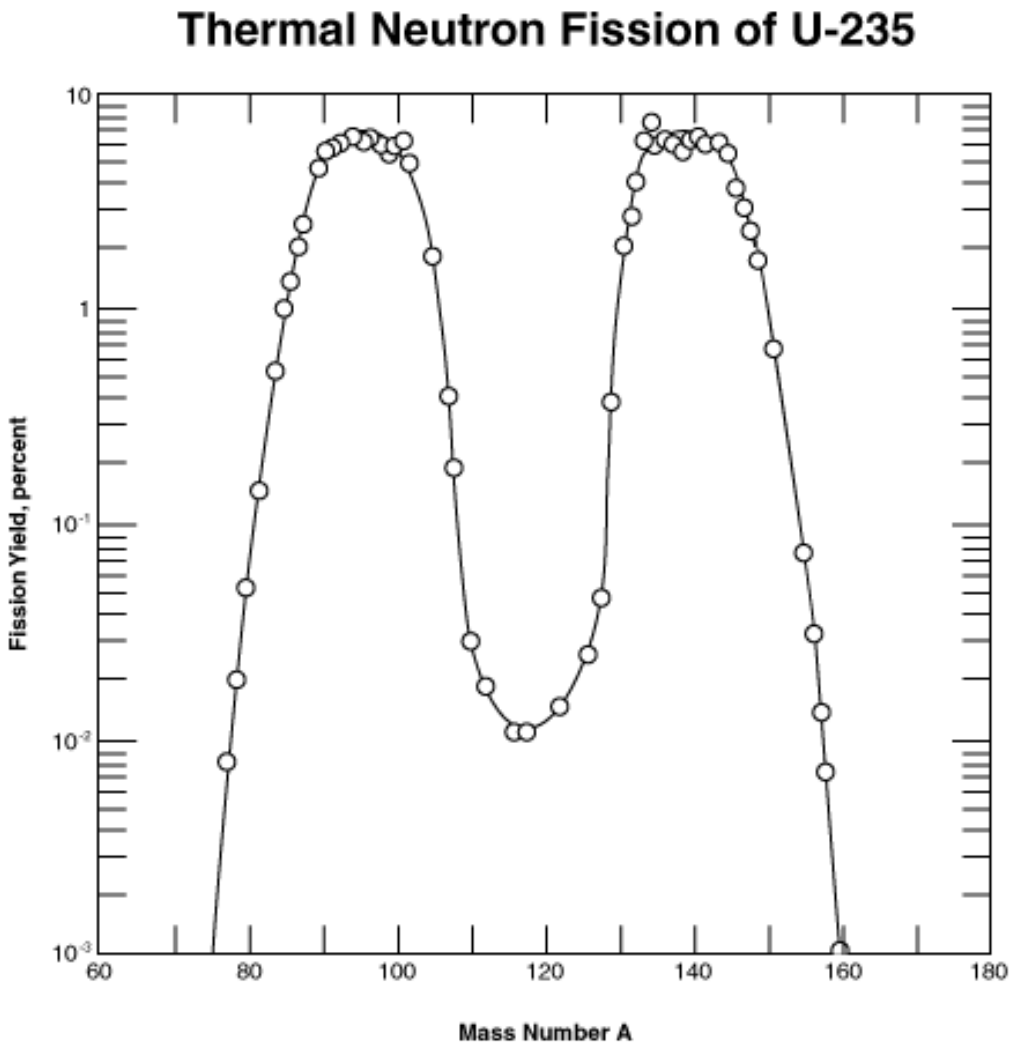

Figure 1. The double hump curve for the thermal neutron fission of U-235 showing the effective fission yield versus mass number of fission fragments. Reproduced with permission from [15].

Many of the fission fragments have short half-lives on the order of milliseconds. This means that in the sample collection studied in this research, the daughter products have mostly decayed away. Over time, and especially for the decades-old particles being

examined in this research, the products tend to decay toward the band of stability shown in Figure 2.

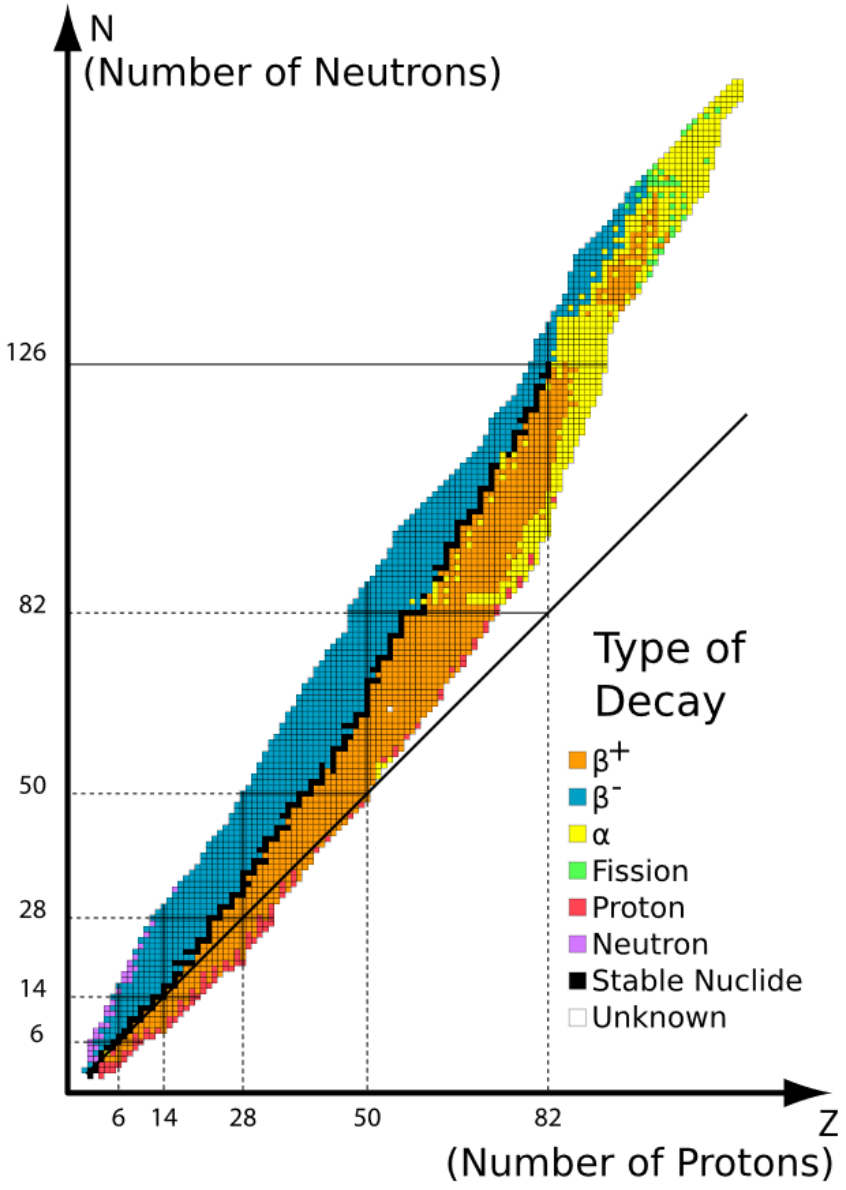

Figure 2. The nuclear band of stability. Nuclides tend to decay toward the black isotopes or centerline that represents stable nuclei. Reproduced with permission from [16].

Because the fission products are neutron rich they primarily undergo beta decay, converting neutrons to protons [13]. Other decay mechanisms such as alpha decay also occur in order to approach the band of stability [16].

Fallout Formation Mechanics

Now consider the formation of the fallout particles being comprised of fission fragments, environmental debris and some fraction of un-fissioned nuclear fuel. The fission fragments will only exist on the parts per million level within the fireball in comparison to environmental debris for a near surface burst. Much of the research concerning fallout formation took place in the 1950s and 1960s during the period of nuclear testing at the Nevada test site and atoll islands in the Pacific. Adams specifically contributed with some of the more robust compilations of data and fallout models using these test results [17]. A major consideration is the extreme temperatures of the fireball and the fact that the nature of matter at those extreme temperatures is not very well known. Therefore, models must be simplified and extrapolations must be made based on known data and test measurements. As an example, tests taking place on a large predominantly iron tower in the desert can be examined to deduce information regarding the condensation of iron and soil minerals as the fireball cools.

The concept of vaporization, mixing, and condensation of the particles is fundamental to the understanding fallout particle formation. By better understanding the formation of the particles, we can begin to find ways to un-mix the fallout in terms of actinide concentration, and compositional components. Any information of this nature is known to hold value in better understanding how actinides mix with chemical precursors in soil [18].

From the nuclear tests, fallout particles from surface/tower detonations show that the visual appearance and composition of the fallout particle depends on the location of the test, where inside the fireball the material existed, and when/how it cooled [17]. Some examples from Adams' research are shown in Figures 3 and 4. It can be see that some particles are uniform, revealing that the material solidified after mixing, with radioactive material throughout. Other particles solidified in such a way that smaller droplets agglomerated to the outer layer in the condensation process. There are more curious textures such as homogeneously porous samples, as well as un-melted regions. By examining just two different environmental test locations, it is clear that the debris greatly affects the composition and structure of the particles.

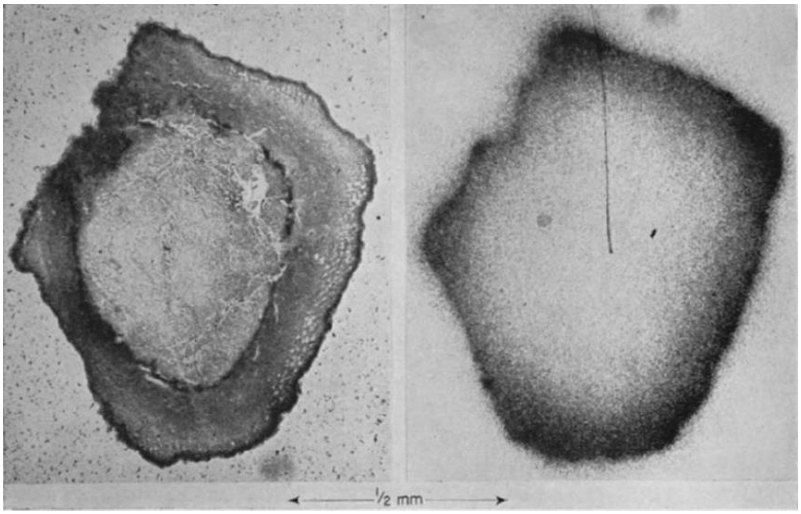

Figure 3. Bikini atoll fallout particle showing sample cross section with outer layer solidifying on smaller particle. Autoradiography on right showing radioactivity associated with outer layer. Reproduced with permission from [17].

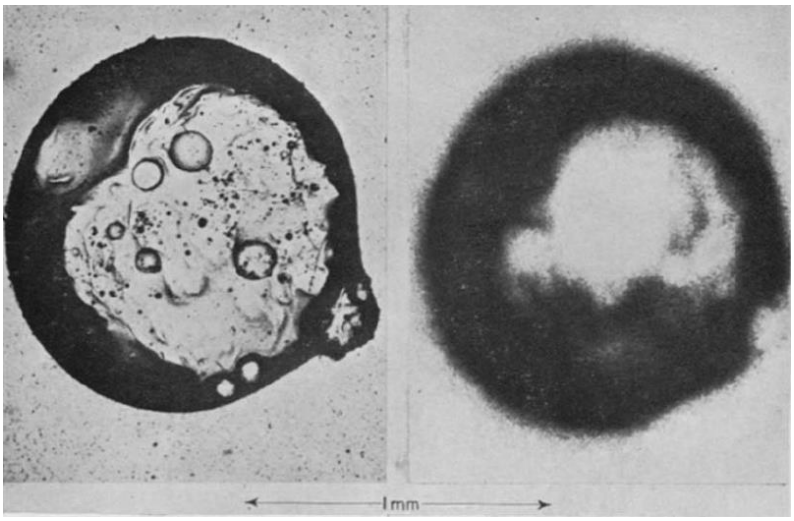

Figure 4. Nevada tower shot fallout particle showing sample cross section with irregular solidification and mixing. Autoradiography on right showing radioactivity associated with specific visual characteristics. Reproduced with permission from [17].

Adams examined fallout particles from mainly three different test locations. These included the Nevada test site, the Bikini Atoll, and the Pacific water shots. Adams concluded that particle formation is predominantly determined by two processes. The condensation of vaporized material within the fireball and the entrainment and heating of the surface material in the fireball. The particles consist of uniformly melted and cooled surface material mixed with bomb fragments. Some particles also exhibit the condensation of actinides on the outer surface of the particles. Furthermore, the lack of surface material, i.e. an atmospheric burst, would contain much smaller particles most of which would not accumulate appreciably on the ground [17].

It is known that not all of the nuclear fuel in the weapon undergoes the fission process. This would lead us to expect fallout particles to contain unspent fuel and other actinides. For the purposes of this study, the actinide concentration and associated precursor composition is the focus for the better understanding of fallout formations. This

is due to the fact that fission fragments will have mostly decayed away in the 60 years since the analyzed particles were found.

Miller [19] described a large effort to understand the thermodynamics of fallout formation. The two major processes of condensation are discussed similar to Adams' discoveries. These include either the complete solidification in a vapor-liquid phase and a vapor-solid phase where material condenses on the surface of solid particles. The problem is understanding the temperatures at which different elements condense and also how they tend to behave/interact with actinides in the fireball. By understanding how the material within the fireball behaves prior to condensation, we can extrapolate information about how to expect fallout to form in unknown environments with unfamiliar vaporized material [19]. This leads to the concept of fractionation and the models associated with refractory and volatile particles. Fractionation results from the different components and combinations of elements within this fireball having different condensation temperatures [20].

Fallout particles are typically categorized as early and delayed fallout. These early particles are those that reach the ground during the first 24 hours following detonation [14]. All fallout particles are important and have useful information contained in their material, both early and delayed. However, in the event of a real-world detonation, a collection team will typically be sent out to collect early fallout samples for analysis. The samples from this study were collected years following the nuclear test and stored in barrels. They were not examined until years later. Little is known about specifically how fallout forms inside the fireball, and how different environmental conditions affect the formation of the fallout. A major goal of this research and previous research in this field is to better understand the

partition of actinides in fallout samples, the time-temperature history of fallout formation, and also to test new models which make predictions about fallout formation [21].

2.2. Recent Work

In recent years there has been increasing interest in nuclear-centered research especially supported by the Department of Defense for national security purposes [10]. Some of this recent research has been conducted by LLNL and AFIT researchers. The goal of the research is to gain an overall better understanding of the process of fallout formation. Better understanding leads to better prediction modeling for nuclear detonations as well as more efficient analysis by the recovery teams and scientists. The following sections describe a progression of recent work in fallout particle analysis.

Monroe

Monroe conducted research in 2013 on 12 fallout samples from a single historical nuclear test. These samples are also included in the sample set for this research. Monroe's research analyzed the mounted samples using some of the same spectroscopic techniques used in the research including X-ray Fluorescence Microscopy (micro-XRF), SEM/EDS and autoradiography. This research sought to find a correlation between elemental composition of the particle and radioactivity. The radioactivity is assumed to likely have originated from alpha emitters (i.e. actinides) from unspent nuclear fuel. The actinides have a potential use in determining design and manufacture information. Some of Monroe's major conclusions relate to the methods used. The micro-XRF method was determined to be of little value due to the lack of vacuum conditions in the experiment, and was only suitable for bulk analysis. Therefore, the XRF data could not be aligned well with the

autoradiography, and elements such as aluminum, magnesium and silicon were not detected. Therefore, the XRF was determined of value for bulk analysis if the SEM/EDS was unavailable or time was limited. The final conclusions were a result of comparing the elemental maps and the autoradiography. Calcium and aluminum maps were observed to be co-located with actinides in the images. Figure 5 and 6 show the optical and autoradiography images Monroe used. Figure 7 shows an example of the SEM/EDS maps on one sample (designated AF08) compared to the autoradiography also shown in Figure 7.

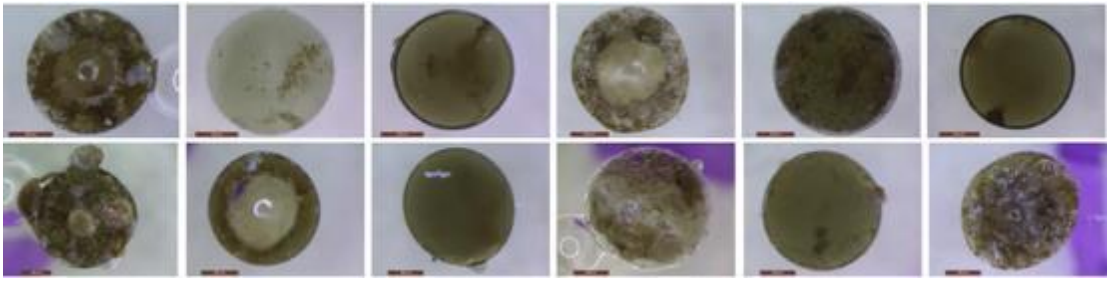

Figure 5. Optical images of the 12 samples used by Monroe [21]. These samples exhibit homogeneous and heterogeneous mixing. These samples are included in the sample set for this research.

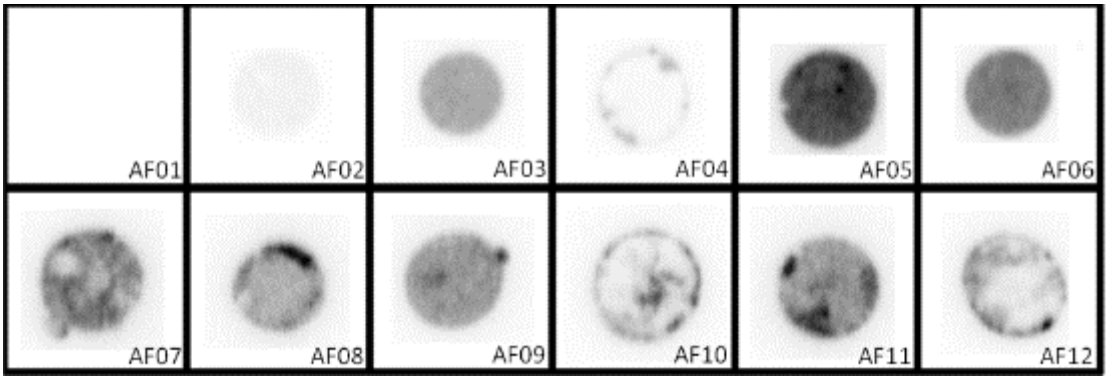

Figure 6. Autoradiography images of the 12 samples from Figure 5 [21]. The images are not oriented with figure 5.

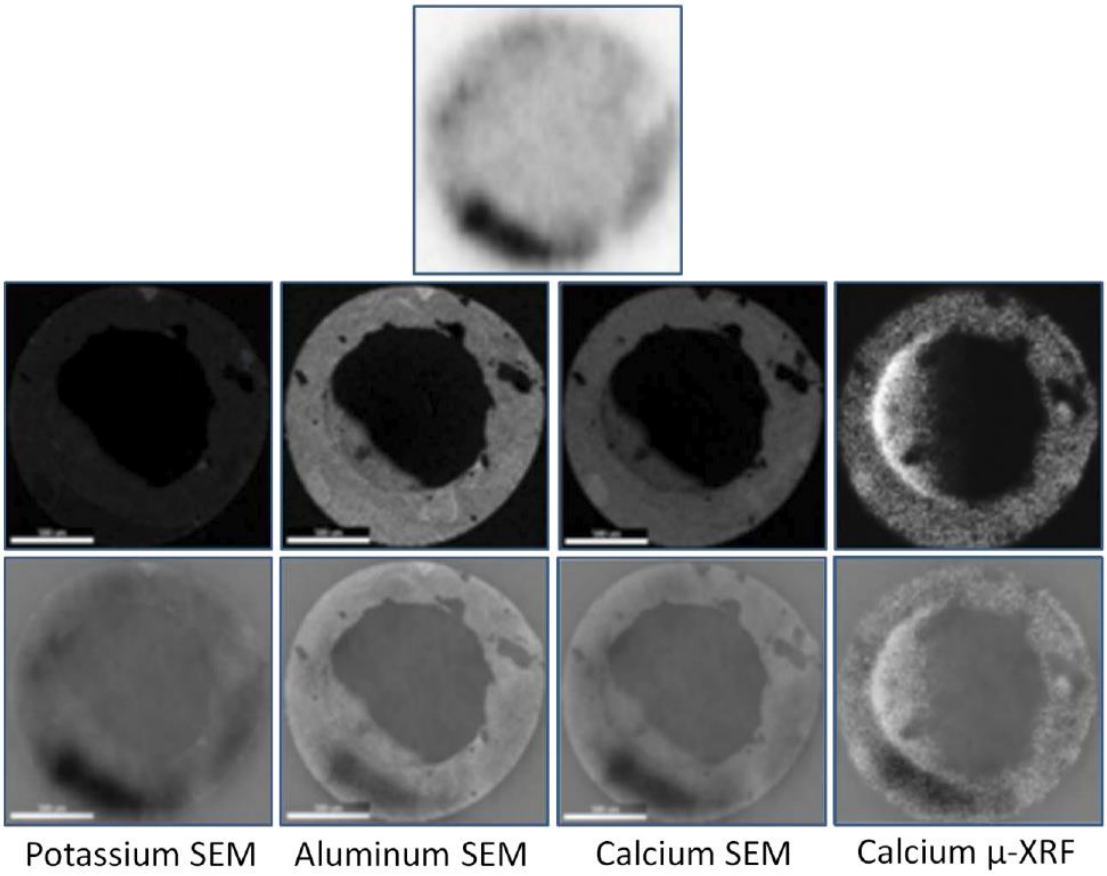

Figure 7. One sample from Monroe's set showing the process of overlaying the autoradiography on SEM elemental map images. Autoradiography map (top) with (from left to right in the middle row) potassium SEM map, aluminum SEM map, calcium SEM map, and calcium micro-XRF map. Bottom row is the result of the overlay. [21].

Dierken

Dierken, in 2014, continued similar research to Monroe, but expanded the sample set to 48 particles each roughly 1 mm in diameter. These samples are included in the sample set for this research. Similar to Monroe, the chemical composition and activity of the samples were measured by SEM/EDS, micro-XRF and autoradiography. The low resolution and inability to align the images appropriately led to a lack of quantitative results. The conclusions focus heavily on the glass composition referring to mafic or

feldspar type glass and how this might be correlated with actinide concentration rather than specific elemental compositions. Dierken states that higher activity levels are associated with mafic glass and homogeneous particles. Further, this suggests that the unspent fuel exists in areas with composition more susceptible to diffusion. By definition mafic glass is a silicate material rich in iron or magnesium [8].

Holliday

In 2016, Holliday conducted and compiled research in order to further find relationships between chemical composition and plutonium distribution in nuclear test fallout samples. The study used autoradiography and SEM/EDS along with optical image analysis. His work incorporated Monroe, Dierken, and other LLNL researcher's results. One interesting aspect of his research is that the focus does not lie with correlations specifically for chemical composition, but rather correlations with the mineral compounds. It was shown that condensation mechanisms were not the driving force for the chemical composition in the sample particles, but rather the simple mixing and melting of material describes the elemental variation within the samples. It follows that high radioactivity areas in the particles were not associated with concentrations of single elements, but rather compounds such as mafic glass. This observation is opposed to looking at just silicon or calcium as a correlating variable. Overall, he described the fallout particles using four compositional precursors. The precursors he found represent the idealized elemental composition describing the entire sample set. The endmembers were silicon dioxide, mafic glass, felsic glass, and other inclusions in the particles. These inclusions were described as locations on the particle face that have a high element concentration such as a particular basic oxide [12].

The precursors were found by using the PCA model described in the next section. PCA is used similarly in this research to make precursor estimations for further analysis with MCR-ALS. In Figure 8 below, the EDS map of the particle shows high concentrations of calcium are correlated with the radioactivity shown in the autoradiography image on the right. The calcium appears to have a correlation with radioactivity, but this may not be the case.

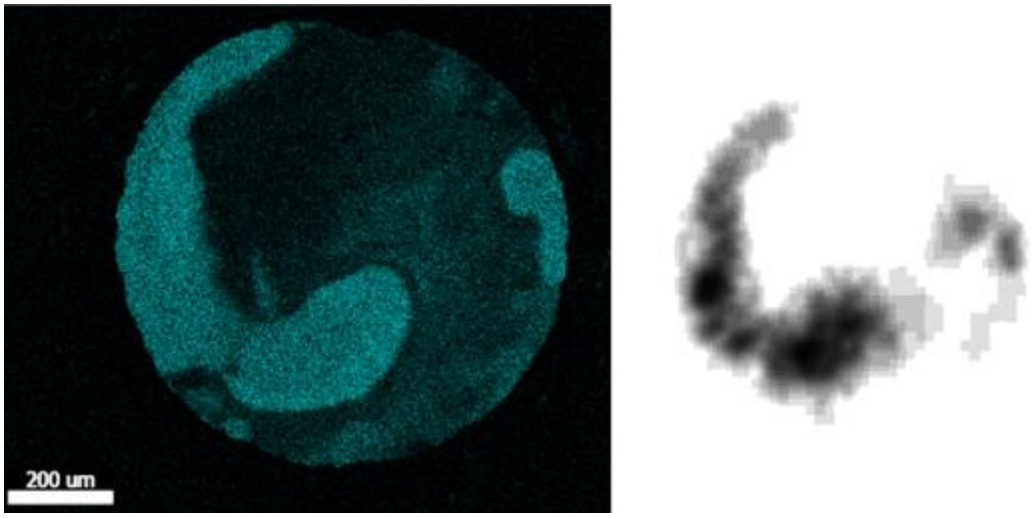

Figure 8. Dierken sample showing SEM calcium elemental map aligned with autoradiography [12].

Figure 9 below provides another image showing that an area high in calcium actually reveals a drop in the activity. Other elements with calcium drive the correlation with activity. It appears that radioactivity is never associated with inclusion areas rich in a single element [12].

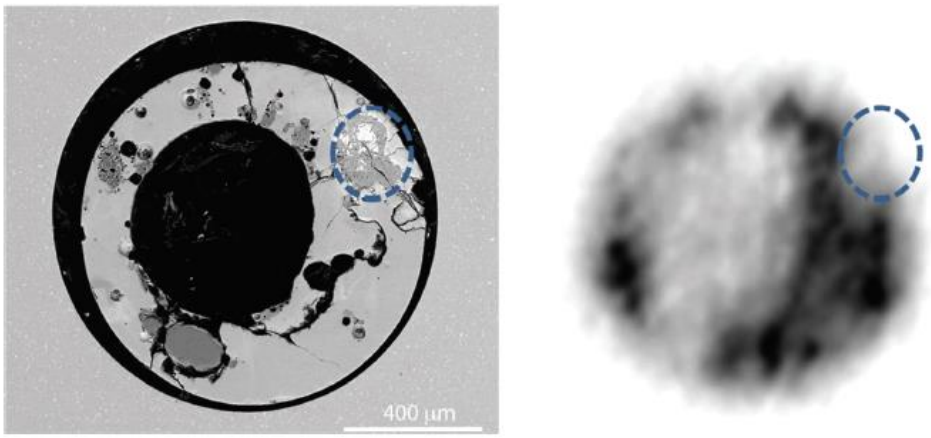

Figure 9. Sample image highlighting a calcium rich area that does not exhibit high radioactivity [12].

Holliday's data suggests that the plutonium's distribution in the sample particles is dictated by the physical properties of the mineral compounds in the sample, and not the chemical characteristics of single elements. Furthermore, the melting and mixing model tends to fail using the elemental correlation assumption, as the melting point of SiO_2 (1600^{o}C) is higher than mafic glass (1261^{o}C) which incorporates plutonium. The felsic glass (720^{o}C) is anticorrelated with plutonium. This lead the author to investigate viscosity as a driving factor in fallout formation and plutonium segregation in the particles. Viscosity decreases with melting temperature for felsic glass, mafic glass, and pure SiO_2. Looking at Figure 10 below, the conclusion is that the lower viscosity of mafic glass may contribute to the mixing and plutonium incorporation.

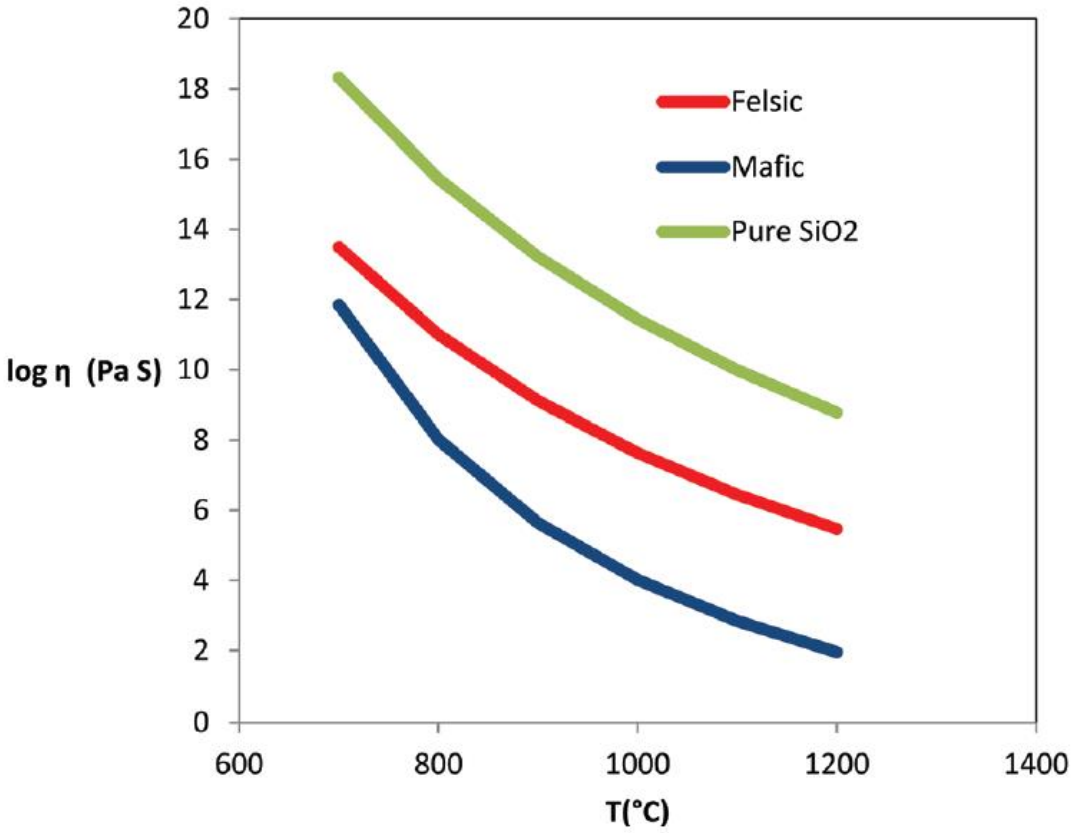

Figure 10. Logarithmic plot of viscosity versus melting temperature for three different mineral compounds [12].

Castro

In 2016, Castro sought to develop a way to quantify the results of the previous qualitative analysis to provide a measurable correlation between particle composition and actinide concentration. The resulting method used was principal component analysis, which would became a common method used in this research to determine the major sources of variation within the sample data set and future research data sets. This method is discussed in detail in further sections of this chapter. Spectroscopy results similar to those previously discussed were used in order to gather compositional data and activity for

the analysis. The research consisted of two major efforts. The first was to develop a standard reference data set that simulates fallout material in an urban environment. This was successfully accomplished. In regards to this research, PCA was then applied to the data to confirm that this method can be used to identify sources of variance in the particles. In this second effort, Castro conducted PCA on another set of only 11 samples determining that Ca resulted in the highest variance and was co-located with the areas of highest activity [7]. These samples are also included in the complete data set for this study.

When confronted with a large compilation of compositional spot data on samples, it is difficult to distinguish samples which are statistically different from the group. This is where PCA is most effective, in considering each data point as a linear combination of each variable, namely each elemental composition. Figure 11 shows the first and second principal component scores plotted against each other for each data point. The result gives a representation of variance for each sample. The result shown in Figure 11 gives a clear representation of which samples are compositionally different as shown by the colors. This

verified that PCA is useable for fallout analysis using SEM/EDS compositional data [7].

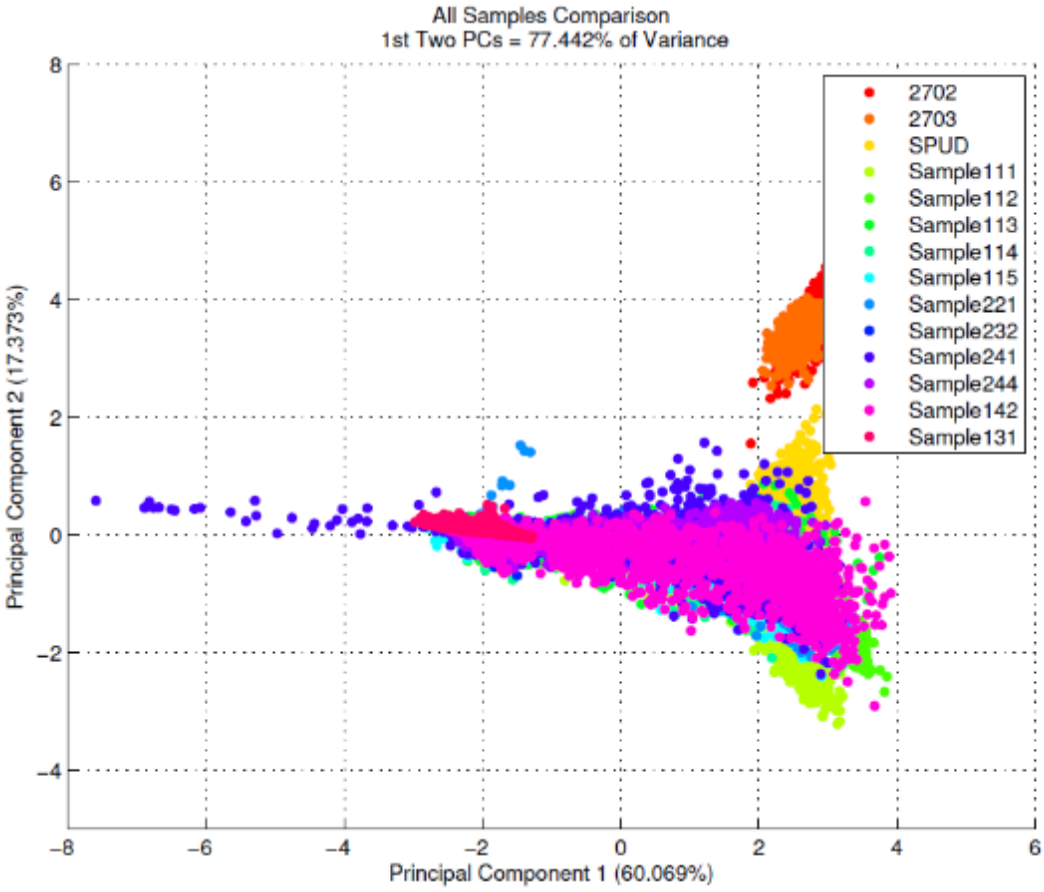

Figure 11. PCA results for the fallout samples and reference samples in Castro's research. PCA separates compositionally different samples from the dataset [7].

Haws

In 2017, Haws conducted research similar to Castro on a new sample set from a historical nuclear test. The sample set included 50 half-mm diameter, spherical particles mounted in an aluminum puck and polished into hemispheres for internal analysis and SEM/EDS mapping. Autoradiography was conducted as well. From the SEM/EDS, Haws obtained spot data including nearly 2000 total spots and the elemental composition for each of those spots. The elements include Na, O, C, Mg, Si, Al, K, Ca, Ti, and Fe. The data

points for carbon were eliminated as this element held no contribution to the variance in the data when PCA was conducted. This is because carbon only exists prominently in the epoxy molding used in sample preparation. Oxygen data was removed as it created noise and the molecules are considered to be oxides. Haws conducted PCA on this data to find the elements and samples where the most variation in the data originated. In Figure 12 below, the principal components 1 and 2 for the data points are plotted versus each other [9].

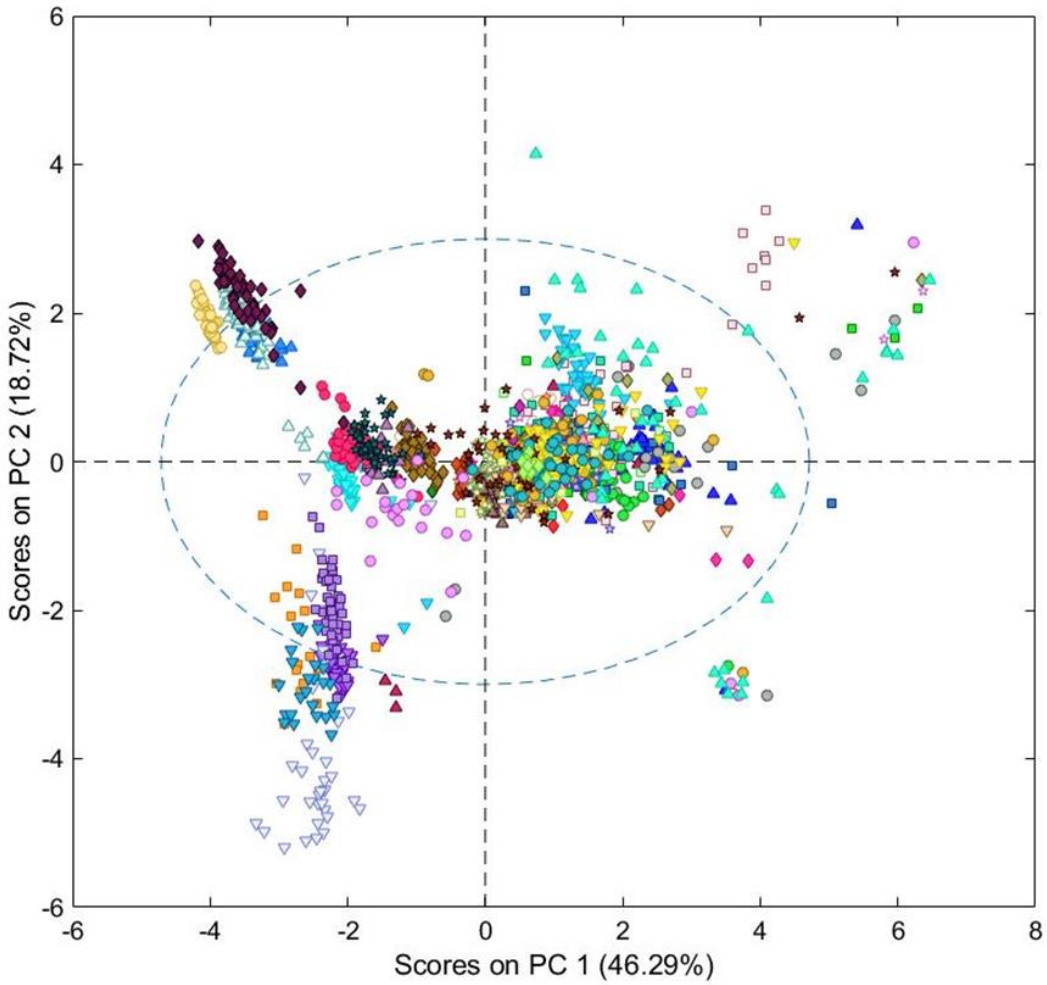

Figure 12. Plot of sample EDS spot scores for PC 1 versus PC 2. Spots with similar composition cluster together and those furthers from center represent greatest variation. Each color represents a sample the EDS spot measurement [9].

Each data point plotted in PC-space is considered a linear combination of each variable, the elemental composition, and by plotting the PC scores against each other, a pattern emerges to visually observe variation in the data. In Figure 13, Haws plots the weighting factors for the principal components to show the elements that account for the variation shown previously.

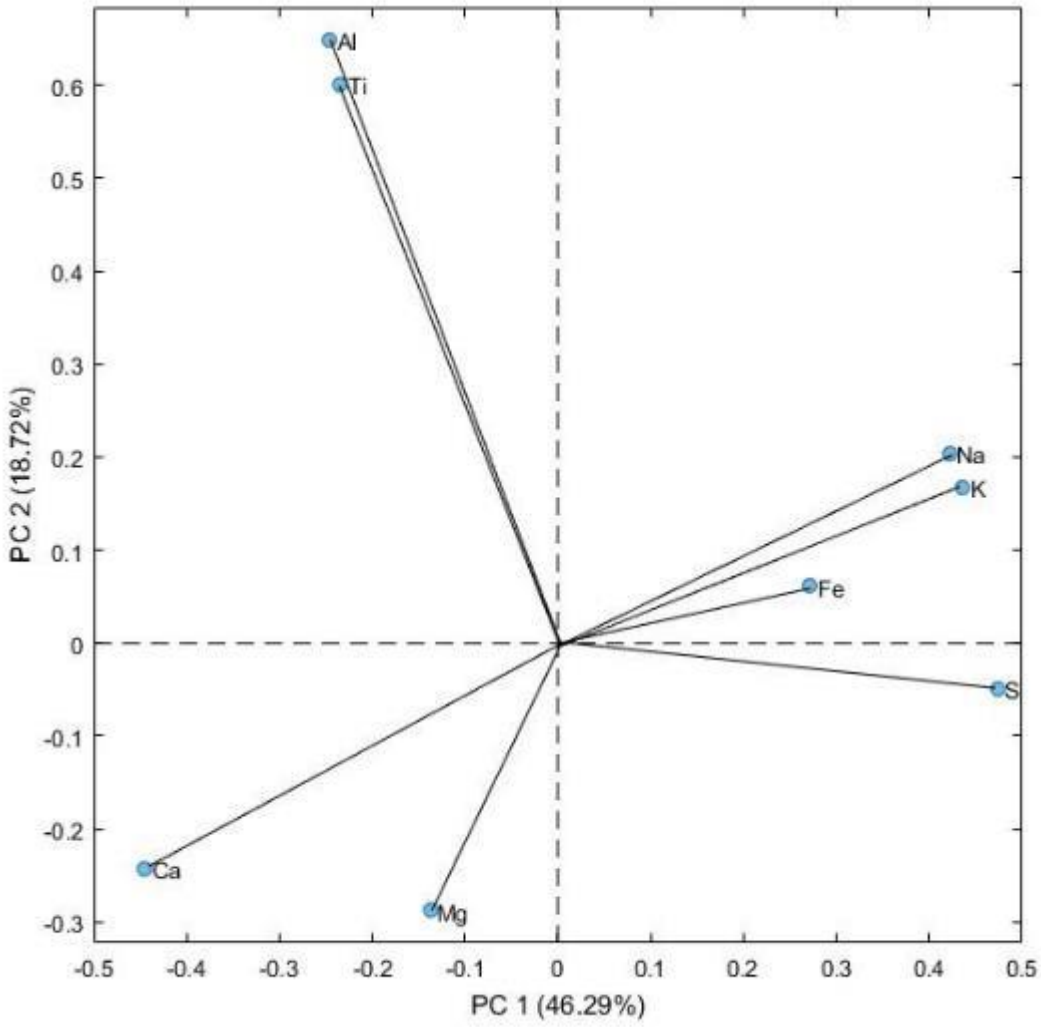

Figure 13. Plot of elemental variable weightings for PC 1 versus PC 2. This is correlated with the PCA plot in Figure 12 [9].

The final conclusions made based on this method of analysis was that the samples could be grouped into 3 main groups. One group consisted of porous samples high in Mg and Ca. The second group consisted of homogeneous samples with uniform activity (shown in the autoradiography) and high in Al and Ti. The third group was heterogeneous with varying activity. Overall it was concluded that samples rich in Al and Ti as well as those with homogeneous cross-sections were of most value and correlated with high activity therefore unspent fuel.

Fitzgerald

In 2017, Fitzgerald conducted research in order to formulate a more rigorous statistically based method of analysis on nuclear fallout particles which takes advantage of *a priori* knowledge of the composition of environmental debris. This method is known as multivariate curve resolution-alternating least squares (MCR-ALS). Fitzgerald developed a code which can take any SEM/EDS data set containing compositional mass fractions and output the collection of elements that were originally mixed in a sample set. Essentially, while previous research focused on correlating specific elements with high radioactivity, this model un-mixes the elemental composition, revealing possible compounds or mineral precursors that existed prior to the nuclear event. Using this information, we can investigate whether these precursors were from the original soil, environmental debris, or if they originated from vapor condensation within the fireball evolution process [4].

Fitzgerald demonstrated this technique first on a synthetic data set as a basis for evaluating the performance of the model and proceeded to use the method to un-mix real historical test sample data. The synthetic data set consisted of a modeled silicon-based soil

sample with randomly induced variation. Figure 14 shows the validation of the model using synthetic data.

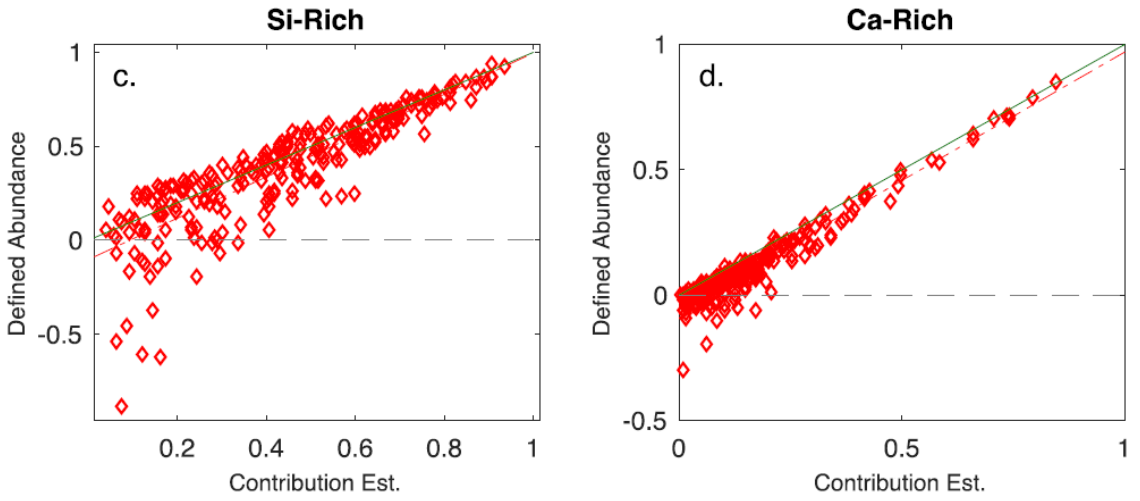

Figure 14. Fitzgerald synthetic data set model validation. The defined abundance of each compound is plotted versus the model estimation. The green line represents perfect agreement between the model estimates and the defined abundance. The linear relationship suggests the model is fitting the defined compound definitions [4].

Figure 14 shows the contribution of each element that is estimated by the model plotted against the defined value for the data. The linear relationship observed indicates that the resulting compositional estimation using MCR-ALS matched the defined composition very well. This validation led to the use of MCR-ALS on real-world fallout compositional data, which resulted in similarly accurate results.

The fact that this model takes into account *a priori* knowledge makes it advantageous over PCA. MCR-ALS reveals compositional signatures that can be reduced to precursors, or compounds that mixed into the particle during fallout formation such as quartz, feldspar or other geochemical compounds. By understanding how these precursors mixed into the particle during formation and fireball evolution, we can better understand how the actinides behave in the formation process with these compounds in different

environments. A better understanding of how these precursors mix with actinides in the fireball allow for more efficient analysis of particle composition [4].

2.3. Theory

Autoradiography

Autoradiography is a widely used technique to detect radiation using film. The film is exposed to a radiation source, and the radioactive decay of atoms within the source interact with the film leaving a trace image behind. This technique uses the same concept as in basic photography where light interacts with film in order to produce an image. Autoradiography has many applications, including medical practices such as tracking the absorption of radioisotopes by imaging the radioactive particles within the body [22].

For this research, autoradiography is used to effectively measure radioactivity in fallout particles. Film is exposed to cross-sections of particles for a specified amount of time. This process results in a darkened image outlining the activity as a function of location on the cross-sectional surface of the particle. Two factors determine the darkness of the image: the amount of time the film is exposed and the activity of the material. For this reason, autoradiography is not ideal for quantifying activity by itself [23]. Rather it better serves to provide a qualitative or relative activity level of regions of the particle cross sections. For this research, determination of specific activity as a function of location on the cross-sections are used in order to co-locate unspent fuel with geochemical compounds in the material.

All ionizing radiation impacting the film will deposit energy and contribute to the image on the film. As mentioned, relative activity can be measured by simultaneously

imaging different samples for the same time and conditions. The area in which the radioactivity originates can be measured by placing film in direct contact with the source. The decay products which deposit energy travel directly away from the source in an omnidirectional path. Alpha particles typically have a definitive energy and short path length of travel, whereas beta particles have a longer path length and a varying energy distribution. The stochastic nature of the direction of travel and energy of radioactive decay products results in an image that is somewhat blurred. The blurring of the image results primarily from the beta particles [24]. However, qualitative deductions can be made using this technique as it provides valuable information regarding actinide location on particle cross-sections.

Using autoradiography for this research requires assumptions as follows. Photon interactions with the film are minimal and uniform due to the large mean free path relative to the film thickness. The fission fragments which result from a nuclear detonation have decayed due to their relatively short half-lives and the time since the nuclear test [13] [14] [25]. The long-lived fission fragments decay by gamma decay, but photons have a long path length and minimal interaction with the film. Therefore, gamma radiation in this case can be generally disregarded. This research considers the autoradiography image to be a result of alpha and beta decay solely from unspent nuclear fuel radioactive decay. It is important to note that autoradiography would not be a viable method of measuring particles soon after the detonation, as the activity would be overwhelmed by the distribution of fission products and may not reflect the distribution of unspent fuel [26].

Scanning Electron Microscopy

In this project, a scanning electron microscope was used to determine the chemical composition of specific locations on each nuclear fallout sample surface. The scanning electron microscope (SEM) scans a beam of electrons across the sample surface under vacuum. The electrons excite the atoms in the sample, producing other electrons and characteristic x-rays that give information about the topography or chemical composition of the sample (Figure 15).

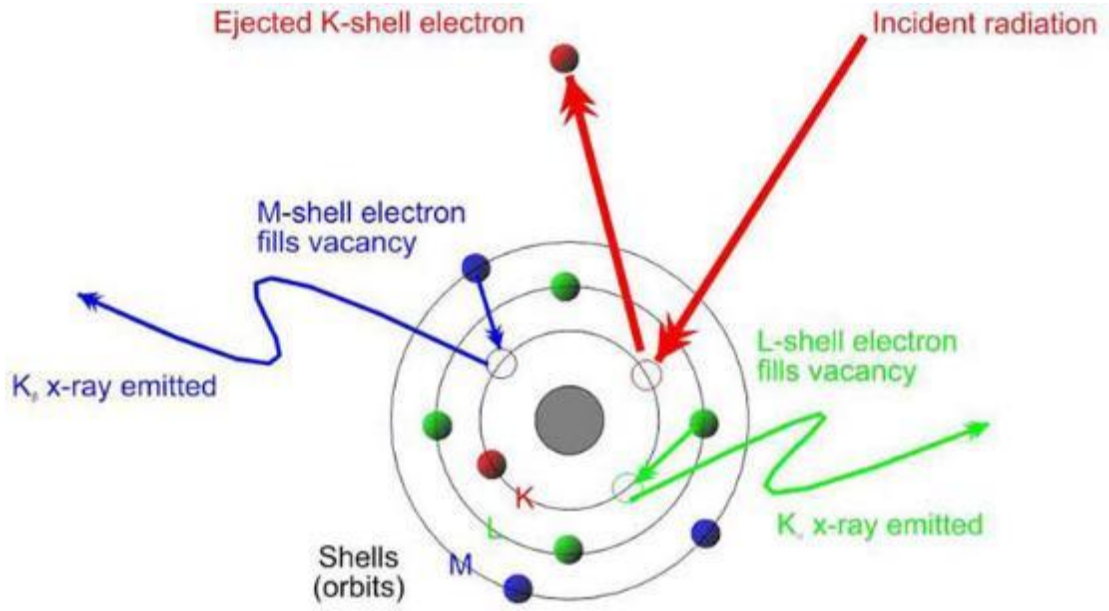

Figure 15. Illustration of the shell model for electrons moving to different shells and emitting x-rays.

X-rays are emitted due to excitation of inner atomic electrons, and the subsequent transition of outer electrons in the atom into an inner shell. The energy of the x-ray is dependent upon the transition electron's shell. Each element has specific, known shell energy levels that are programmed into the SEM software to be easily recognized when the x-ray energy is measured. Using this information, the composition of the sample at the

specific location the electron beam interacts is determined [27]. This is known as x-ray energy dispersive spectroscopy (EDS).

Backscattered electron (BSE) imaging utilizes electron elastic scattering. As the electron beam generated by the microscope comes into contact with the sample, some electrons are reflected back at the detector. The energy of these electrons is proportional to the square of the atomic number of the interacting element. The higher the atomic number of the element, the more electrons that will deflect back to the detector. The resulting image produced by the microscope is a gray-scale image where the lighter portions of the image indicate higher atomic number and darker portions indicate no interaction or low atomic number. This contrast allows for a visual representation of how the samples are geochemically mixed [27]. Below is an example of a BSE image showing the chemical composition characteristics as a function of contrast.

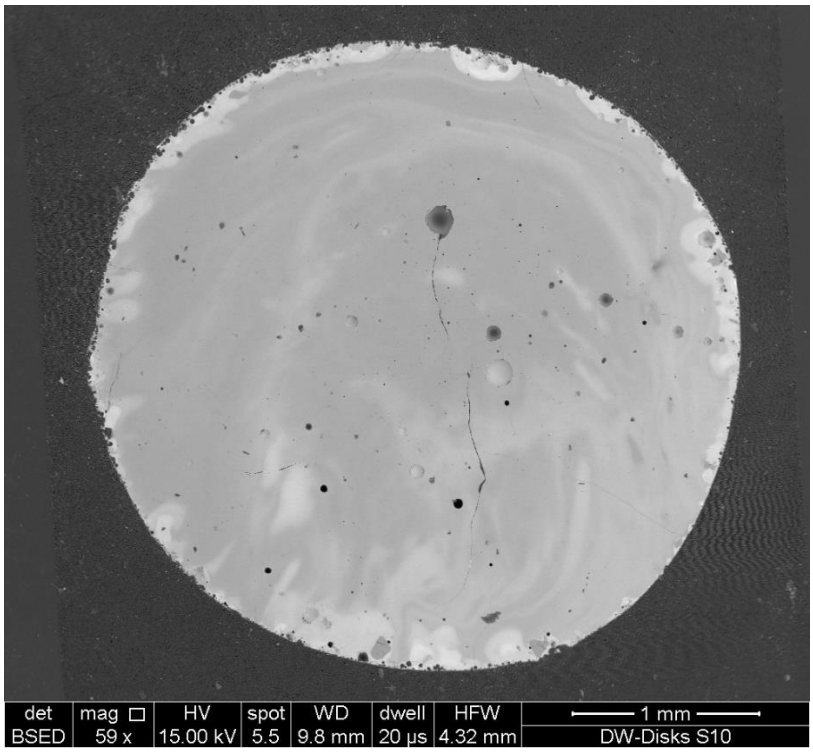

Figure 16. BSE image example. The elemental variation can be seen by differing shades of the sample surface.

Secondary electrons (SE) are emitted from the atom's k-shell following interaction with the electron beam. This process involves inelastic scattering to free atomic electrons. The number of secondary electrons detected depends, in part, on the topography of the sample surface. By scanning the electron beam across the sample and collecting the secondary electrons, an image of the topography of the surface is created. Figure 17 shows the SE image of the same sample shown in Figure 16. The reader is referred to the bibliography for more information regarding SEM imaging. [22] [27] [28].

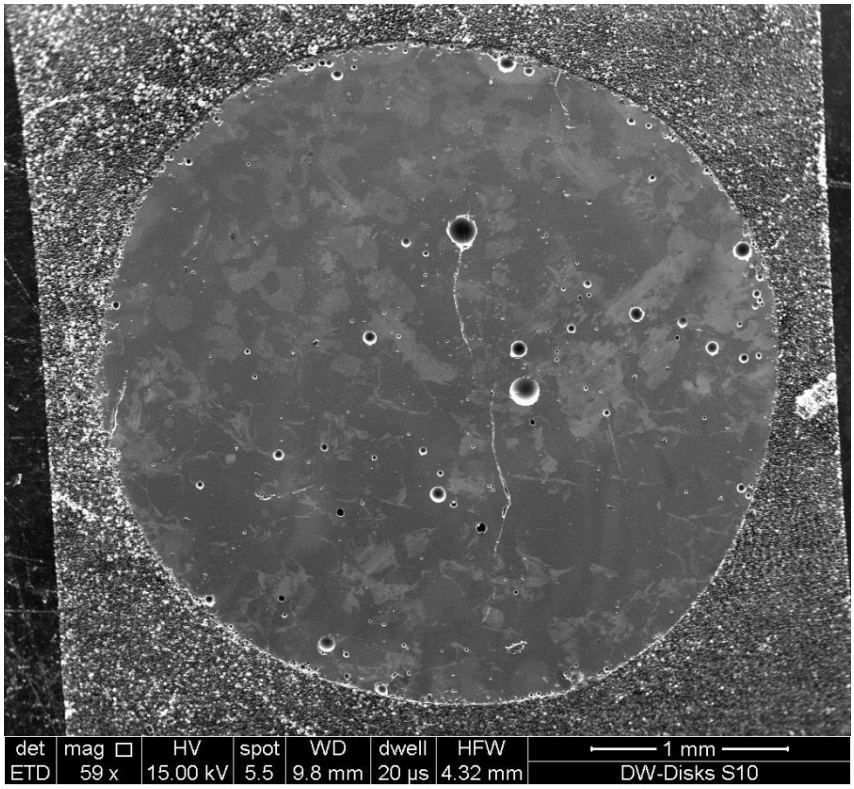

Figure 17. SE image of the same sample shown in Figure 15. This image highlights the higher degree of sharpness and visible edges on the sample. Note the surface appears different in this image than in the BSE image.

Principal Component Analysis

PCA is a mathematical method of finding patterns in large datasets. The method generates a means of expressing data variation in terms of one variable instead of multiple variables, through linear combination and statistics. For example, this research considers compositional data with eight different elements in the composition of samples. Each data point contains therefore eight different variables as a composition mass fraction. For this research it is assumed that the elemental composition, and therefore the precursors, can be expressed as linear combinations of the other variables. Once the patterns are found using

linear algebra, each data point can be compressed, essentially reducing the number of dimensions in the data, without losing information [6].

The new variables are called principal components. The total number of principal components equals the total number of variables considered in the dataset. Each data point is thus represented by 8 principal component values instead of the 8 original elemental combinations. Each of the original variables is multiplied by a corresponding weighting factor. This factor is calculated using orthogonality between that particular variable and all of the others. The lower the principal component value, the lower the variation between that variable and any other variable in the dataset, for that particular data point. Essentially, the data is projected onto eigenvectors which represent the variance and covariance in the data [29].

The resulting matrix recasts each data point as a value corresponding to each principal component. By plotting sample principal component scores against one another, for example PC1 versus PC2, the samples which are closer to the center of the plot account for very little variation in the dataset as a whole, whereas the data points clustered away from center represent samples which encompass more variation. The model is built to orthogonally capture as much variation as possible in PC1, followed by PC2, and so on. Therefore, the PC1 versus PC2 plot provides a visual representation of which samples account for the majority of variation in the dataset and those which tend toward specific compositions. Minor PCs are still significant however, and can still be examined for recognition of minor components of the mixture such as bomb vapor in this case [6] [30]. The loadings, or eigenvalues, correspond to the original elemental variables and can also be plotted to align with the data clusters. An example is shown below in Figure 18.

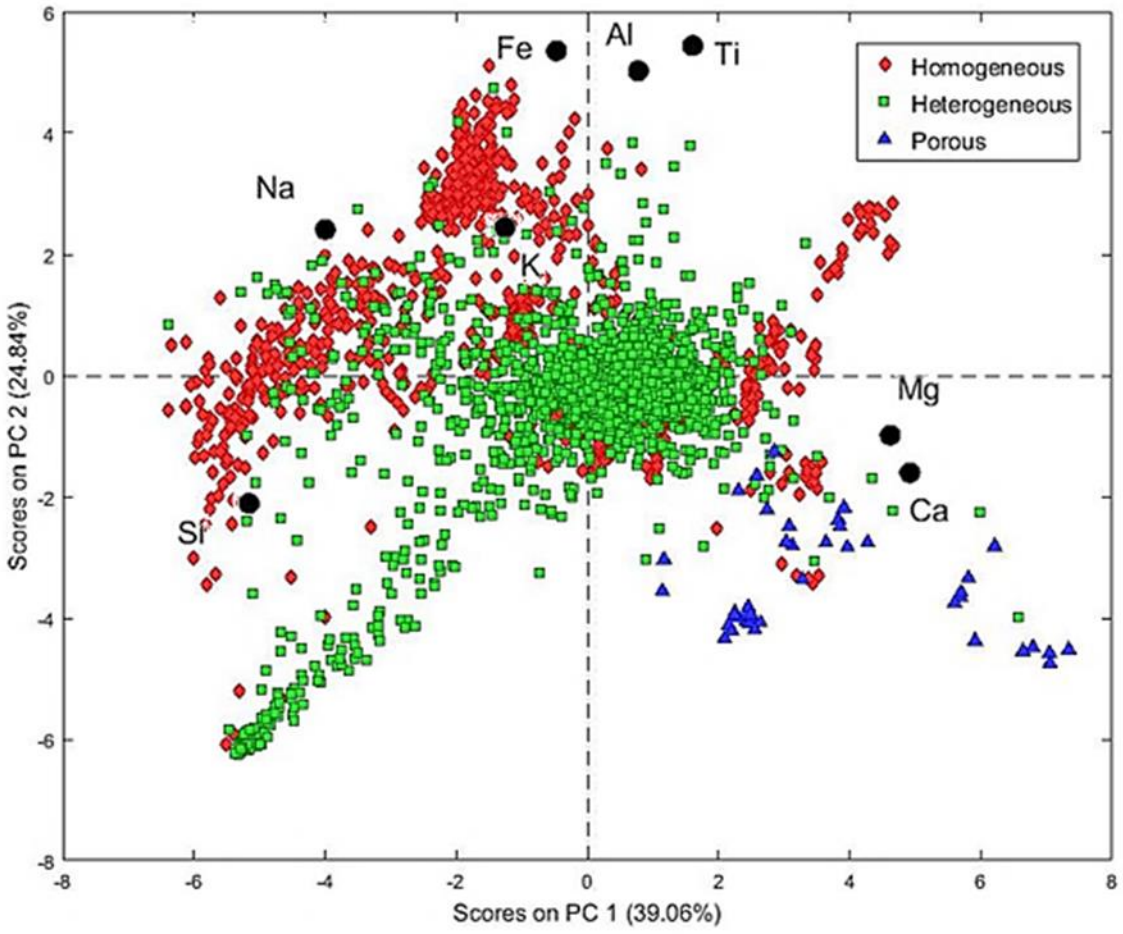

Figure 18. PCA score plot example showing clusters of sample spots near compositional loadings which correlate to the samples.

Without reducing the dimensionality of the data, it would be nearly impossible to compare variables individually for each data point and find correlations and variation dependencies for thousands of data points [31]. This is also a factor in considering the spatial variation in elemental composition where images consist of thousands of pixels. PCA displays the strength of compositional relationships between variables in the dataset. Using the elemental variation, this research further deduces what the precursor compounds mixed in the fallout during fireball formation and how these compounds align with radioactivity using autoradiography.

There are a few assumptions to consider when utilizing PCA as a model for finding variation in the data. First, there is little prior information about the environmental precursors. For this research we do use prior knowledge in model refinement, but it is important to consider the validity of this method without prior knowledge of the compositional makeup of the samples. Also, this research assumes that the variation in the dataset is meaningful and can be expressed by a limited number of orthogonal vectors which represent the elemental covariance in the data [32].

In order to verify that the data has captured the variation effectively, the PCA model is created using a cross validation approach. This approach runs the PCA model on random subsets of the entire dataset, and compares how the subset models fit against each other. This process then averages the differences in results for each partition comparison. The comparison of the root mean squared error between models is used to reveal where principal components begin to represent noise in the compositional variation [33]. This cross- validation is used along with a scree test, an eigenvalue plot which is described in subsequent chapters, to estimate the number of precursors represented by the data [34].

Multivariate Curve Resolution – Alternating Least Squares

MCR-ALS is a linear programming method used in this research and previous research by Fitzgerald [4] to un-mix compositional information from SEM/EDS. While PCA is a viable method for evaluating general mixing trends in a melt and recognizing the major precursors contributing to compositional heterogeneity, PCA methods are unable to quantify the composition or contribution of these precursors because of ambiguities in PC loading and score interpretation. Linear programming approaches, such as MCR-ALS, have been constructed to overcome these limitations. MCR-ALS performs calculations by

iteratively solving for precursor chemical compositions and contributions to minimize the residuals between each iteration. MCR-ALS has been applied and validated for use in un-mixing in geochemistry problems in the field of remote sensing and chemo-metrics [32] [35] [36].

In order to un-mix the data with MCR-ALS, the number or precursors must be estimated. One method of doing this, described in Chapter 3, involves PCA. Once the number of precursors is determined, the equations used inherently in the MCR-ALS code include matrices manipulated to solve for compositions and contributions prior to mixing. The equations are

$$\hat{A} = X\hat{B}^{+} \tag{1}$$

and

$$\hat{B} = \hat{A}^{+}X \tag{2}$$

Where $\hat{A}$ is the estimate of precursor contributions or abundance, $\hat{B}$ is the estimate of precursor compositions, and X is the compositional data set provided by SEM/EDS [4].

The basic idea of un-mixing is based on matrix math. Figure 19 illustrates the "forward" mixing process of $\hat{A}\hat{B}$. While Figure 20 and equation (1) show the inverse problem, un-mixing, addressed in this research.

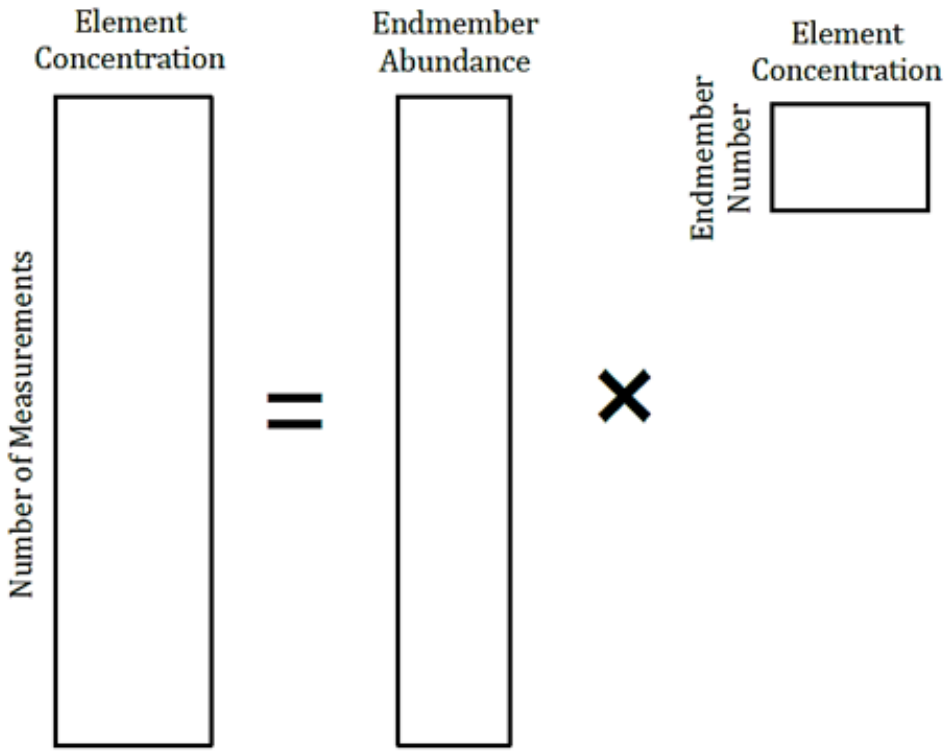

Figure 19. Illustration depicting the "forward" mixing process of AB. Used with permission from Fitzgerald [4].

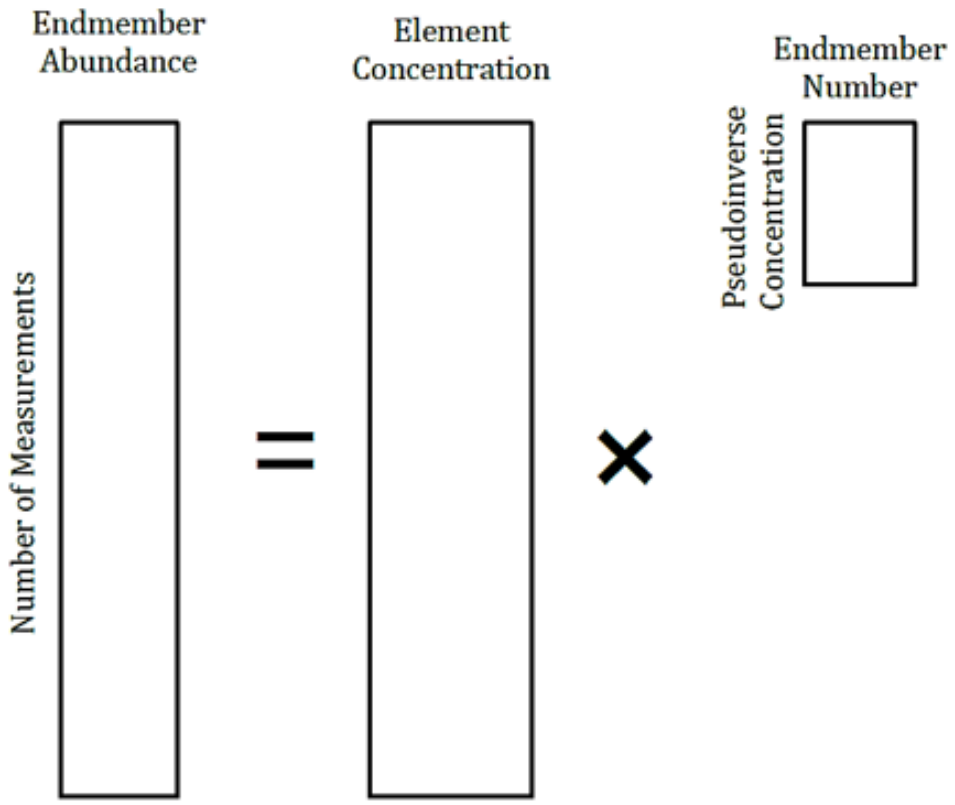

Figure 20. Illustration depicting the un-mixing process of shown in equation 1. Used with permission from Fitzgerald [4].

The MCR-ALS method iteratively solves for a model of precursor compositions which best fits the data set by two steps. The first step holds the composition matrix, $\hat{B}$, constant and estimates the contribution matrix, $\hat{A}$. The precursor contributions are then normalized to the sum of the precursor concentrations at the end of the first step. The second step solves for the composition matrix, $\hat{B}$, while holding the contribution or abundance matrix, $\hat{A}$, constant. The process continues until a convergence is reached or a predefined set of iterations is completed. These solutions minimize the residuals between iterations but may not resemble the "correct" solution – an effect referred to as multiplicative or rotational ambiguity. Multiplicative ambiguity occurs when the estimated precursor contributions

deviates from the true contributions. Rotational ambiguity occurs when the chemical relationship between precursors is systematically offset from the true relationship. In the MCR-ALS process, multiplicative and rotational ambiguity can be reduced by the use of weighting factors for the composition of each precursor. These weightings give less freedom in the iteration to deviate from the initial precursor composition estimate. The constraints allow the user to incorporate knowledge of the chemical compositions of the precursor materials to identify geochemically reasonable estimates [4].

As the model iterates, the compositional information from each SEM/EDS data point is used in an attempt to converge on a compositional model that is representative of the dataset with minimal residual data. The result is a set of compositions that either match closely to the original guess, or some precursors match while others will show major deviations. The process must be repeated with different initializations in order to converge on a well-modeled solution. In each model, there is a resulting q-residual which accounts for compositional information not encompassed in the resulting model. The result essentially tells the user how accurate the initial estimation was, and provides insight into what compositions were unaccounted for in the initial guess. This process is best understood when applied to a problem as shown in the methodology of Chapter 3.

III. Methodology

3.1. Sample Selection and Preparation

The samples used in this research originated from a historical plutonium nuclear test in the 1950s-60s timeframe. A team from LLNL collected large quantities of debris from the test site near ground zero. The debris was then sifted through sieves of differing mesh sizes to separate the samples by size. For this research, specific particles were chosen from the gathered samples to best represent different morphologies present as well as observed textures. Figure 21 shows examples of the particles prior to mounting and selection. This research examined 140 total particles selected from debris collections as shown in Table 1.

Table 1. Fallout sample breakdown for this research. Sample size and shape are indicated.

Number of Samples	**Sample Size**	**Sample Shape**
50	1/2 mm	symmetric
63	1-2mm	symmetric
4	2-3 mm	symmetric
7	3-4 mm	symmetric
14	3-4 mm	irregular
2	4-5 cm	ground glass/ irregular
140		

Figure 21. Examples of fallout particles prior to mounting and polishing.

Three criteria were used to select samples. First, the particles were gathered and separated by size group using the aforementioned sieves. Next, particles of glassy appearance were separated from the collection. Then, the activity of some samples was measured using an alpha or beta particle counter to confirm radioactivity. This research also used previously mounted particles as well as newly mounted irregular shapes and ground glass particles. The above criteria provided confidence that the particles examined are debris from fireball mixing and condensation.

Once the particles were selected, LLNL scientists mounted the samples using various methods including placing the samples into holes drilled into aluminum or stainless-steel pucks, and securing them with epoxy. The largest samples were mounted directly into epoxy. The particles were then polished down to reveal a smooth surface

cross-section for each sample by grinding with corundum polishing paper and finishing with a 0.25-micron diamond paste.

Some samples were mounted individually, and then placed in putty on observation slides for easier analysis. Figure 22 shows a compilation of every sample used in this research. Each set was mounted at a different time, and the letters DW is an unclassified designation for the specific historical nuclear test. The following numbers indicate the sieve grid fineness and distance from ground zero. These aspects are not examined in this research. Additionally, SL refers to the disc slides, Bullets refer to the stainless-steel cylinder mounts, and M1 and M2 refer to mounts 1 and 2 from the same set.

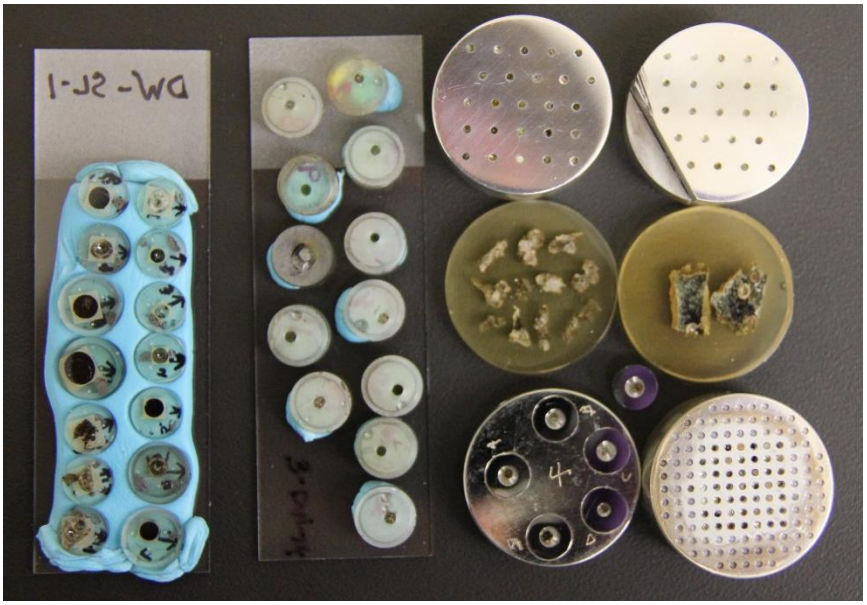

Figure 22. Optical image of all 140 mounted samples considered in this research. From left to right, top to bottom, each sample is grouped as: DW-SL-1, 3-DW-14 (no chemical data collected), 1-DW-14-M1, 1-DW-14-M2, DW-IRR, DW-GG, DW-Bullets and 1-DW-25.

Figure 23 shows an up-close example of the half millimeter sample mounting and how the samples are oriented to aid in identification throughout the analysis. Each mounting was documented and aligned for proper orientation in the SEM as well as

alignment with autoradiography images. Samples were each given a specific designation for documenting results.

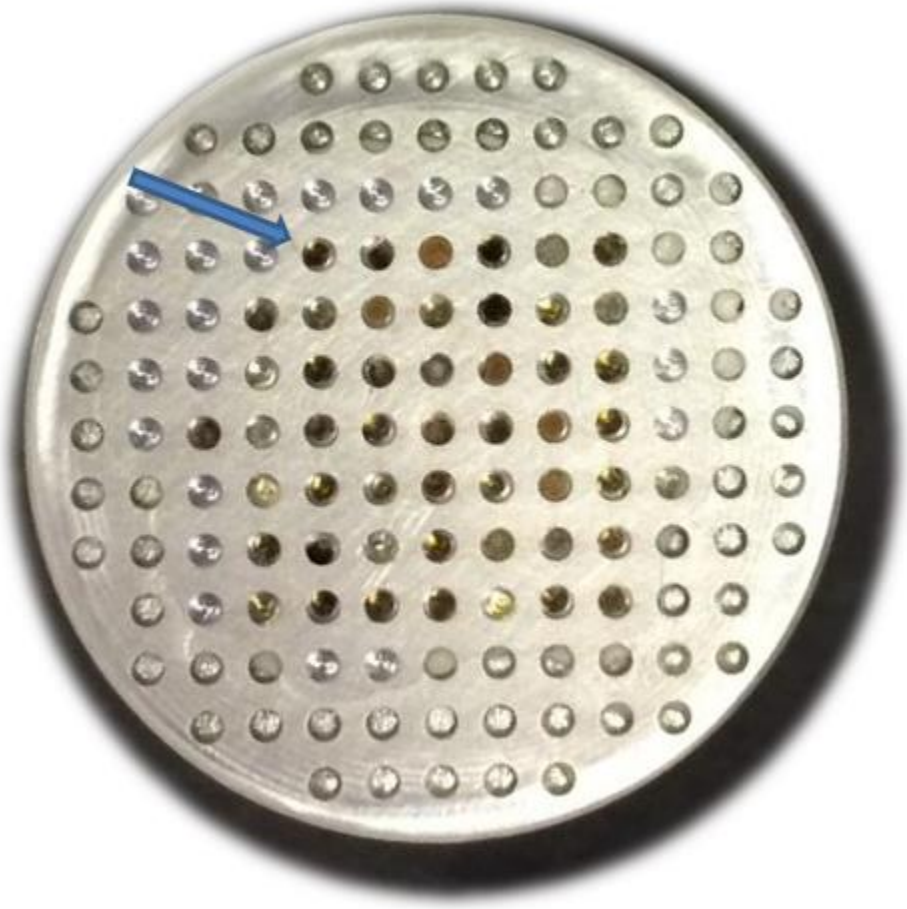

Figure 23. 1-DW-25 half-millimeter samples mounted in an aluminum puck. Note the offset of some samples to aid in autoradiography matching [9].

Optical microscopy was conducted on all 140 samples in order to identify surface features, cracks and defects. Many samples contain defects including cavities and cracks. These images were used to aid in removing data points which were gathered from these irregular locations on the samples. The irregular features are also used to orient the autoradiography images with visual anomalies on the sample surfaces.

3.2. Autoradiography

Autoradiography was conducted on the entire sample set shown in Figure 22. We started by first documenting the orientation of all of the samples. A small, roughly 0.5 square-meter base, light-shielding tent was used to prevent photons from washing out the film during capture. The samples were placed face-down in direct contact with the film in the same configuration as shown in Figure 22 on a standard autoradiography film cassette in a dark room. The tent was closed and all samples were imaged simultaneously for 18 hours. The simultaneous imaging of the samples allows for a relative comparison in pixel darkness in the image. This provides a way in which the precursors found using MCR-ALS can be correlated with radioactivity. The direct contact also eliminates attenuation of the alpha and beta particles as no medium is between the source and the film.

Upon completion, using the working gloves attached to the tent, a protective shield was placed over the film prior to removal from the tent. The samples were then placed aside and the film was taken to the Typhon FLA 7000 digital scanner for processing (Figure 24).

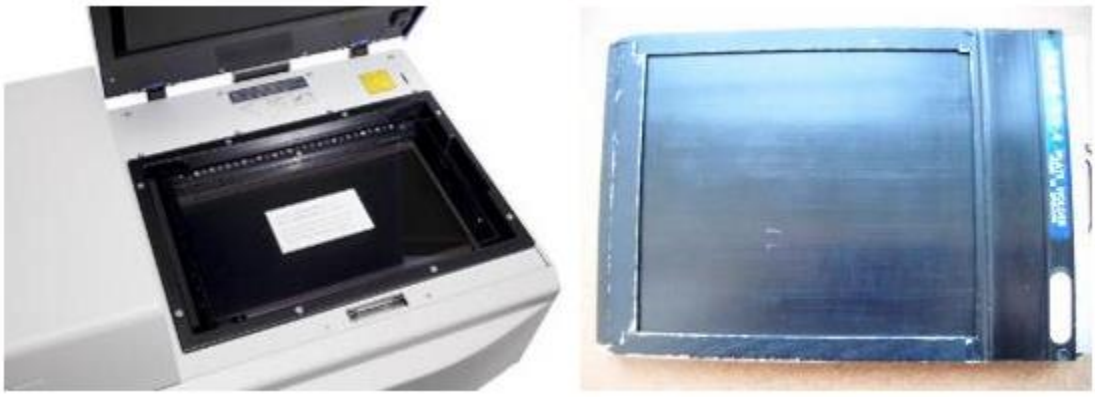

Figure 24. Typhoon scanner and standard film cassette used for the autoradiography.

The film was imaged using the settings in Table 2. The settings were based on previous research and calibration curves provided by LLNL. The autoradiography image was then labelled to appropriately indicate each sample location relative to the optical image shown in Figure 22. The final autoradiography is shown in Figure 25.

Table 2. Typhoon FLA 7000 digital scanner settings used to process the autoradiography image.

Setting options	**Value**
Photo Multiplier Tube	626 Volts
Pixel Size	25 microns
Laser Wavelength	650 nm

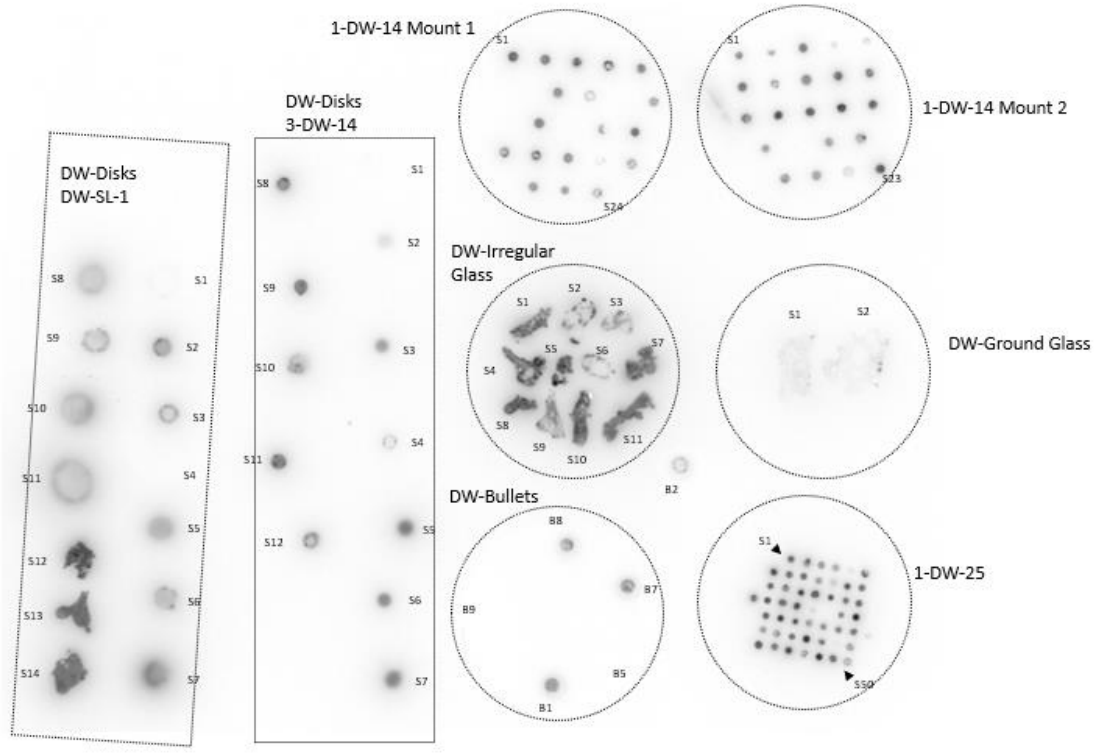

Figure 25. Full autoradiography image of samples for this research [37].

3.3. Scanning Electron Microscopy

Scanning electron microscopy was conducted at LLNL using a FEI Inspect Model F SEM and detector. Each sample mount was placed in the SEM individually for data collection. All mounts were coated with conductive carbon to prevent charge buildup as the electrons impact the sample. This was done by LLNL scientists as a standard SEM sample preparation procedure. Each sample was electrically grounded using either conductive carbon tape or a copper prong in order to further prevent charge buildup. The samples mounted in putty were removed from the putty and placed in the SEM individually. Due to time constraints, and issues with the mountings of the 3-DW-14 sample set, no SEM/EDS data was collected for the 3-DW-14 samples and 5 of the 14 DW-SL-1 sample. The final SEM/EDS data contains data from 123 samples from the same test.

BSE and SE images were taken of each sample to provide detailed, high resolution images which can be aligned with autoradiography. These images were used in classifying the samples as homogeneous or heterogeneous. If a sample contains a visual texture that appears to be diverse and full of inclusions, the sample was classified as heterogeneous. If the sample had a smooth uniform texture, it was homogeneous. A rarer classification was porous. These samples contained a unique web-like texture. These classifications are shown in Figure 26.

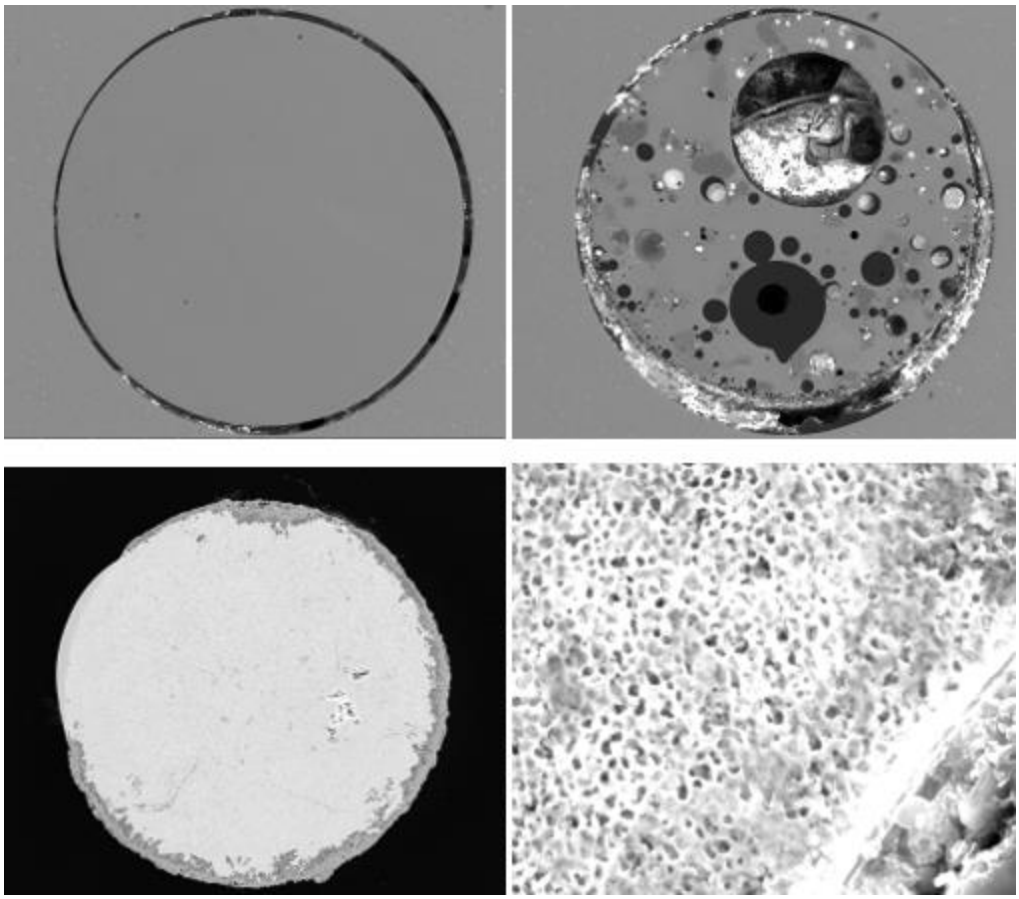

Figure 26. Sample classification examples. Homogeneous (top left), heterogeneous (top right), and porous (bottom left). Also shown is a zoomed in image of the porous texture (bottom right).

For each sample, EDS data was collected using a raster tile method. The SEM was magnified to 300x and a grid of tiles was set up to gather elemental data from specific locations. Each tile contained 16 points called rasters which are 10 by 10-micron squares. This method gathers the average elemental composition across the square raster. That is to say, the average elemental mass fraction for each of ten oxide elements is contained in one raster. These elements include: aluminum, calcium, iron, potassium, magnesium, manganese, sodium, oxygen, silicon, and titanium. Of the 123 samples analyzed, there were various sizes and shapes as mentioned previously. This required a lengthy effort to

cover the entire sample with tiles using the SEM software to appropriately gather EDS data from the entire sample. Figure 27 gives an example of the how tiles were manually aligned over a sample surface.

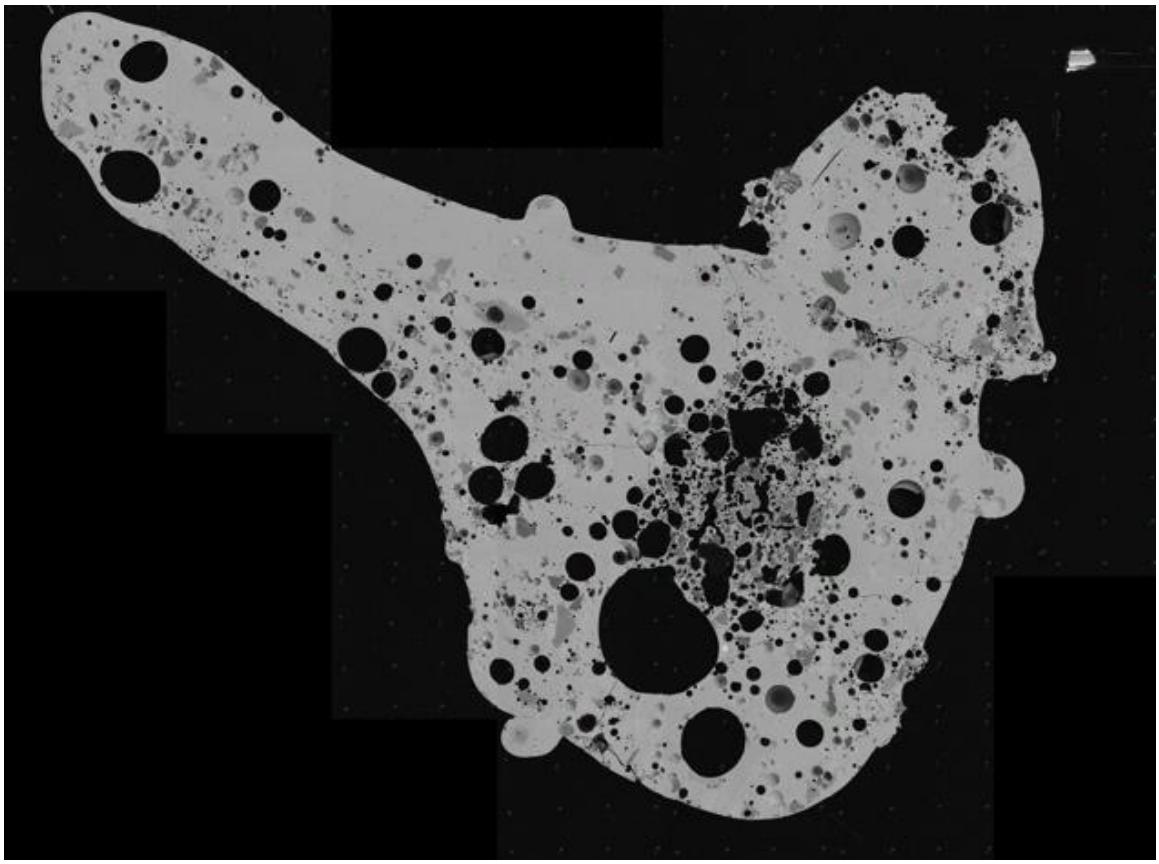

Figure 27. SEM mosaic image of an irregular sample, approximately 3 mm in length. Tiles are shown pieced together to create a full image.

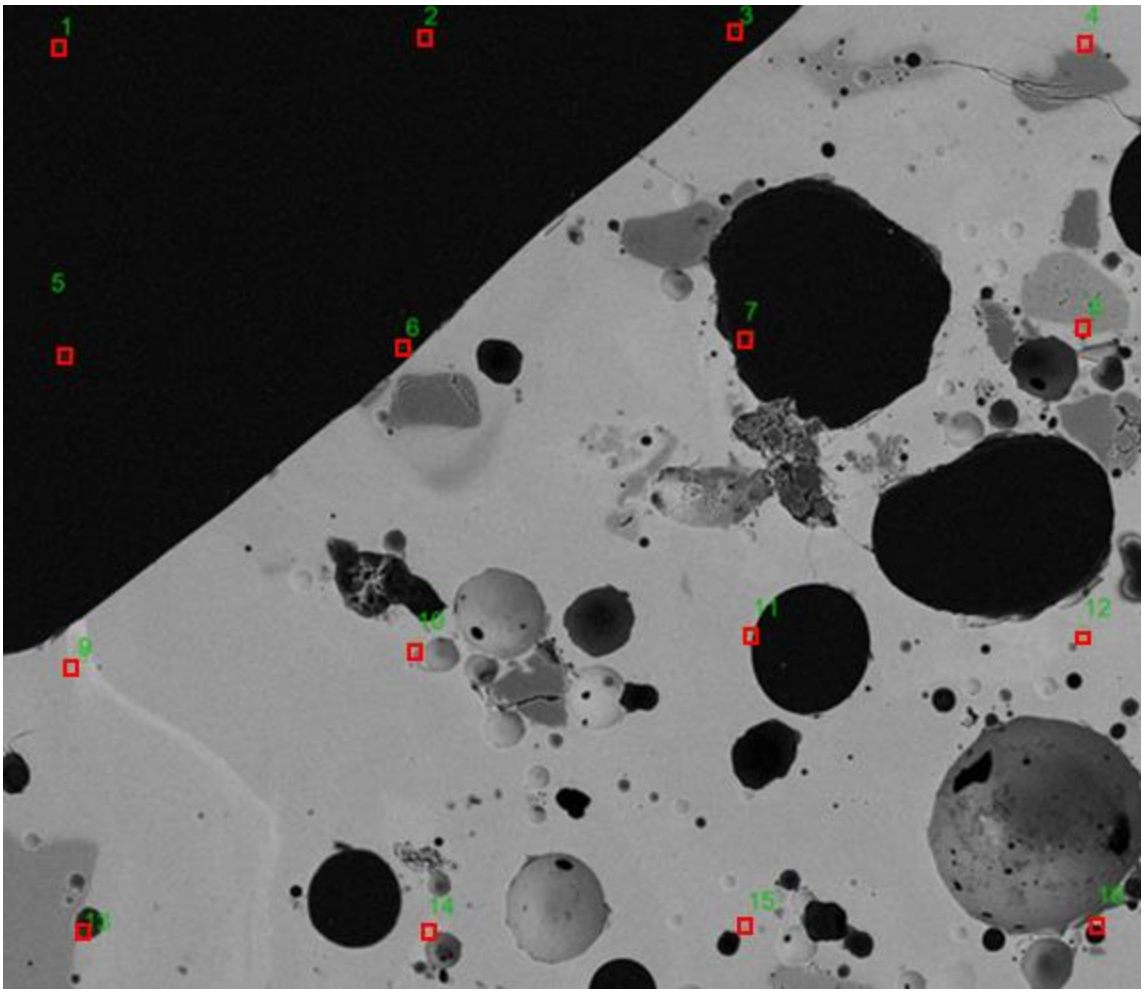

Figure 28. SEM image of a single tile from the same sample as Figure 27. Rasters are shown as red squares across the sample.

Using this method, data was gathered at every point in the grid shown in Figure 28. Many data points were removed from the data compilation because they were located on epoxy or some other anomaly on the sample surface. Further discussion of how the data was refined after collection is in the following section. The size of the tiles remained consistent with each sample. Therefore, smaller samples such as the half-millimeter samples fit entirely within one tile, whereas some irregular large samples were covered by 50-60 tiles. While this naturally produces more data originating from large sample pieces,

by maintaining the same sampling density for all samples, we ensure that the number of measurements is proportional to the size of the object. Therefore, the data as a whole will still statistically encompass the elemental composition of each sample enough to determine variation and conduct statistical analysis.

The settings for SEM/EDS data collection were selected based on previous study. There was a 30 second live time used for each raster, with 16 rasters per tile. Rasters were 10 by 10 micron in size. Acceleration voltage was 15 keV, the image resolution was 1600 by 1600 pixels.

3.4. Principal Component Analysis

Before performing PCA on the data, data points that fell on epoxy, the sample holder or surface defects were eliminated. Of the 140 original samples, only 123 were examined using SEM/EDS due to time constraints. The samples without data include samples 3-DW-14 and samples (1, 6, 7, 8, and 14) from DW-SL-1 as annotated in Figure 25. The total number of data points from the 123 samples include 12,257 total rasters. Blanket criteria were used to eliminate poor quality data. All points with a sum total (elemental mass fraction) below 95% and above 105% were removed. Next, all points with oxygen over 60% (from epoxy) and/or aluminum (from the holder) over 40% were removed. Following this initial culling, the data was evaluated by PCA using the Eigenvector software [38]. Using the generated PC1 vs PC2 plot, outliers were examined individually by tracing back to the raster tile image. If the outlier was on a surface defect or other unfavorable location, the point was removed. This process removed another 12 data points. The final data point count is 4,893 data points. The result of data collection

was 39.9% usable raster data points. This result is expected using the automated tile and raster grid method. In order to individually gather 4,893 good data points, the collection time would have far exceeded the automated method.

Next, using the data points selected, PCA was performed without oxygen and manganese values from the data. Oxygen contributes very little to the chemical variation in the dataset because it is a major constituent of all samples. Manganese concentrations are typically below the detection limit of the SEM, and therefore its variation is not significant [4]. In the PCA software, the data were categorized by multiple classes in order to view the data from different perspectives. These classes include size, shape, sample name, sample number, and apparent degree of mixing.

The first step in evaluating the PCA is to plot eigenvalues against PC number (Figure 29). Using the eigenvalue plot, a scree test is used to estimate the number of precursors that mixed together in the fireball. A scree test looks at the PC number where there is an apparent inflection in the eigenvalue plot. PC 3 or 5 show this behavior, suggesting that between 4 and 6 distinct endmembers likely exist in the dataset, and therefore 3-5 PCs capture true compositional variance [34].

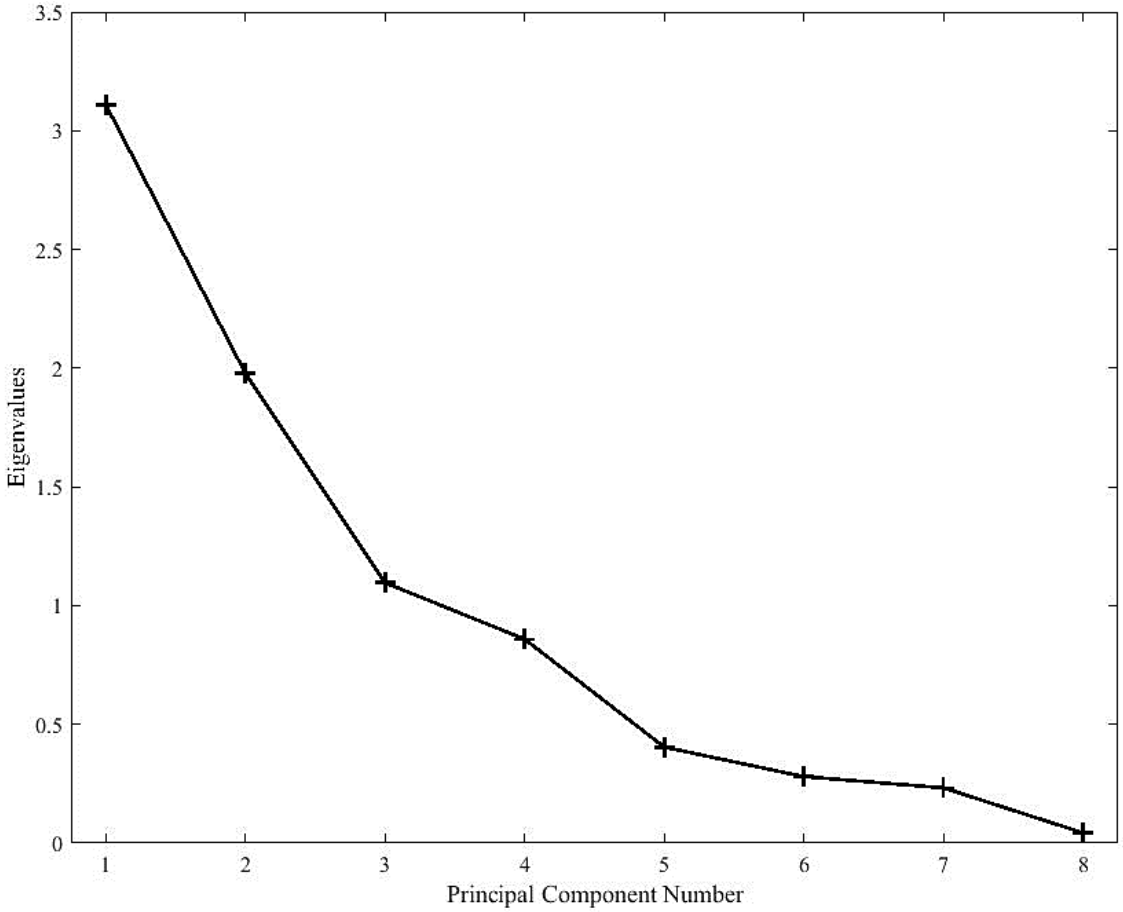

Figure 29. Eigenvalue versus Principal Component Number is plotted. Noticeable inflections are located at PC3 and PC5.

For further examination, the cross-validation approach is used as an alternate method to determine precursor number. This process, discussed in Chapter 2, results in a plot of the root mean squared error of the total (calibration) data set (RMSEC) and the root mean squared error of the calibration validation set (RMSECV). This plot is show below in Figure 30. Using this approach, an estimate of the number of precursors is determined using the point at which the error lines deviate significantly. The plot shows a major deviation at PC3 and PC 5, validating a prediction of 4-6 precursors.

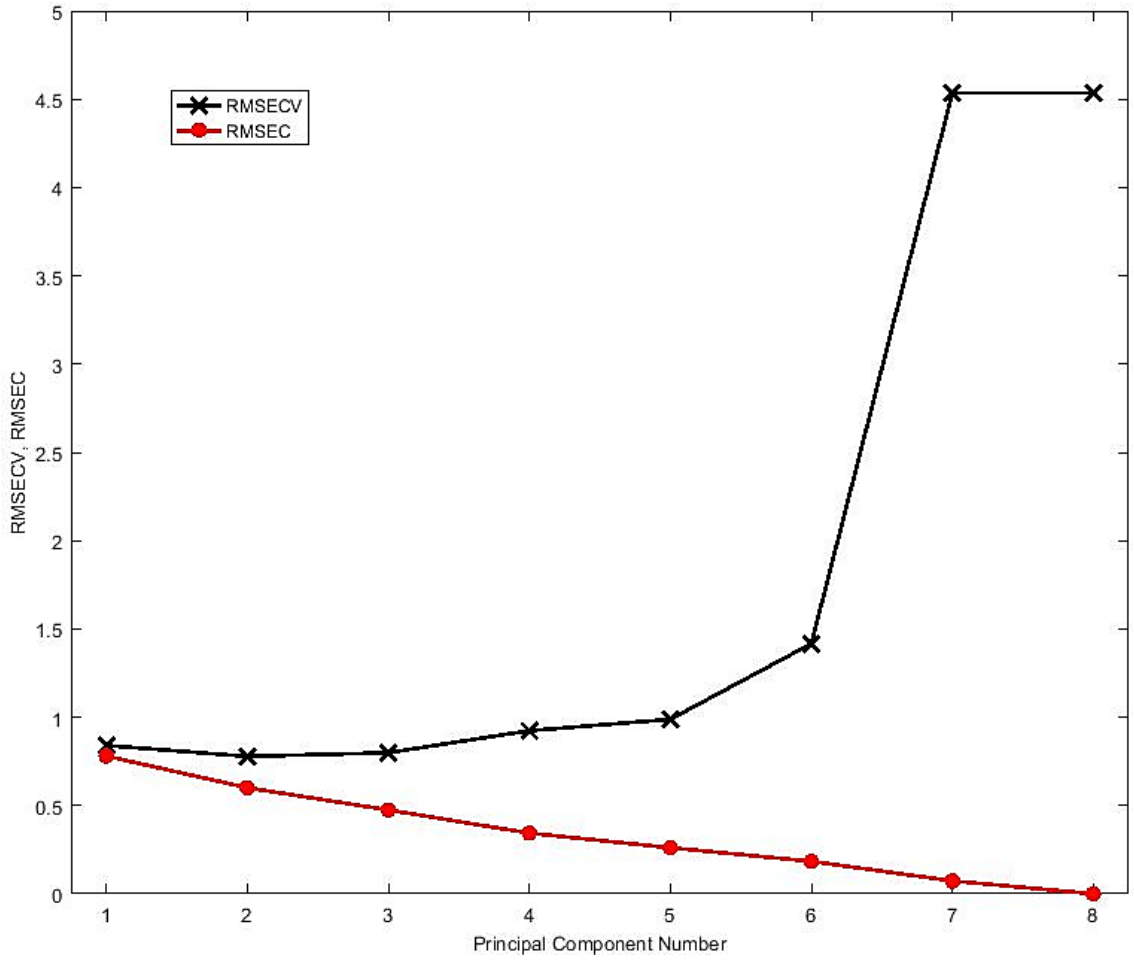

Figure 30. Cross-validation plot displaying RMSEC and RMSECV versus Principal Component Number.

Zooming in on the cross-validation plot (Figure 31), there is a distinct inflection at PC 3 and 5, again suggesting a between 4 and 6 precursors.

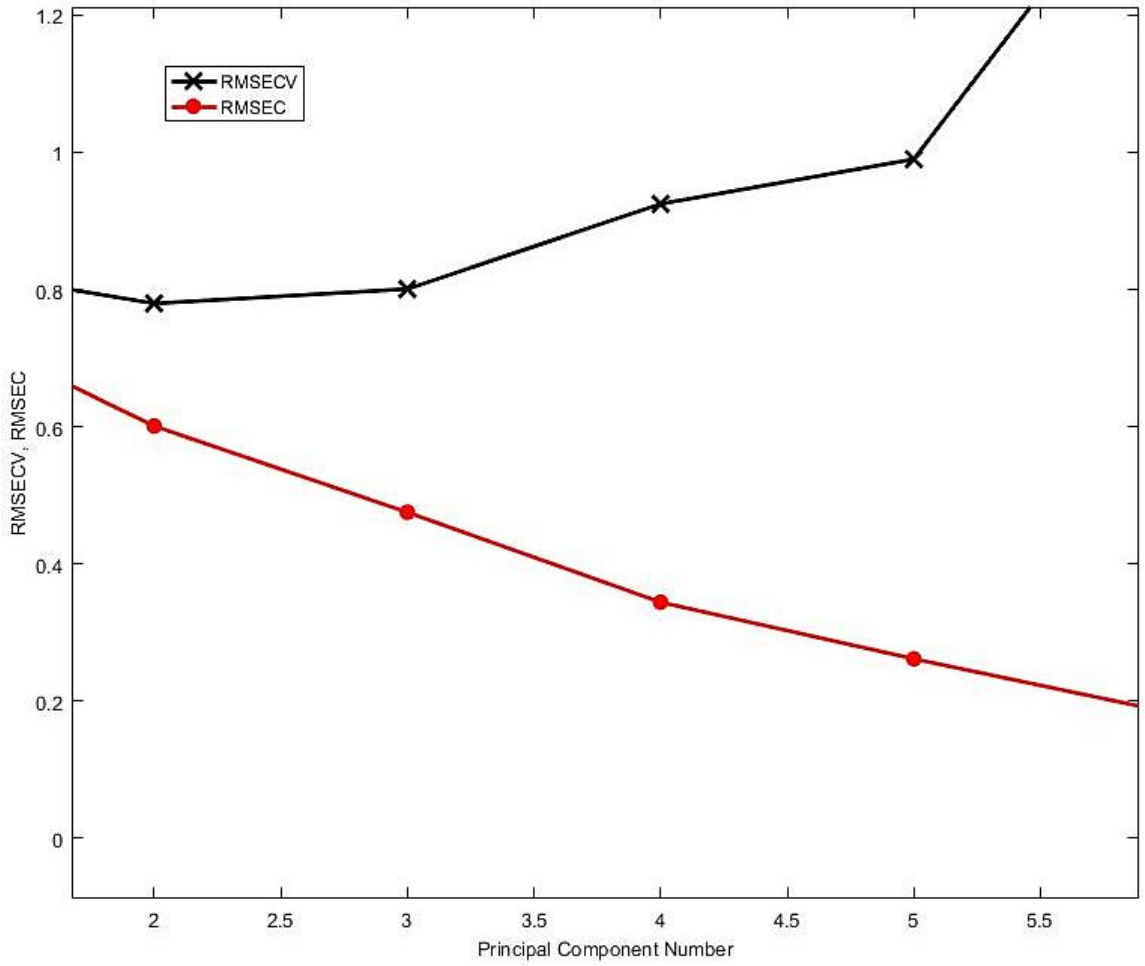

Figure 31. Zoomed-in Cross-validation plot displaying RMSEC and RMSECV versus Principal Component Number. The deviation of the lines at PC3 and PC5 can be seen clearly.

Following these tests, the number of significant principal components is determined to be between 3 and 5. Using 3, 4 or 5 principal components, a different amount of variation information is captured as shown in Table 4.

Table 3. Variance captured by each principal component in this model.

Principal Component	% Variance	% Cumulative Variance
1	39.06	39.06
2	24.84	63.9
3	13.54	77.44
4	10.74	88.18
5	5	93.18
6	3.44	96.62
7	2.84	99.47
8	0.53	100

The captured variation is plotted in Figure 32 showing the cumulative variance vs. PC number. Using all PCs (8) would capture 100% of the variance, but this would capture variation which is not significant to the fallout elemental composition. Every measurement using the SEM will have some degree of error and noise due to machine limitations and human error. The scree test and cross-validation applied previously allows us to confidently assume that the variation captured by PCs greater than our estimate (3-5 PCs) is variation not representative of fallout properties [34].

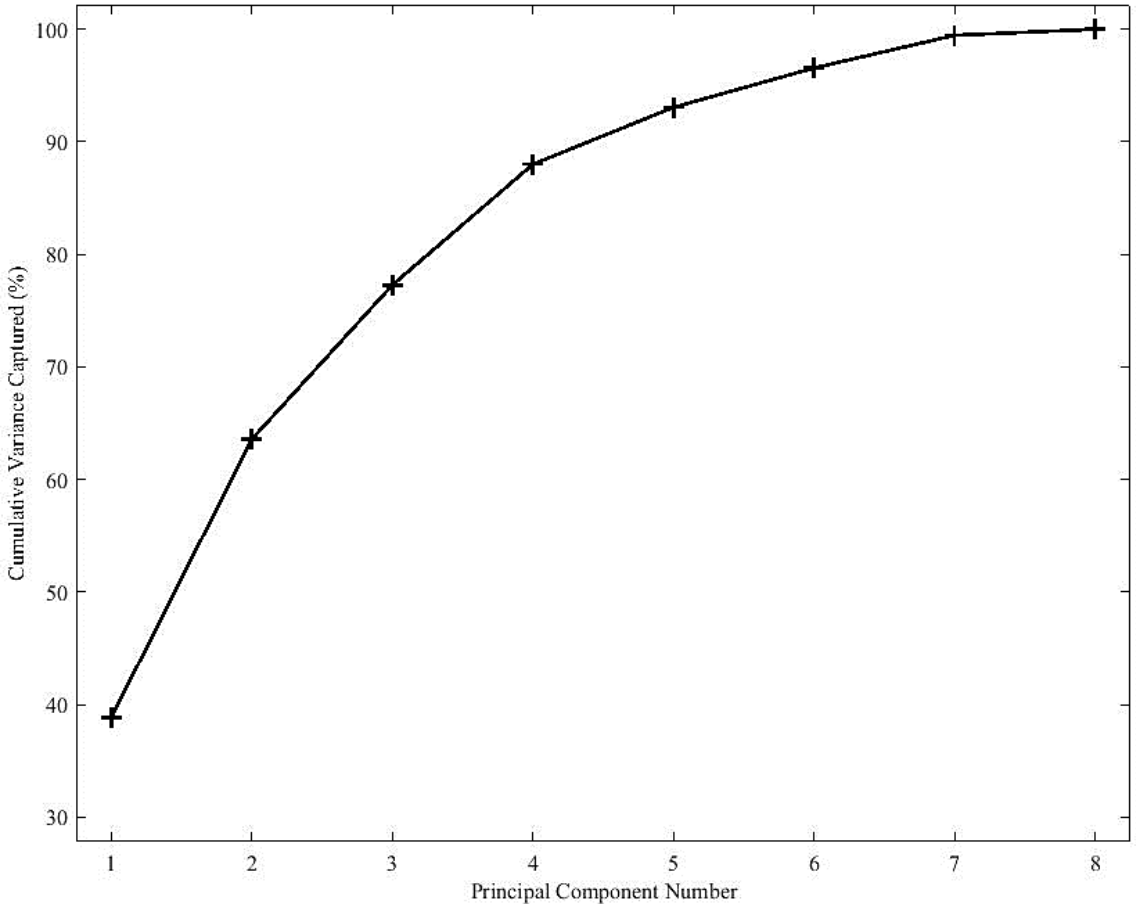

Figure 32. Cumulative variance captured as the number of PCs used in the model is increased.

Once the number of precursors is estimated, an initial chemical composition of each precursor must be defined for the MCR-ALS analysis. This process is done using the MATLAB software data highlighting tool and examining the PC plots of various combinations from PC1 through PC5. Data point clusters are highlighted, and the highlighted sample points' compositional information is plotted. This provides a framework from which initial mineral precursor estimates can be derived. The estimates are discussed in Chapter 4. Further analysis using MCR-ALS allows for a final estimation of precursor number and significant PCs. The process of this decision is iterative. The aforementioned tests provide a guideline for a reasonable initial estimate. Different

estimates initialized in MCR-ALS will fall within the guideline based on these findings. Estimates can also be guided using previous research such as soil geological surveys and previous research which examined soil composition. The resulting estimate should be geochemically sensible.

3.5. Multivariate Curve Resolution – Alternating Least Squares

Once the number and chemical composition of the precursors are estimated, the valid compositional data from the rasters is input into the program with the initial guess. This is illustrated in Chapter 2 in the Theory section. The iterative process runs using weighting provided by the user. These weighting are entered into the MATLAB code as values from 0 to infinity. The larger the number, the stricter the code will be when converging on a solution for that particular precursor.

The output provides a solution that best fits the compositional data as well as the contribution of the mixtures for each data point. The reasonableness of the guess is determined by observing how well the final model matches the initial estimate. For example, in this study, quartz matched very well in all applications of MCR-ALS. However, different other combinations of minerals were attempted in the estimate in order to find a solution that fit the data well. Once a final model is built, the precursors are examined in the sample data specifically.

3.6. Spatially Aligning Precursors and Autoradiography

Precursor compositions can be plotted in PCA space using the loadings for each variable in PCA. Those rasters which cluster near the precursor composition can be viewed in various PC combinations. By then examining the specific sample, tile and raster numbers

where the data point originated, the point can be visually found on the BSE image from the SEM analysis. Using this image, the autoradiography image can then be aligned visually with the BSE image to examine how dark the autoradiography is for that precursor on each particular sample. The process is tedious for larger samples as the tiles are small compared to the entire mosaic tile compilation and the autoradiography can be distorted and blurred. For this reason, a scale of relative darkness was used to qualitatively describe the level of radioactivity at each examined data point. This scale includes: None, Low, Medium, High and Very High. Other sample characteristics can also be documented at this stage, and this allows for further conclusions about fallout formation. Specifically, how minerals mix with unspent fuel, and additionally, how the shape, size, and degree of mixing impact how that mixing occurred. The results are discussed in Chapter 4 along with the complete procedure utilizing the described methodology.

IV. Results

Principal component analysis and multivariate curve resolution-alternating least squares was performed on elemental composition data collected from the surface of 123 nuclear fallout samples. All samples originated from a historical nuclear test referred to as DW for the purposed of this research. Compositional data was obtained through X-ray Energy Dispersive Spectroscopy raster sample data collection. Chemical variation within the sample set was used to derive mineral precursors (i.e. compounds existing in the environment prior to the nuclear event) within the fallout samples. The mineral precursors were estimated and iteratively refined using MCR-ALS, to ensure the precursor estimates capture as much chemical variation as possible in the data set. Using these precursors, the location of precursors within the samples are spatially aligned with autoradiography images in order to determine if specific precursors are correlated with high radioactivity.

Three different precursor estimates were made and input into the MCR-ALS program. The final, and best fitting estimate resulted in a model of five precursors. These precursors were plotted in principal component space, and rasters which exhibit similar compositional characteristics were co-located in PC space. Five rasters were chosen for each precursor and traced back to the SEM image along with associated characteristics and autoradiography. It was discovered that feldspar showed signs of being co-located with high radioactivity areas, and quartz was anticorrelated with radioactivity.

Further analysis of bulk data suggests that large, homogeneous, spherical symmetric samples encompass the most variation in compositional data, and contain most of the activity.

4.1. EDS Compositional Data Modeling: PCA

EDS was conducted on 123 samples using the raster method described in Chapter 3. The resulting 12,257 rasters were then modeled using the principal component analysis on the Eigenvector software in MATLAB [38]. The dataset was filtered as described in Chapter 3, resulting in 4,893 rasters and analysis was performed using various combinations of principal components and sample class perspectives. After data refinement, each raster data point consists of 8 elemental composition mass fractions. The initial PC1 versus PC2 plots encompass 63.9% of the chemical variation. This makes this plot the most valuable in determining and extrapolating precursor estimate information.

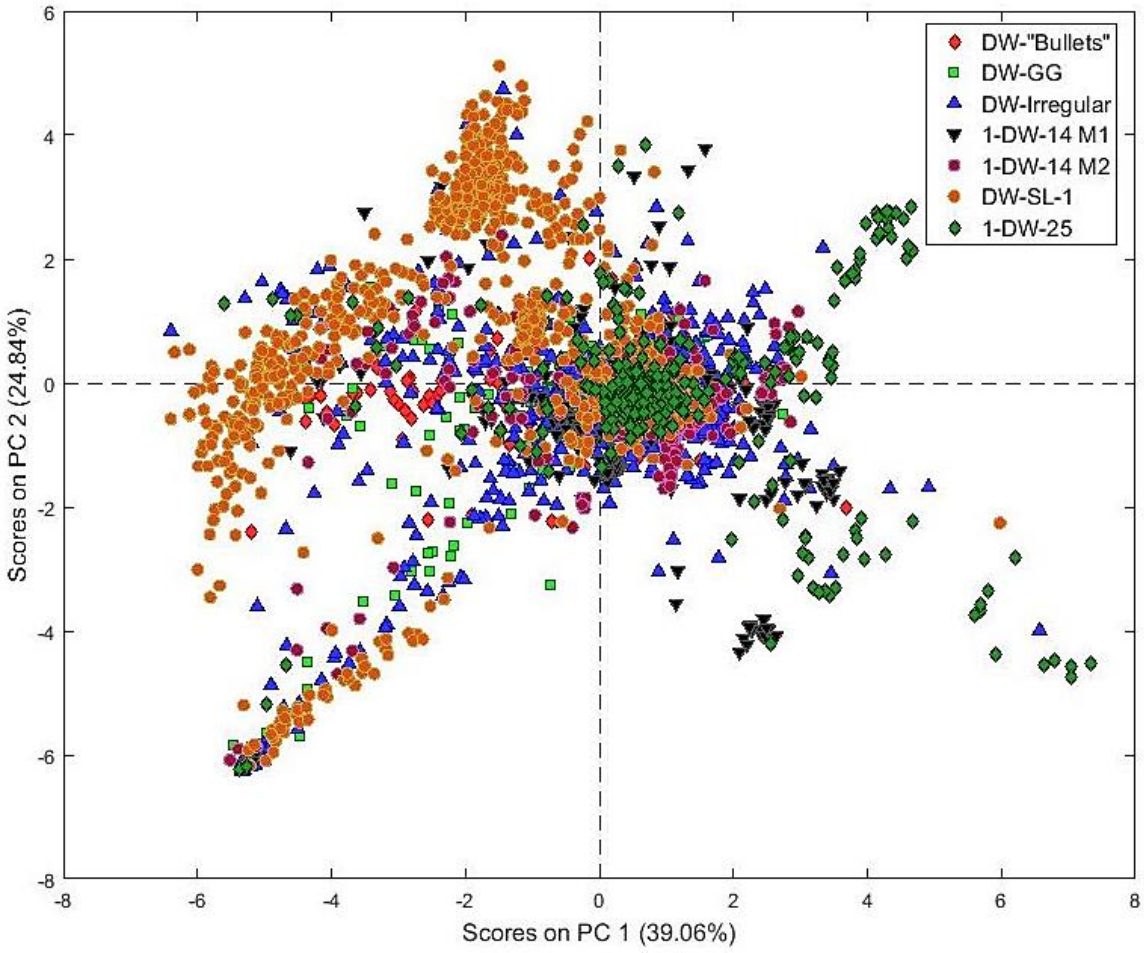

Figure 33. Complete refined DW sample raster data plotted in PC1 vs PC2 space. The data is categorized by sample set.

The initial PCA plot shown in Figure 33 is categorized by specific sample set. Initial observations show that the DW-SL-1 (Refer to Figure 22 and 25 for sample designations) set of particles encompass a large portion of the variation, as they are further from the center of the PCA plot. In order to make further observations with regard to clusters and sample characteristics, the same PC 1 versus PC2 plot is shown for various categorizations.

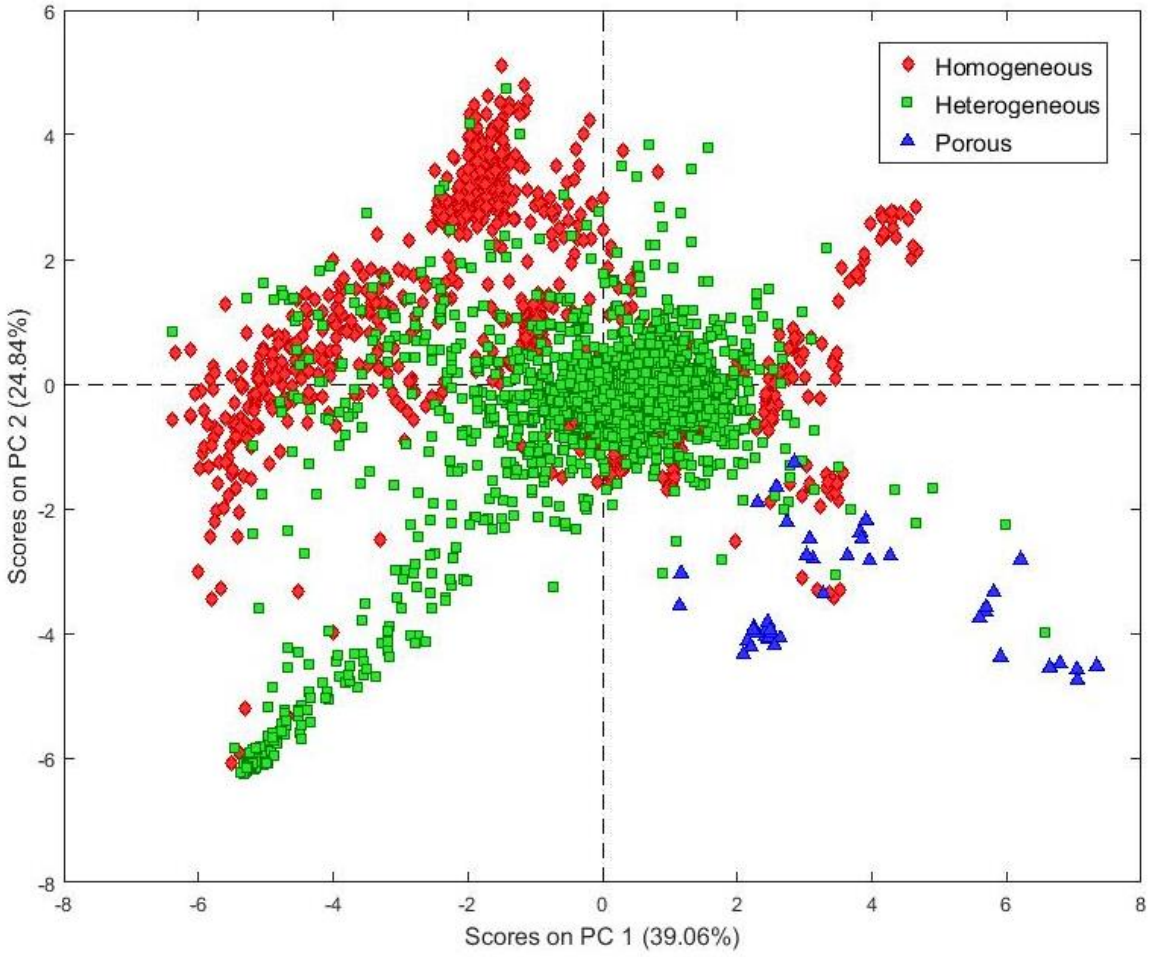

Figure 34. Complete refined DW data plotted in PC1 vs PC2 space. The data is categorized by degree of mixing.

Figure 34 is the same PC1 vs PC2 plot as Figure 33 with sample points categorized by the apparent degree of mixing, namely homogeneous, heterogeneous, and porous. Examples of each are displayed respectively in Figure 35. Initial observations suggest that the radioactivity discussed in the following sections may have a significant correlation with the apparent degree of mixing. The clusters present in this graph reveal that porous samples are significantly different in chemical composition than homogeneous and heterogeneous

samples. However, some samples contribute little to the variation including both homogeneous and heterogeneous samples that gather at the center of the PCA plot.

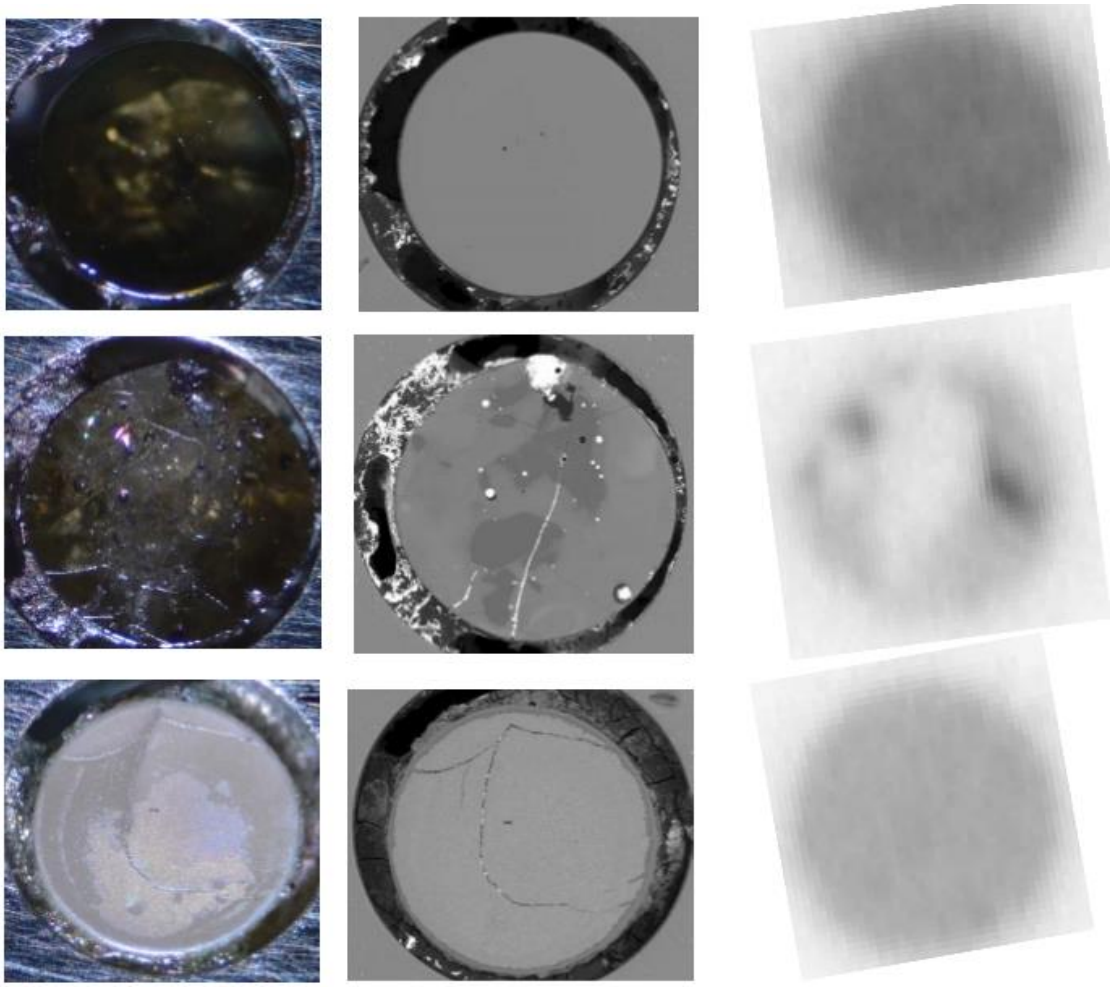

Figure 35. Comparison of homogeneous (top row), heterogeneous (middle row) and porous (bottom row) images. The optical image (left column), the BSE image (middle column) and autoradiography (right column) are shown.

Degree of mixing is not the only factor that is clear in the sample clusters. The plot in Figure 36 categorizes samples by the size. As described in Table 1.

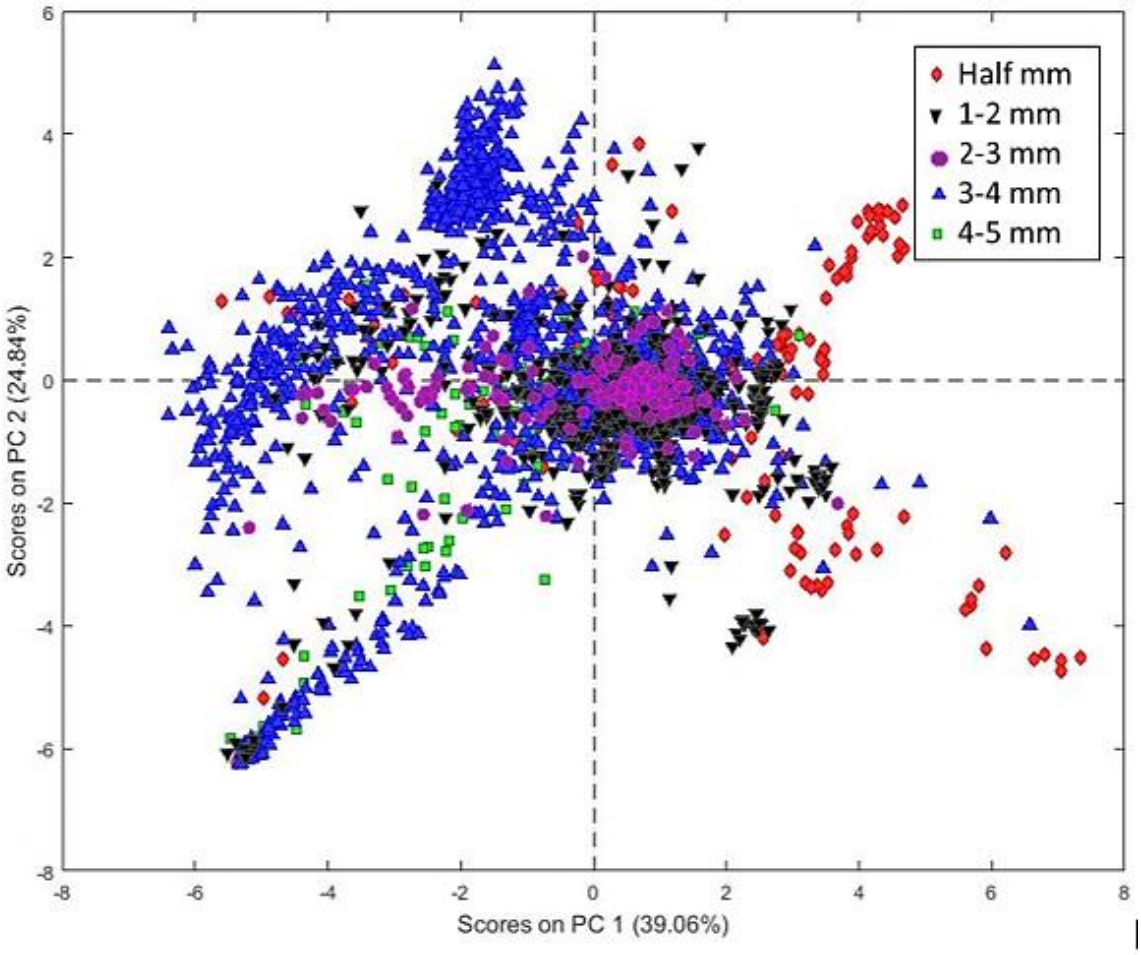

Figure 36. Complete refined DW data plotted in PC1 vs PC2 space. The data is categorized by sample size.

The 3 to 4-millimeter size samples on the left and the half-millimeter samples on the right dominate the variation present in this graph. There are some clusters of 1-2-millimeter samples and random dispersions of others, but there is a clear trend as to which samples contribute to most of the variation. Figure 37 displays yet another perspective, the samples are categorized by shape.

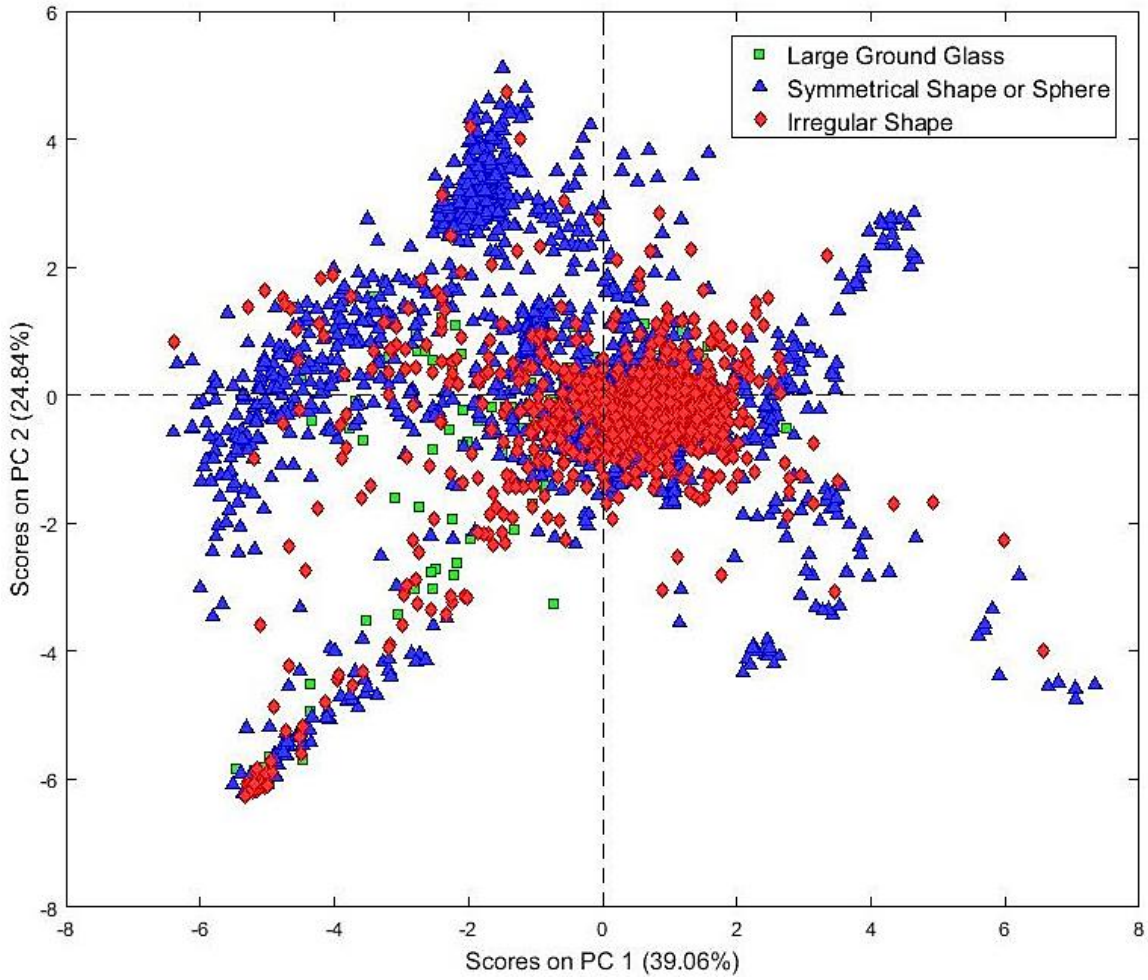

Figure 37. Complete refined DW data plotted in PC1 vs PC2 space. The data is categorized by sample shape.

This plot reveals another characteristic that dominates the chemical variation. The symmetrically shaped fallout glass samples contribute most of the variation in principal component space. There are generally dispersed rasters from other shapes, but it appears as though the variation in the samples comes mostly from the symmetrically shaped fallout glass.

Considering the plots above, the initial observation is that symmetrical samples that are homogeneous and 3-4 millimeter in diameter and symmetrical samples that are porous

and half millimeter in diameter contribute the majority of the elemental variation. Similar plots were made plotting different combinations of PC1 through PC5 in order to determine if other trends were revealed. The observations held in comparisons using all five PCs and their contributions (with five PCs there is a total of 10 different combination plots.).

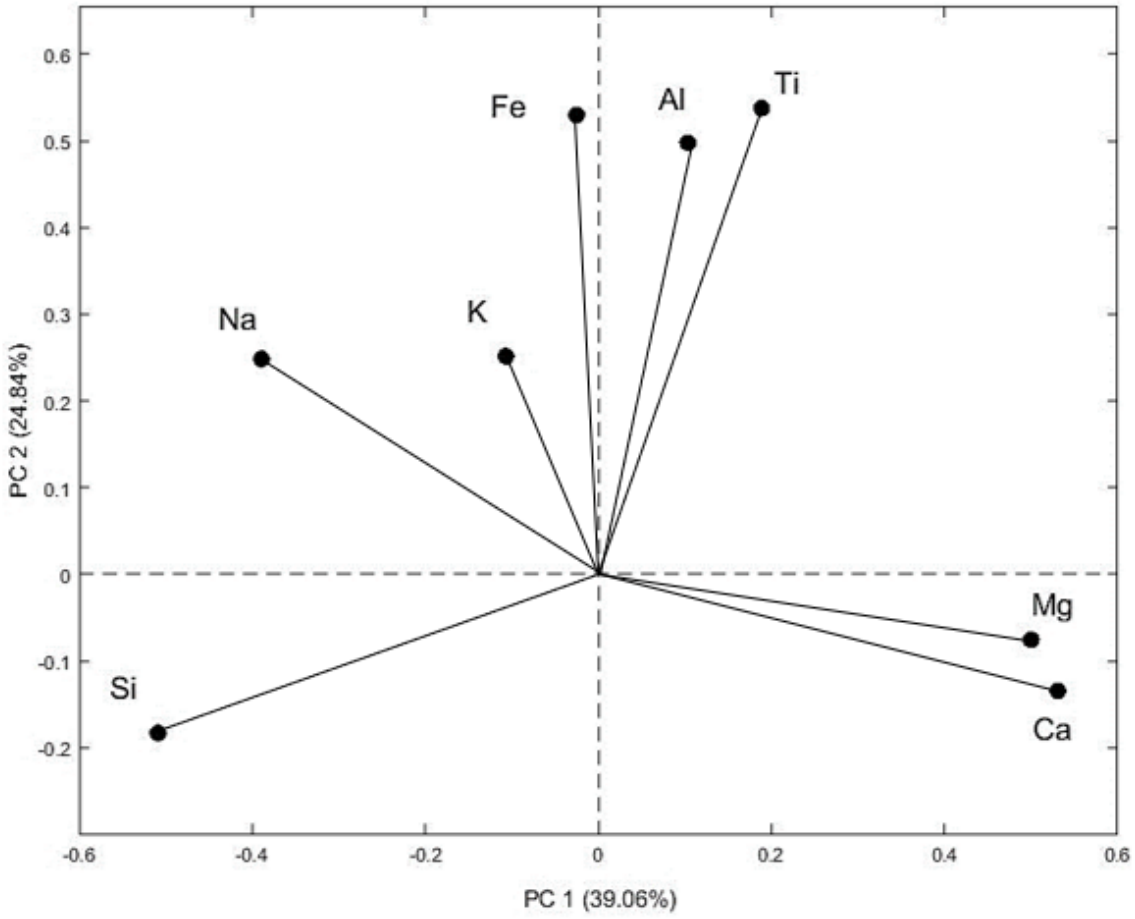

Figure 38. Chemical loadings for each element considered in the DW dataset. The loadings shown are PC1 loadings versus PC2 loadings.

The elemental loadings can be viewed in a similar fashion in order to get an initial understanding of the chemical make-up of the clusters (Figure 38). From the loadings plot, initial observations suggest that clusters appear in the silicon region as well as the calcium

and magnesium regions. By overlaying these loadings onto the PC score plot it becomes clear where clusters reside.

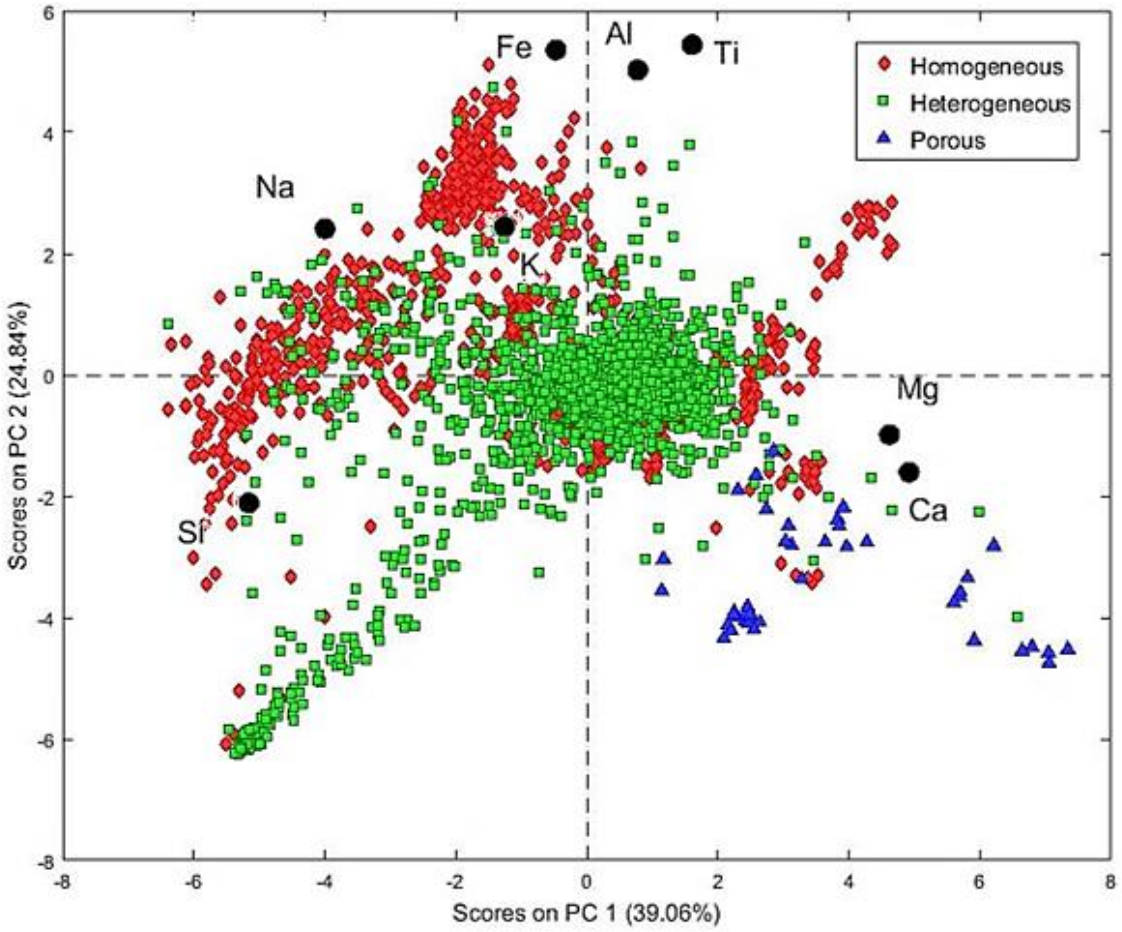

Figure 39. Complete refined DW data plotted in PC1 vs PC2 space. The data is categorized by degree of mixing and includes the chemical loadings overlaid.

Figure 39 reveals that clusters tend towards a combination of each chemical. As a raster point tends toward a chemical loading, this means that this chemical composition may have a higher mass fraction value for that specific raster. Using cluster analysis, the chemical combinations can be observed and utilized to make estimates of what mineral compounds are present in the sample.

Using the eigenvector software, different principal component scores were plotted against one another in order to find cluster trends. Six major clusters were found, all of which are present and visible on the PC1 versus PC 2 score plot. This allows for a simple presentation. Figure 40 shows where the clusters are located on the scores plot. Each cluster was individually highlighted using the eigenvector software. The highlighted clusters consist of individual raster points from the data. The compositional mass fraction data for each of the rasters highlighted is then graphed in order to give a complete compositional picture of the possible precursor described by this cluster.

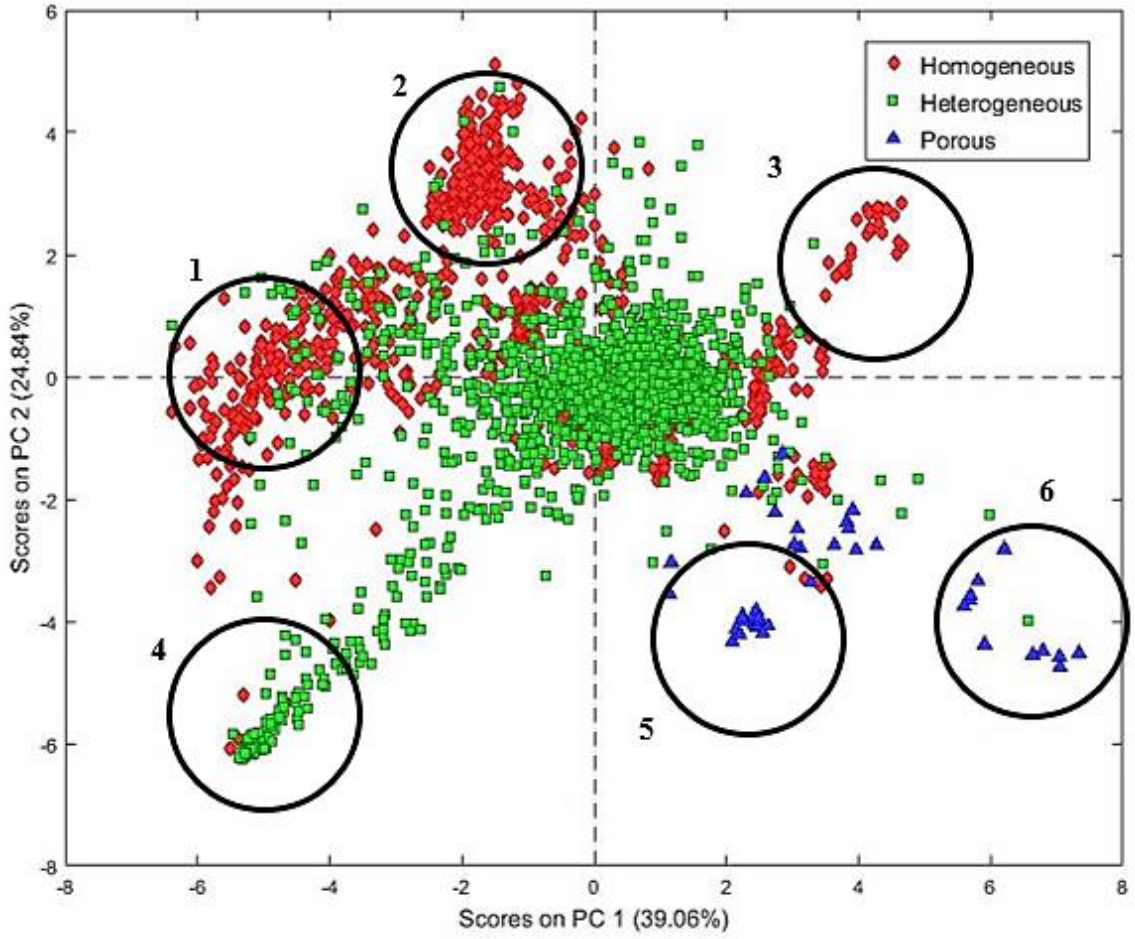

Figure 40. Complete refined DW data plotted in PC1 vs PC2 space. Apparent clusters are encircled.

The cluster compositions shown in Figure 41 provide the baseline for the initial precursor estimates. While other clusters may be present, the highlighted clusters are those which appeared consistently across multiple PC score plot comparisons. Compositions are used to find a close approximation of a precursor mineral for un-mixing in MCR-ALS.

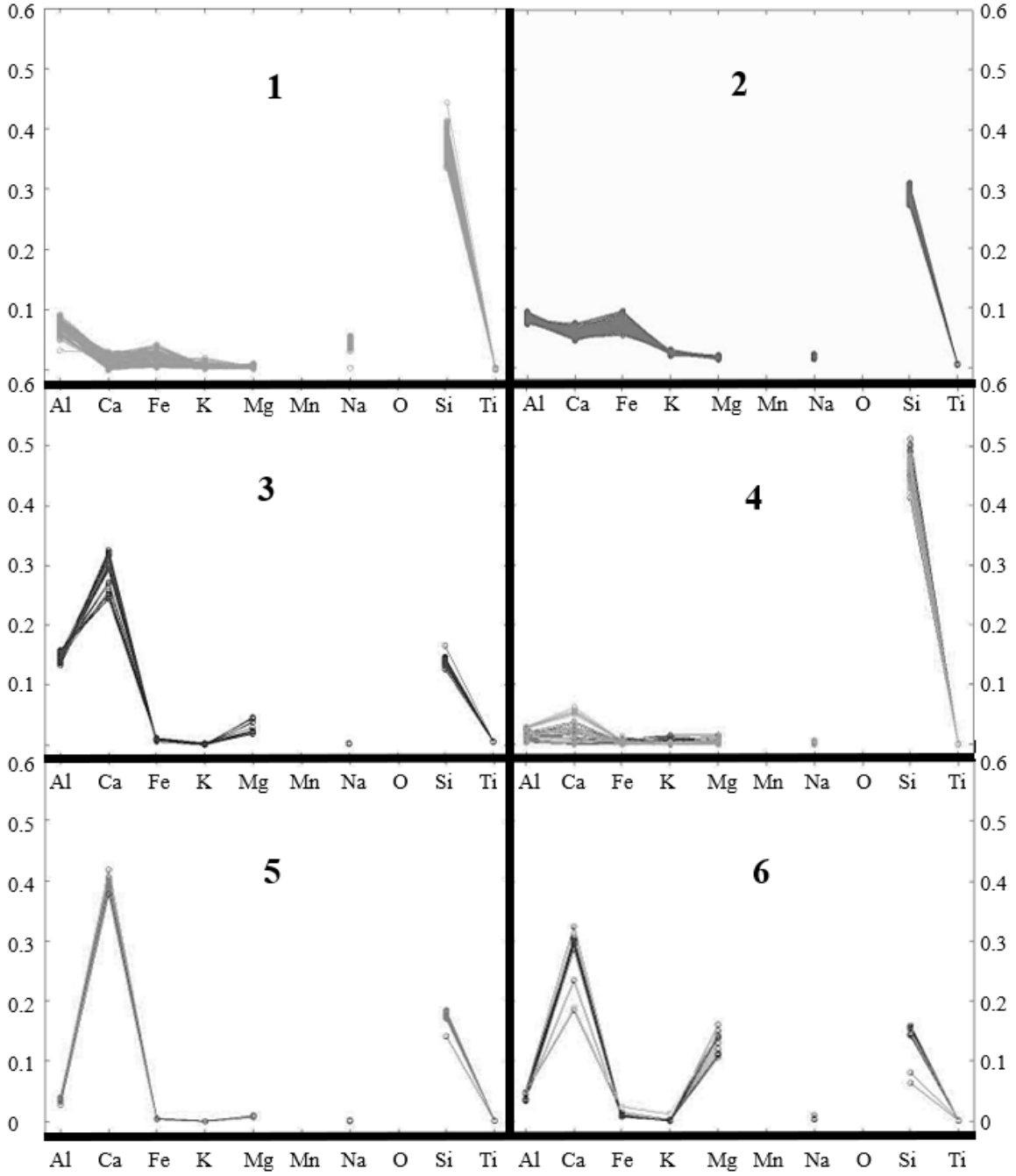

Figure 41. Six initial cluster compositions are shown. Y-axes are mass fraction values for the rasters highlighted. Mn and O are omitted.

4.2. EDS Compositional Data Modeling: MCR-ALS

The compositions resulting from the raster clusters in PCA are used in conjunction with Deer, et. al. [39] and the mineral database on www.webmineral.com in order to find minerals which closely match the compositions found in clusters [39] [40]. The initial precursor estimate is shown in Table 4. As stated in previous chapters, there is error present in the data due to noise in the compositional information. These estimates are used as an initial iteration for the MCR-ALS program to iterate and converge on a set of mineral compositions which can account for a majority of the chemical data from the samples. Final mineral compositions are not deduced until un-mixing occurs using MCR-ALS, and new guesses are made using the resulting mineral estimates from the program.

Table 4. Six initial precursor compositions are shown from direct matching to the highlighted clusters.

Mineral Guess	Al	Ca	Fe	K	Mg	Na	Si	Ti
Erionite-Na	0.0727	0.0016	0.0004	0.0278	0.0016	0.0457	0.2826	0
Clinohomquistite	0.0750	0.0131	0.0513	0.0020	0.0590	0.0130	0.2827	0
Hibschite	0.1266	0.0282	0	0	0	0	0.1317	0
Quartz	0	0	0	0	0	0	0.4674	0
Hillebrandite	0	0.4213	0	0	0	0	0.1476	0
Monticellite	0	0.2561	0	0	0.1553	0	0.1795	0

The minerals above each have a specific origin in nature. Some of these minerals are not common in nature. For example, hibschite is a mineral of magmatic origin found near volcanic sites in nature, whereas quartz is common in soil around the world [40]. Therefore, each of these minerals likely does not exist in these exact compositions within the samples. However, we can begin to discern that minerals which exhibit similar compositions do exist within the samples.

Quartz can reasonably be estimated to exist in large amounts prior to any nuclear event that created these samples. A major assumption of this study is that no significant changes occur to the mineral compositions during fireball evolution and fallout formation. This is a process of current scientific inquiry, and may not be true in all cases. The mineral compounds mix together and condense, but the correlations between elements in the precursors are not modified. Additionally, the elements themselves are assumed to undergo no transmutation through decay or other processes within fireball conditions. As described Chapter 3 methodology, the MCR-ALS method un-mixes the compositional data and converges onto compounds which existed prior to the nuclear event. Depending on how close these resulting compounds are to the initial guess, new estimates may need to be formed in order to ensure all compositional information is accounted for in the model.

For the purposes of an initial estimate, the closest mineral composition that match the PCA clusters are used as a first step toward un-mixing. The following results provide valuable information regarding the true nature of the compositional data, and how the number of precursors and precursor composition estimate may be different. This allows for a re-evaluation of the data cluster composition, and for further consideration as to what types of minerals are likely to exist in the soil based on previous research [4].

The initial precursor estimates in Table 5 are used in the MCR-ALS MATLAB program to develop a refined compositional precursor estimate which takes into account all compositional data in all rasters. The MCR-ALS program is designed to put weightings on each precursor guess individually. For the purposes of this research, each weighting is set to a 0.1 value in order to give the program freedom to adjust if the initial guesses are

off. A higher weighting gives the program less freedom to deviate from that specific precursor existing in the final model. The resulting model is shown in Figure 42.

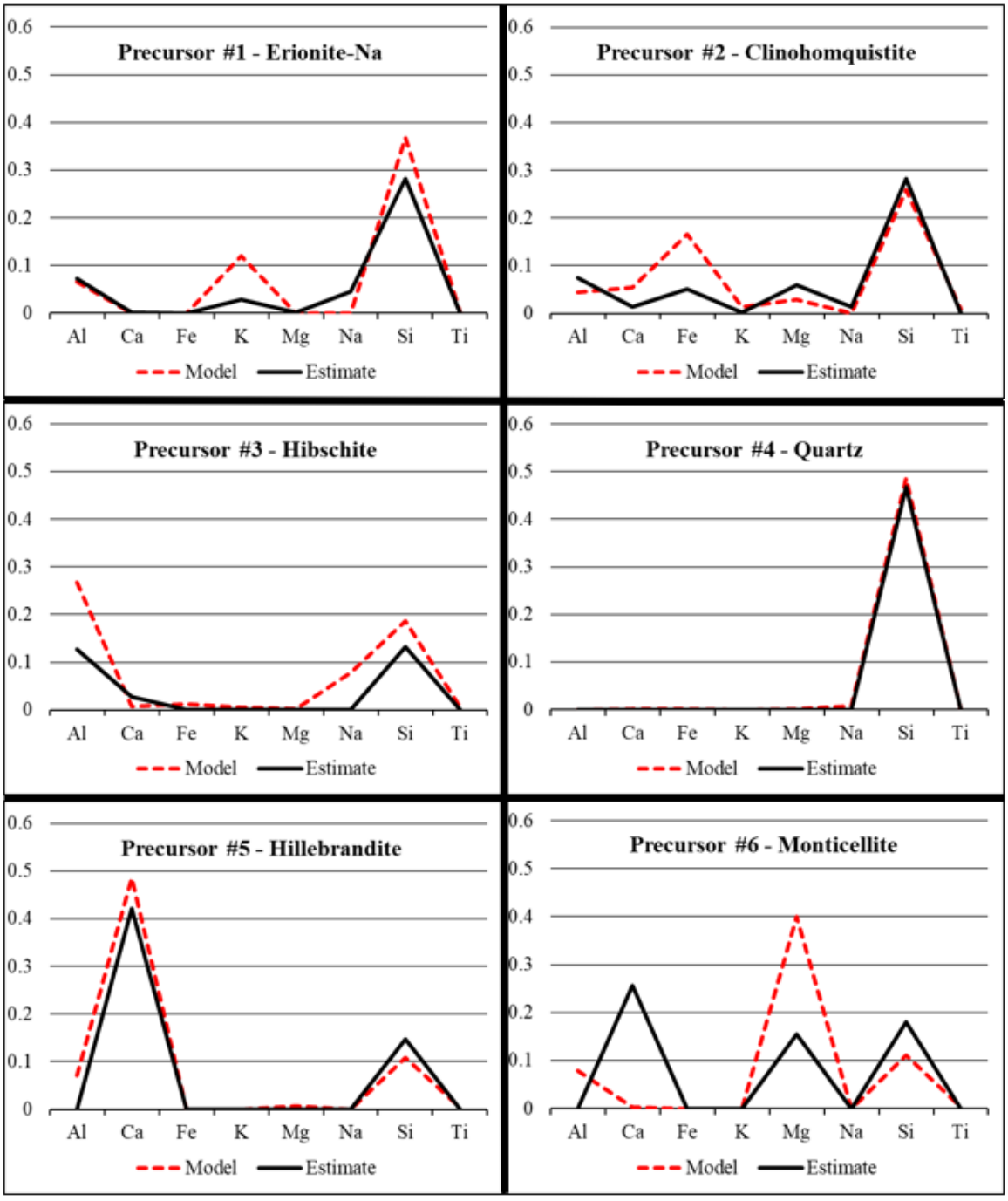

Figure 42. Six initial precursors are modeled using MCR-ALS. The model and initial estimates are plotted above. Y-axes are mass fraction values.

The resulting model accounted for 99.97% of the compositional information in the data, however, the initial estimate is clearly not representative of the complete dataset. The model converged on a result varying greatly from the estimate. The model converged on quartz and hillebrandite especially, accounting for 32.61% and 45.93% of the data respectively. The other precursors, which the model deviated from, present an issue with the initial estimate. It was expected that quartz would converge almost exactly, and this provides confidence that the model is accurately converging on real minerals from the data. Hillebrandite is a mineral that is white and fibrous and occurs in nature near limestone [40]. This calcium silicate could potentially account for a precursor in addition to quartz. However, a new estimate must be built in order to confirm this result.

The other precursors, accounting for only 21.46% of the data combined, show that the compositional estimates made for these precursors may not exist in the data. As mentioned in the theory and methodology, this error could be a result of too many precursors, i.e. one precursor is in effect attempting to utilize compositional information while simultaneously removing data which would be needed to satisfy another precursor estimate. The Q-residuals can be used for insight into missing precursor guesses, or possible error in the estimate. Figure 43 shows the Q-residuals.

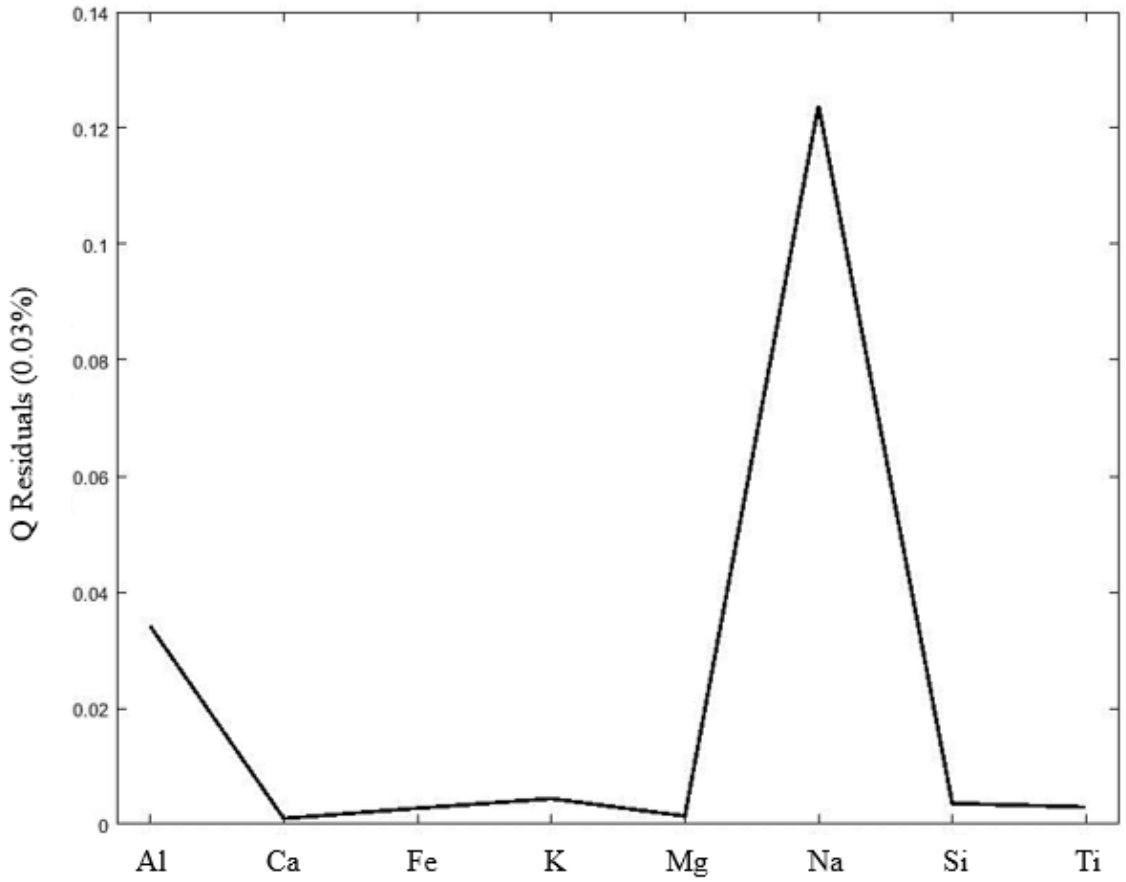

Figure 43. Q-residual values are plotted for the model of six initial precursors. The Y-axis is equivalent to mass fraction values.

It is important to note that the model itself will attempt to converge and encompass as much compositional data as possible. The Q-residual is inversely proportional to the amount of elemental variation that is captured within the model [4]. The Q-residual is highest for aluminum and sodium; however, the mass fraction on the y-axis is much lower than a meaningful value in comparison to the model values. It is desirable to minimize the residuals throughout the estimation process.

In order to build a new estimate, LLNL scientists and soil literature were consulted in order to re-evaluate the clusters found in PCA [39]. The resulting estimate, provided by

LLNL scientist Jennifer Matzel, PhD., is shown in Table 5. Matzel provided these estimates based on previous research and the known geology of the soil near the test site where the fallout was originally formed.

Table 5. Four initial precursor compositions provided by LLNL scientists based on soil geochemistry.

Mineral Guess	Al	Ca	Fe	K	Mg	Na	Si	Ti
Quartz	0	0	0	0	0	0	0.46743	0
Feldspar	0.09983	0	0	0.14466	0	0.08506	0.31174	0
Calcite	0	0.71469	0	0	0	0	0	0
Amphibole (Actinolite)	0	0.08838	0.18472	0	0.0536	0	0.24773	0

The estimate in Table 5 was input into the MCR-ALS program with a weighting of 0.1 for all mineral guesses. The program was adjusted for 4 endmembers, and unlike the previous estimate, this guess was based on soil knowledge rather than PCA cluster analysis.

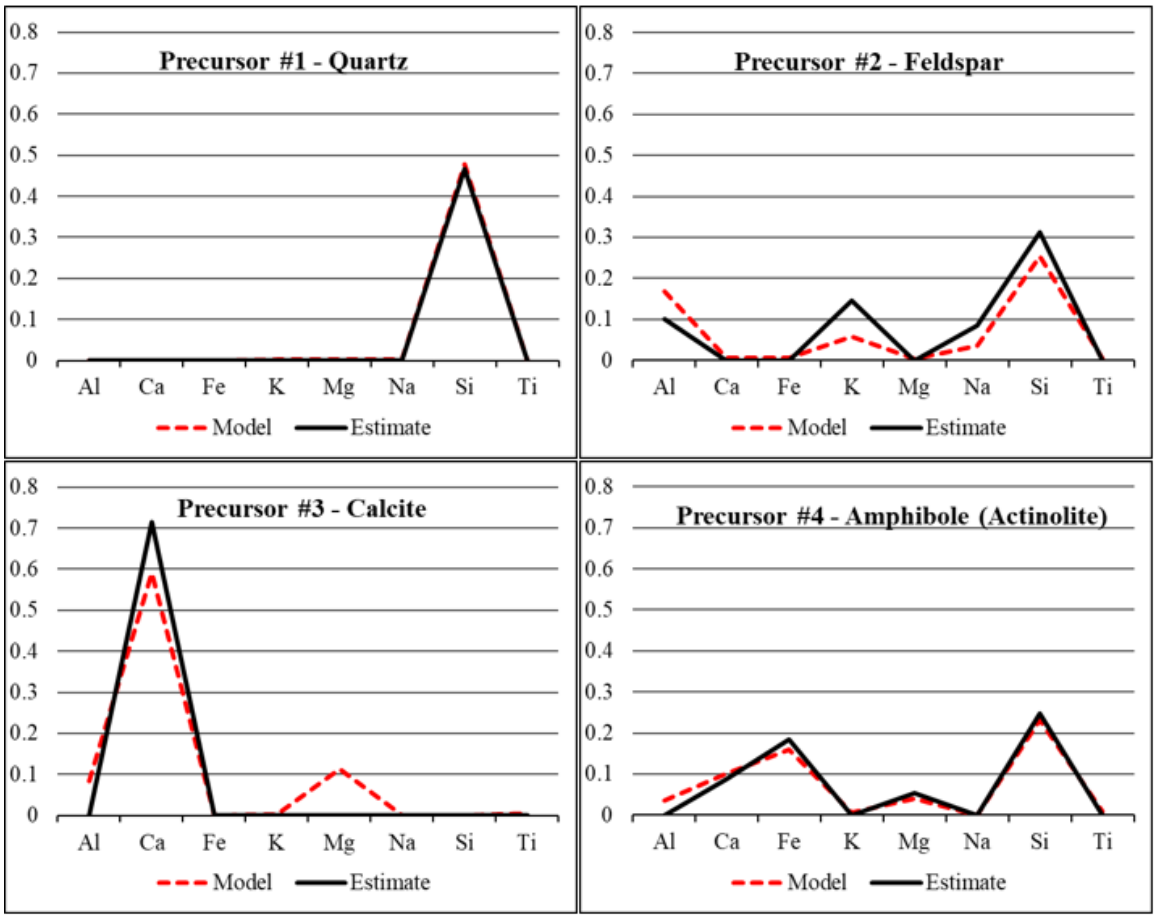

Figure 44. Four initial precursors are modeled using MCR-ALS. The model and initial estimates are plotted above. Y-axes are mass fraction values.

The resulting model of minerals converges close to the initial estimate, as shown in Figure 44. The model accounted for 99.82% of the compositional information with quartz 42.24%, feldspar 16.31%, calcite 34.95%, and amphibole 6.32%. There are different types of feldspar that are common in nature, and this could be the source of some deviation from the estimate. Additionally, the model is adjusting aluminum and magnesium clearly in every model precursor. The Q-residuals for this data, shown in Figure 45, suggests a possible gap in potassium, magnesium and sodium within the model.

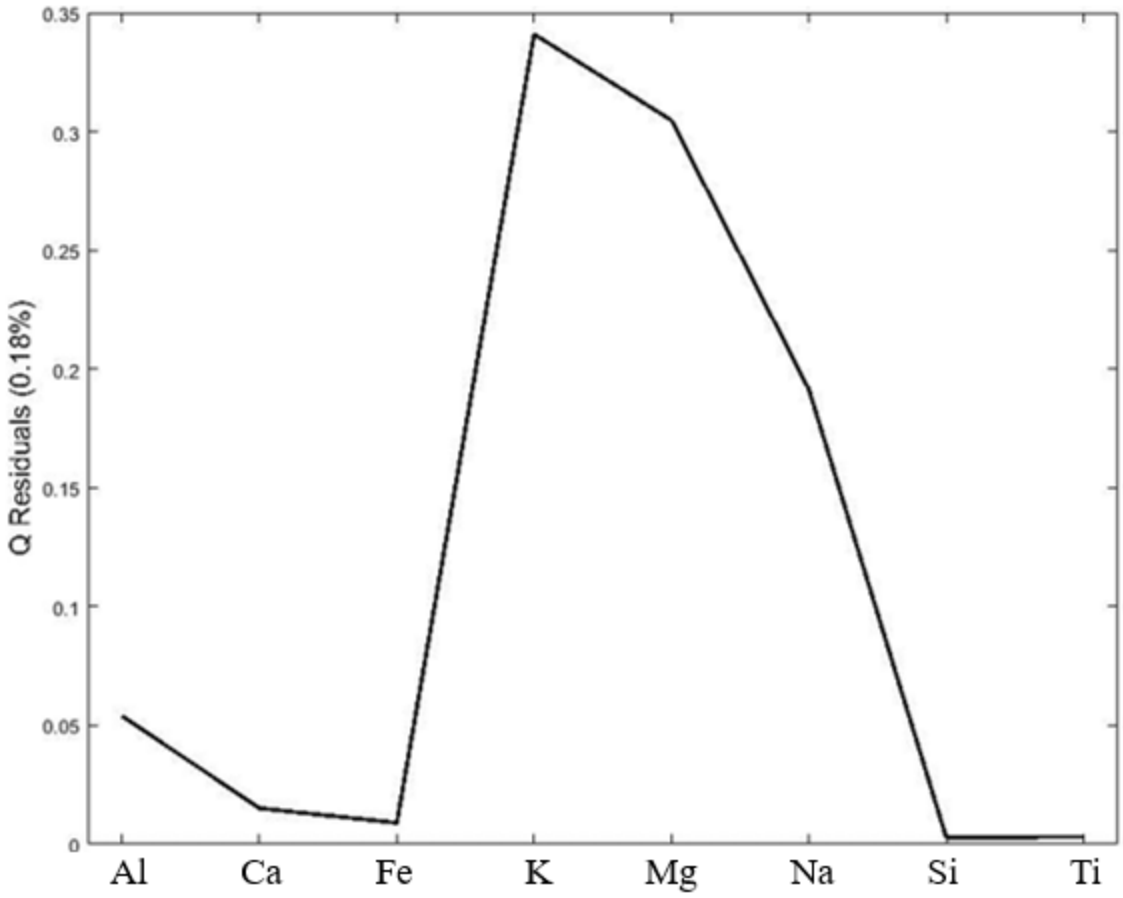

Figure 45. Q-residuals are plotted for the four-precursor estimate. Y-axis is equivalent to mass fraction values.

Using this information, a third estimate was developed using a different feldspar recommended by LLNL scientists, as well as a mineral from the original guess using cluster analysis. This estimate was developed after dozens of various estimate combinations using geological information about the test site soil, previous research and cluster analysis were attempted. The following result based on visual comparison of the model convergence and the initial estimate was a 5-precursor guess with a combination from various sources. One mineral used from the original cluster analysis was Monticellite, a mafic type mineral of the olivine group of minerals. The new initial estimate is shown in Table 6.

Table 6. Five initial precursor compositions derived from previous modeling, clusters, and soil information.

Mineral Guess	Al	Ca	Fe	K	Mg	Na	Si	Ti
Feldspar (Fitzgerald)	0.1106	0.0119	0.0009	0.0373	0.0012	0.0537	0.2972	0.0002
Quartz	0	0	0	0	0	0	0.4674	0
Calcite	0	0.7147	0	0	0	0	0	0
Amphibole (Actinolite)	0	0.0884	0.1847	0	0.0536	0	0.2477	0
Monticellite	0	0.2561	0	0	0.1553	0	0.1795	0

This third estimate was modeled as five precursors in contrast to the previous guesses of six and four. Note that as stated in the PCA methodology, 4-6 precursors were determined to be present within the data. The resulting model seems to have matched the data very well as shown in Figure 46.

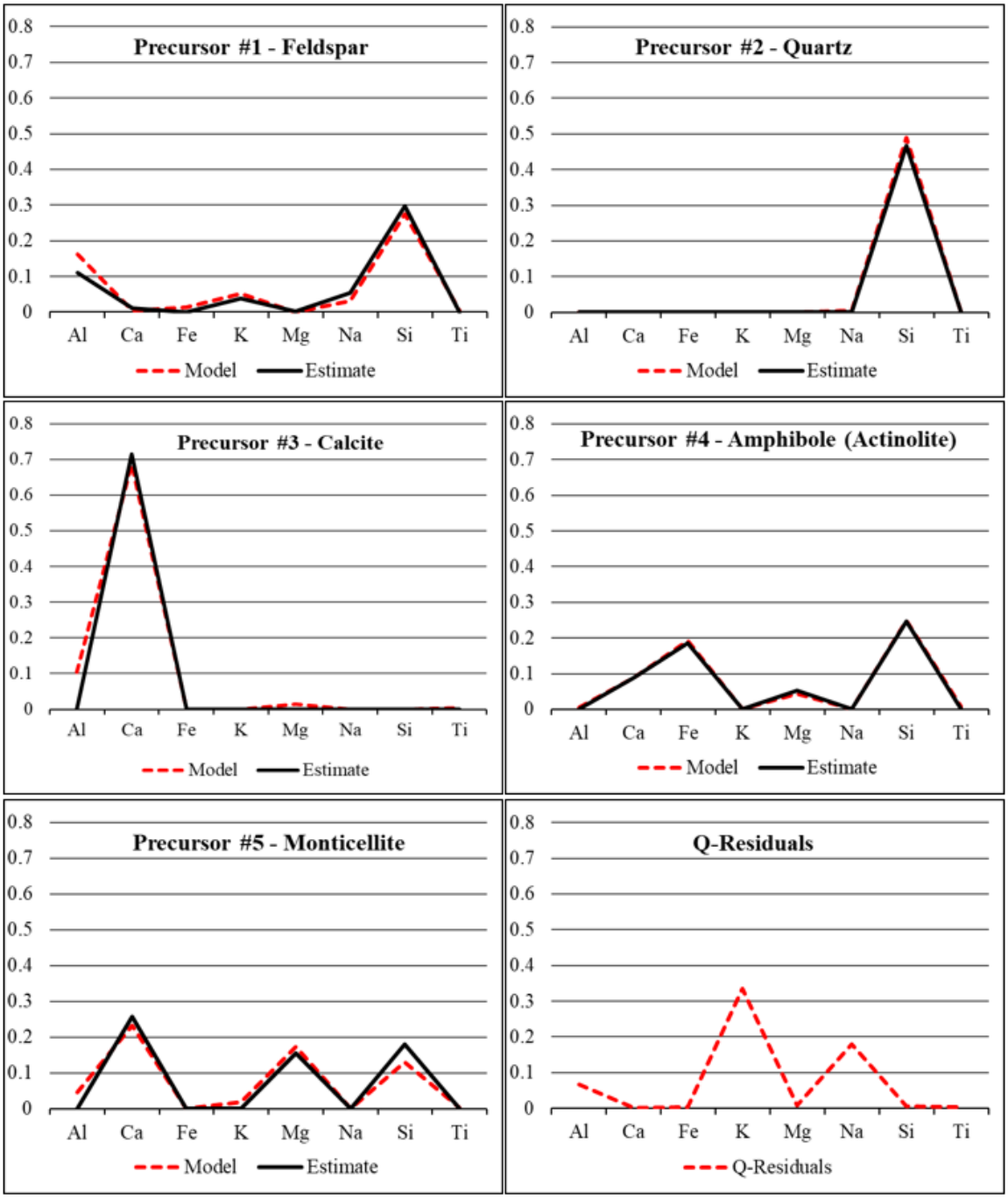

Figure 46. Five initial precursors are modeled using MCR-ALS. The model and initial estimates are plotted above. Y-axes are mass fraction values.

The plots in Figure 46 display the initialized estimate and resulting MCR-ALS model compositions. It can be seen that again quartz (silicon-rich) matches nearly exactly

and amphibole (actinolite) matches nearly exactly as well. Calcite (calcium-rich) is also extremely close with the exception of some aluminum component. Observing the variations in estimate and model plots for each mineral along with the Q-residuals for this model, it can be seen that some aluminum, potassium and sodium are possibly unaccounted for in this model. However, the model still accounts for 99.88% of the compositional information. This residual for this model is only 0.12%. With 4,893 quality data points used, 0.12% is equivalent to roughly 6 rasters out of the 4,893 data points. Meaning that a relatively small amount of chemical data is unaccounted for in this model.

Table 7. Five initial precursor guesses and the percentage of fit they each have to the model. This is a root-mean squared percentage.

Precursor	% Model Fit	% Cumulative Fit
#1 Feldspar	25.21	25.21
#2 Quartz	38.59	63.80
#3 Calcite	25.04	88.84
#4 Amphibole (Actinolite)	5.42	94.26
#5 Monticellite	5.62	99.88

This model fits the data well enough compositionally, that these precursors can be assumed to be present (or some closely related compositionally) within the fallout samples. Table 8 above shows that the last 2 precursors may only account for a small portion of the samples, but based on the model composition matching the estimate in Figure 46, these precursors model the data very well.

4.3. Precursor Locating and Correlation with Autoradiography

In order to find sample data points that exhibit the same or similar composition to that of a precursor, the precursors compositions are modeled into PCA as another compositional data point and highlighted as stars in Figures 47 through 52. The sample

data points co-located with the precursor points are those which are examined spatially and compared with autoradiography images of the same location. This comparison allows for conjecture as to what sample characteristics, as well as what precursors, are correlated with actinide location in fallout.

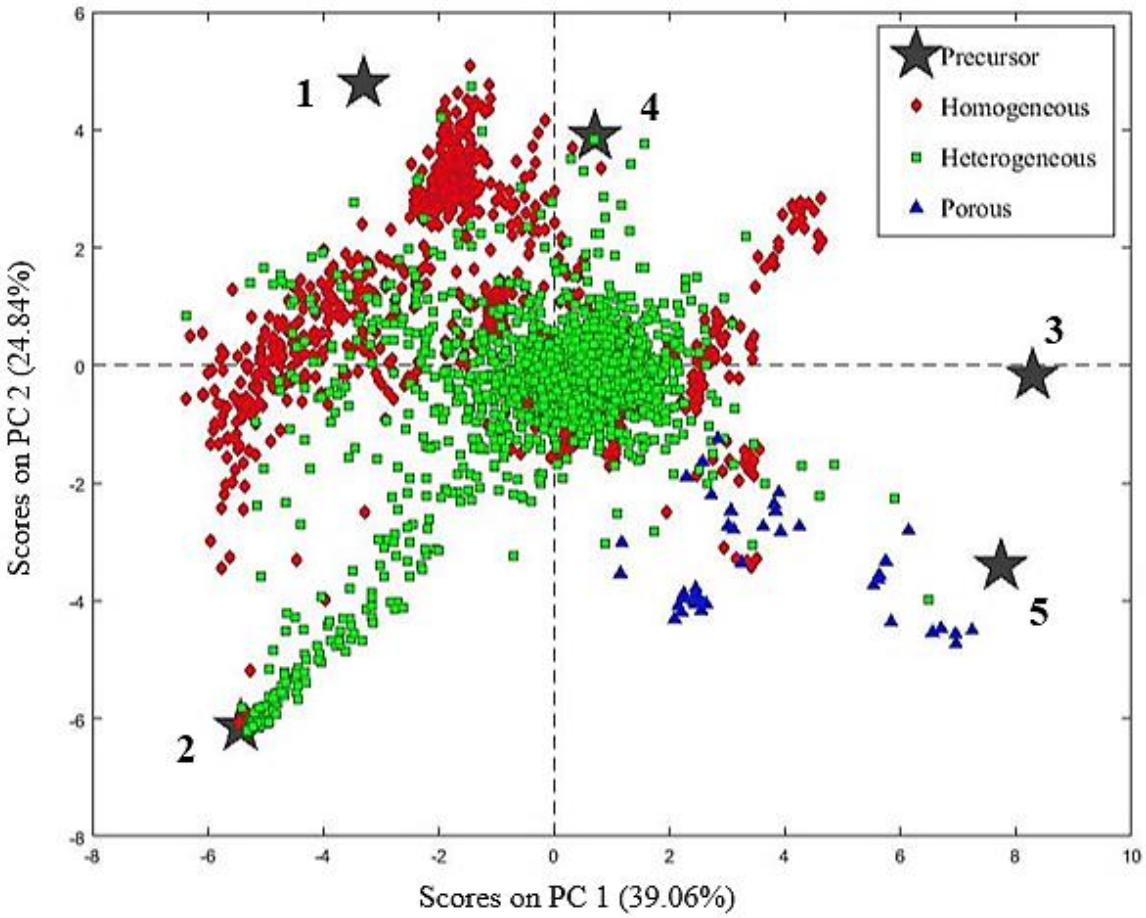

Figure 47. PCA plot displaying the specific location of precursors in PC space for the PC1 versus PC2 perspective. The precursor numbers correspond to the numbering in Table 8.

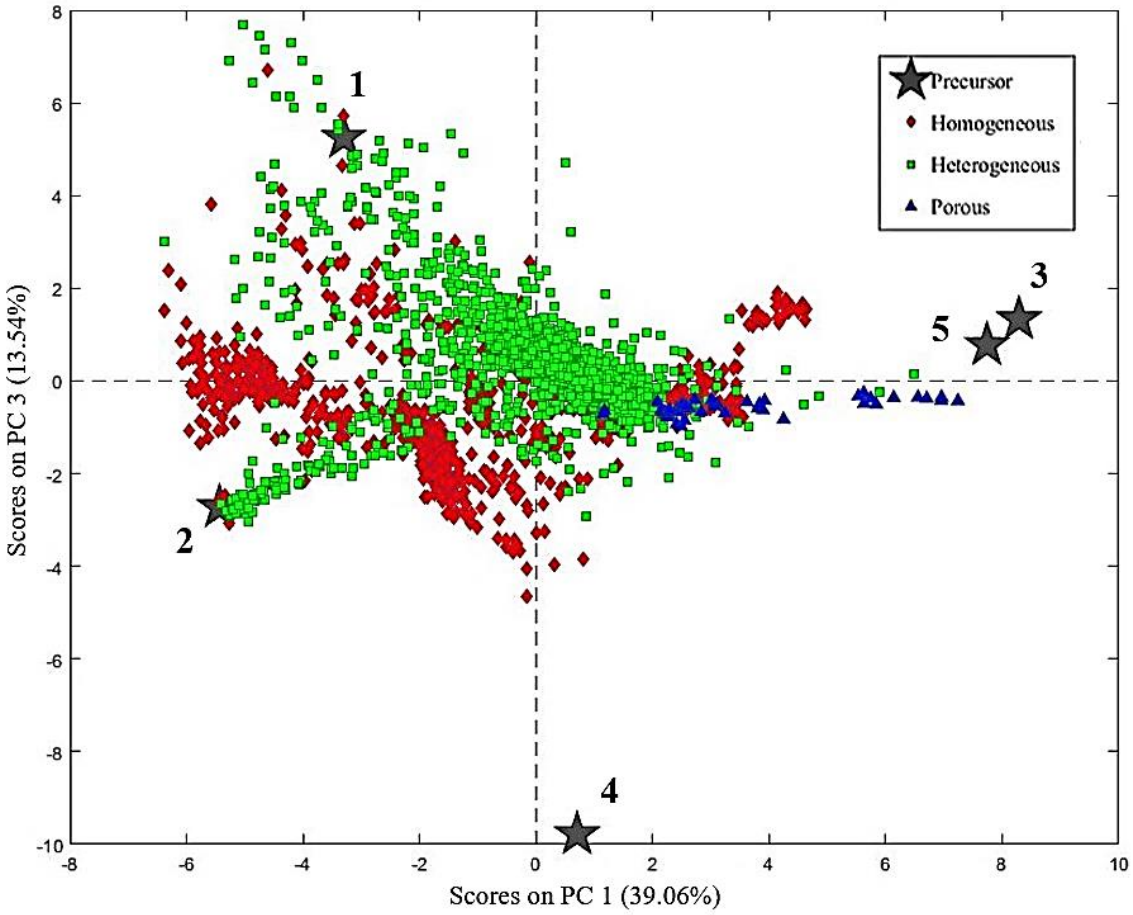

Figure 48. PCA plot displaying the specific location of precursors in PC space for the PC1 versus PC3 perspective. The precursor numbers correspond to the numbering in Table 8.

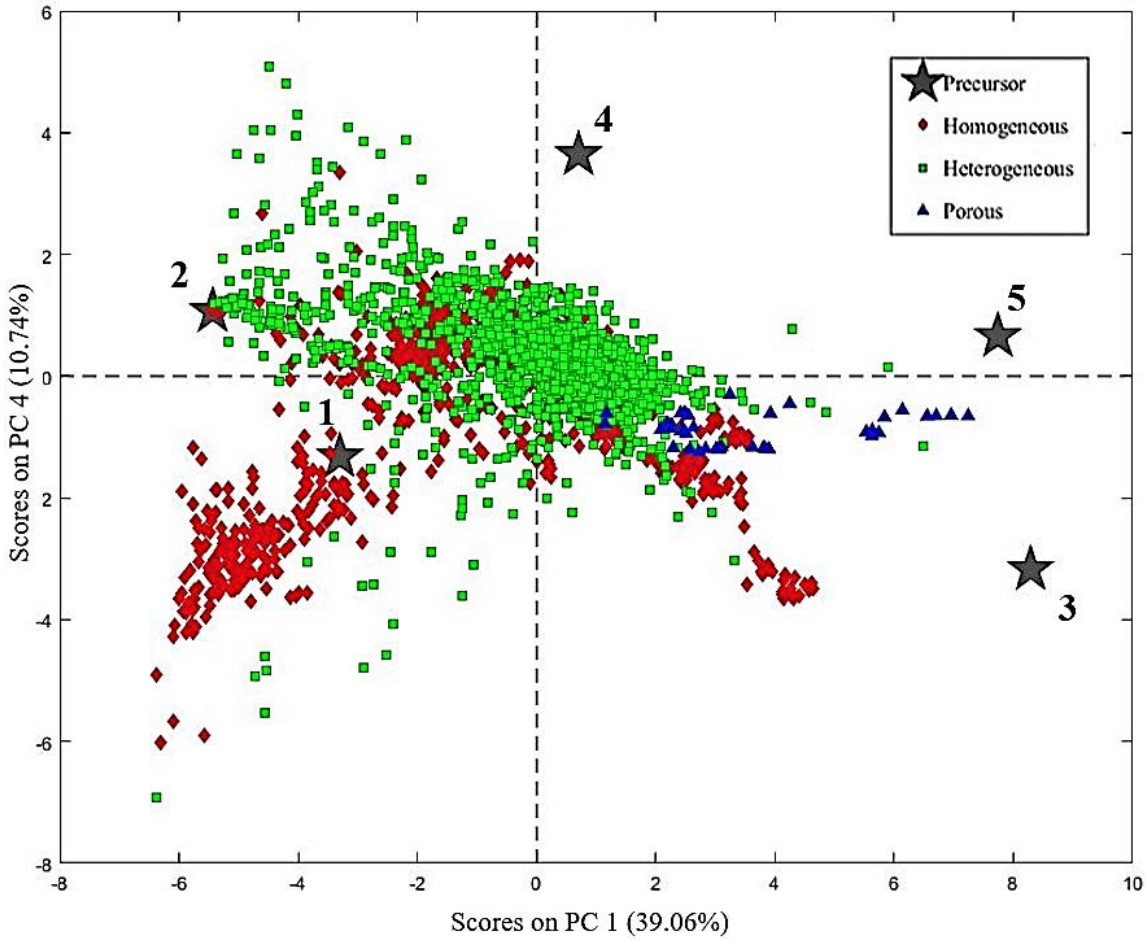

Figure 49. PCA plot displaying the specific location of precursors in PC space for the PC1 versus PC4 perspective. The precursor numbers correspond to the numbering in Table 8.

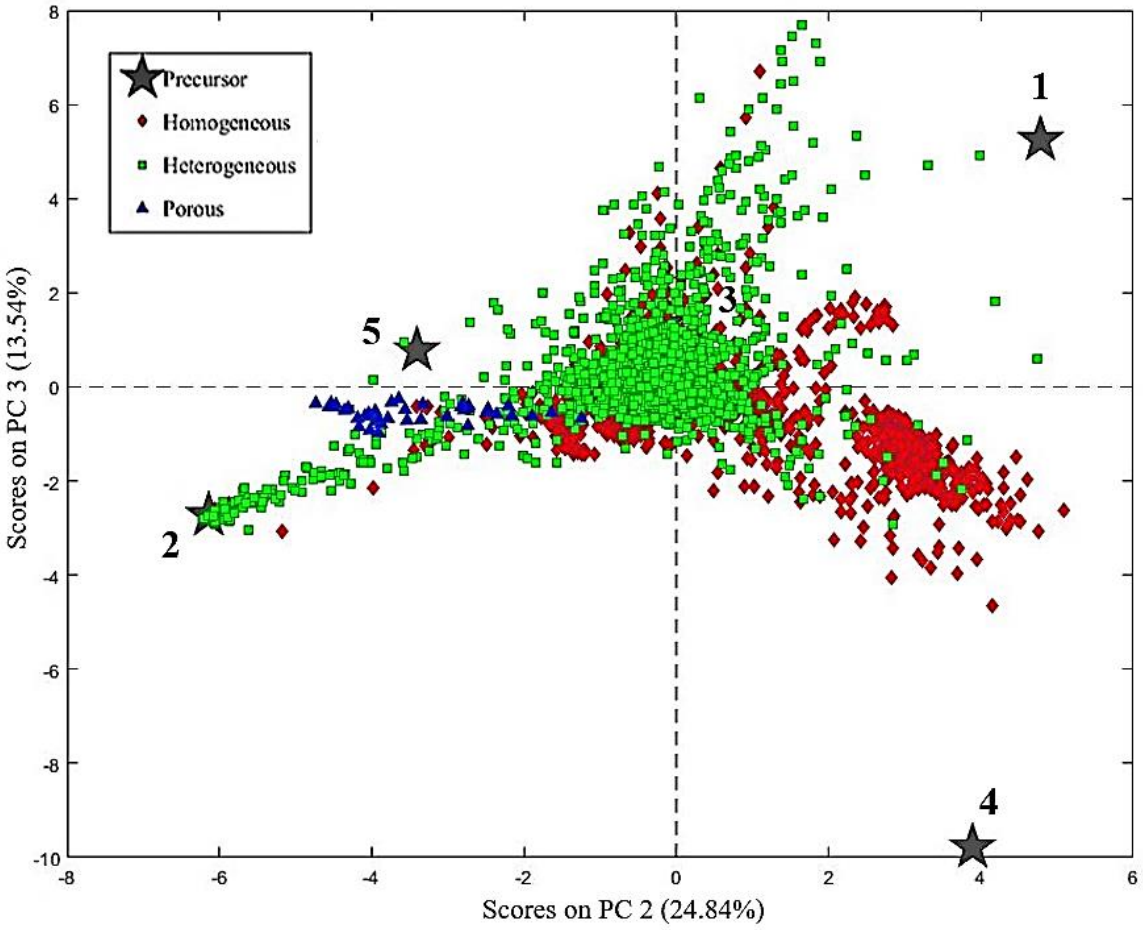

Figure 50. PCA plot displaying the specific location of precursors in PC space for the PC2 versus PC3 perspective. The precursor numbers correspond to the numbering in Table 8.

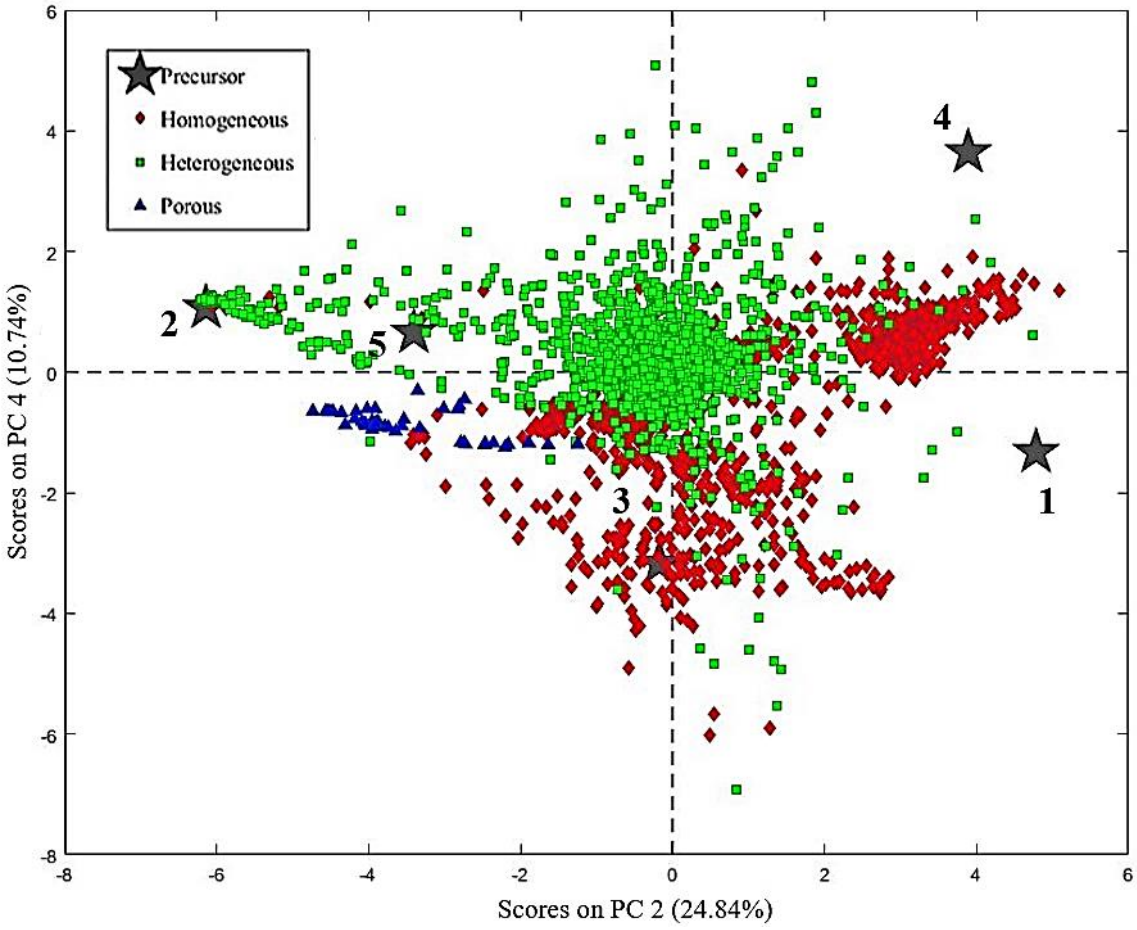

Figure 51. PCA plot displaying the specific location of precursors in PC space for the PC2 versus PC4 perspective. The precursor numbers correspond to the numbering in Table 8.

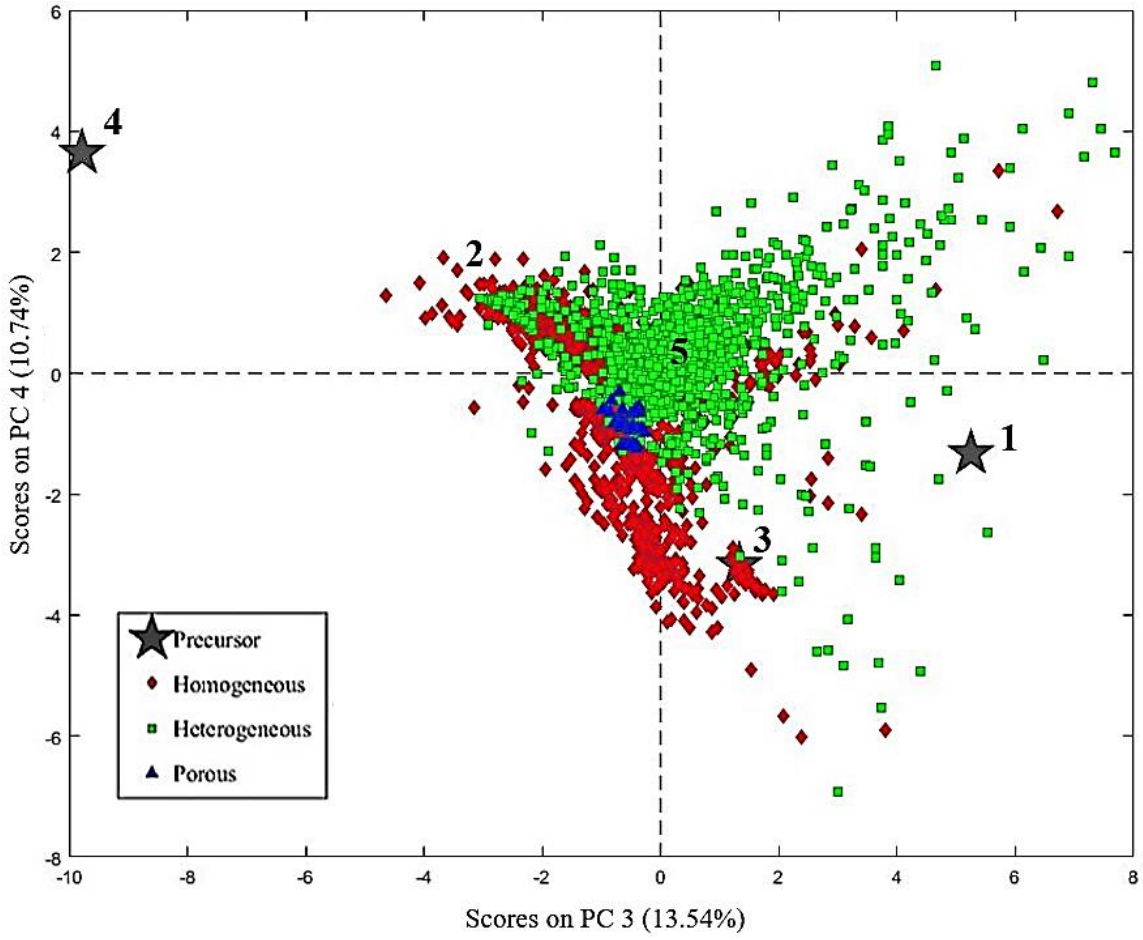

Figure 52. PCA plot displaying the specific location of precursors in PC space for the PC3 versus PC4 perspective. The precursor numbers correspond to the numbering in Table 8.

Initial observation suggest that some precursors are not present in the dataset, however, the MCR model converges on solutions using all compositional information, not specific sample raster compositions. The samples which exhibit precursor compositions are those which tend toward the area identified by each precursor. The fact that clusters do not fall directly around a precursor suggest that raster spots may contain combinations of more than one mineral within the region examined by the SEM. Additionally, viewing the PC scores in various combinations up through principal component 4 (i.e. PC1 v. PC3, PC3

v. PC4, etc.), the precursors do fall in clusters. It was determined that 5 precursors exist, therefore 4 PCs are considered to be variationally relevant for this research. The cumulative variation encompassed by each PC is shown in Table 4 in Chapter 3. Each combination of principal components encompasses the variation equal to the sum of each PCs individual variance percentage from Table 4 as well.

Each precursor was examined individually in order to visually identify locations on sample surfaces which represent each precursor compositionally. The five sample rasters that were closest in proximity to each precursor when plotted in principal component space were examined and found spatially on the sample SEM image. This location was then aligned spatially with the autoradiography image of the same samples in order to determine the relative darkness of this location. Furthermore, relationships between precursor and activity of the samples at the precursor locations are discussed.

Precursor 1: Feldspar

This precursor was best viewed in clusters observed in plots of PC1 v. PC3 (Figure 48) and PC1 v. PC4 (Figure 49). The first raster location is on an irregular sample designated IRR-6. The raster is located on a specific object tile shown in Figure 53 and 54. The autoradiography is aligned in Figure 55 showing no activity for this raster.

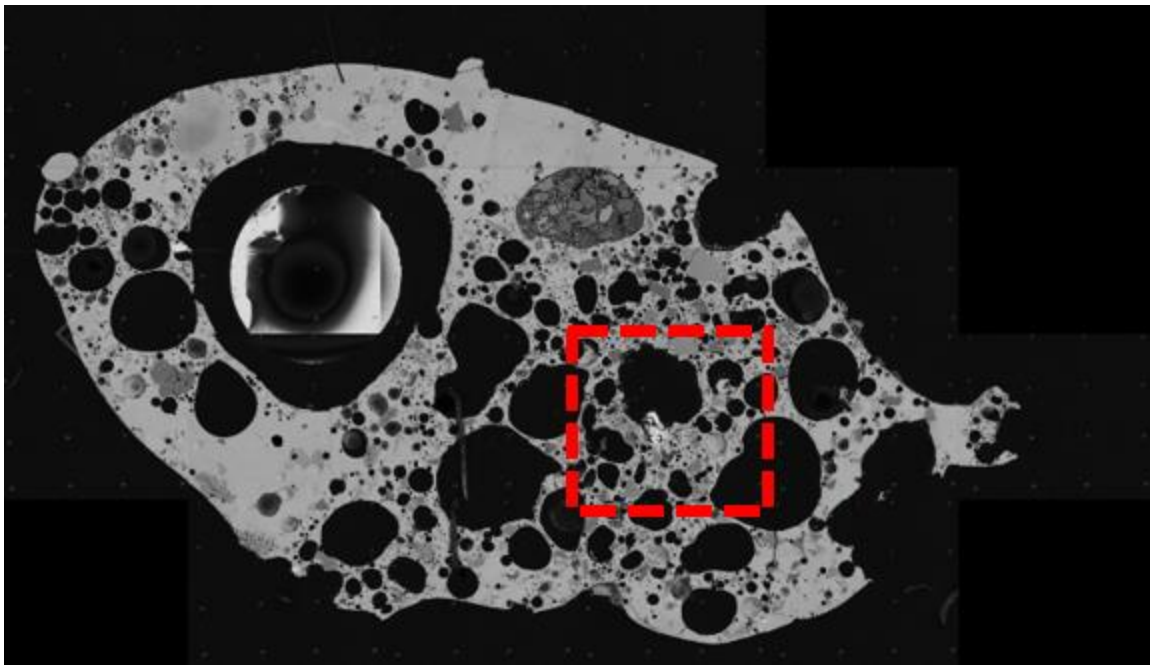

Figure 53. Tile compilation of sample DW-IRR-6 with tile highlighted containing feldspar raster.

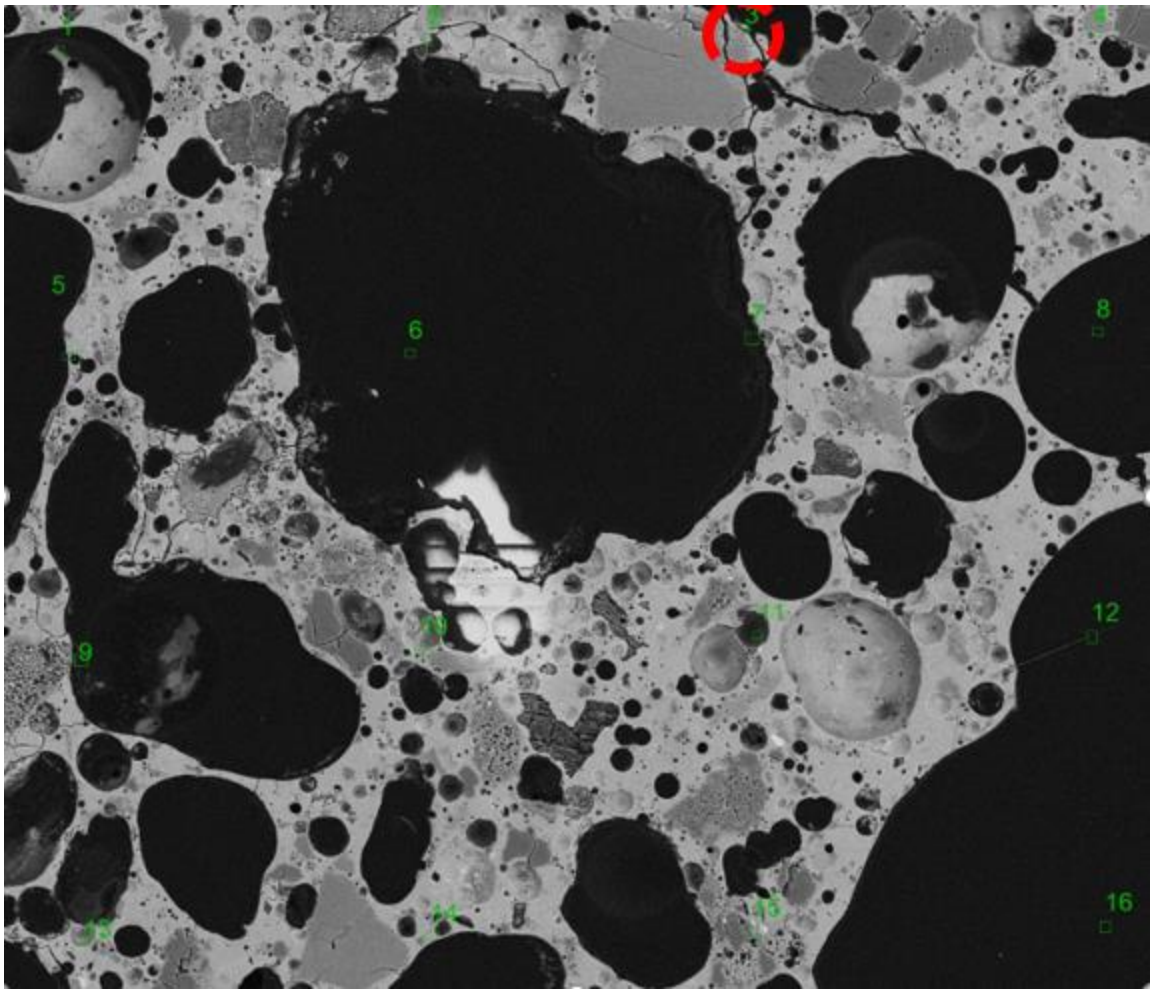

Figure 54. Tile image sample DW-IRR-6 with raster highlighted containing feldspar composition.

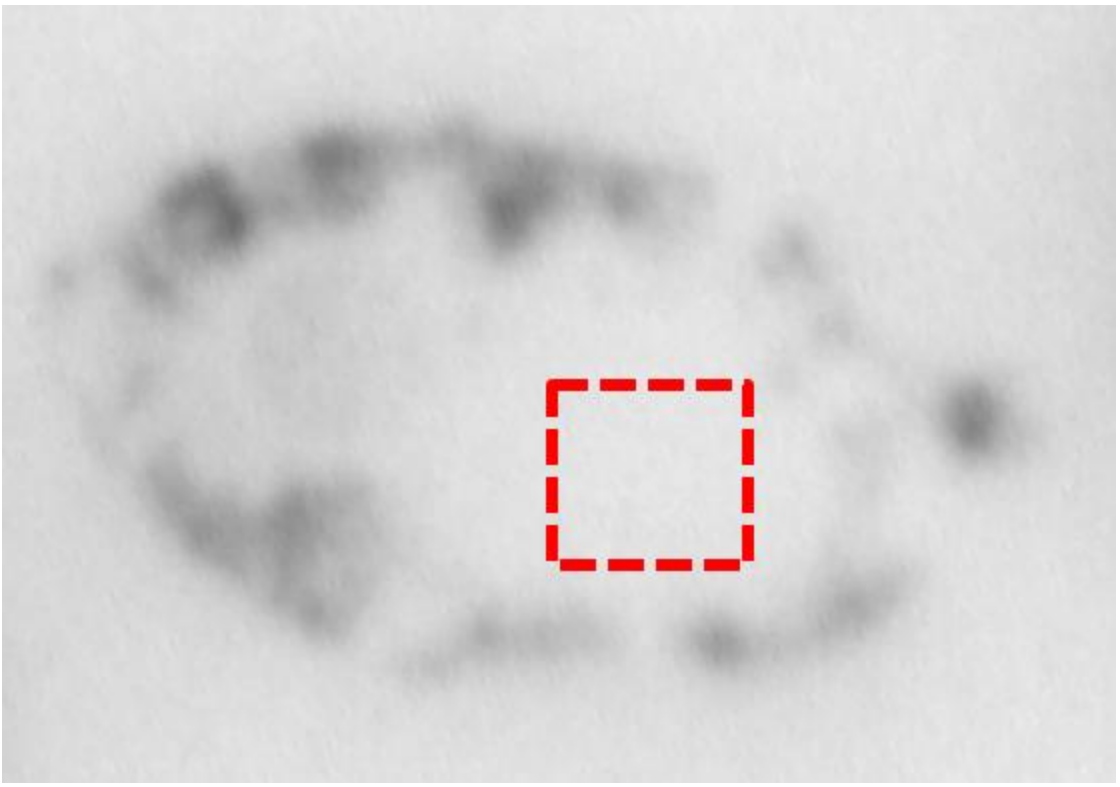

Figure 55. Autoradiography image sample DW-IRR-6 with tile area highlighted with seemingly no activity.

The second raster appeared on a larger ground glass piece. The autoradiography shown in Figure 56 is an inverted light image that better highlights the areas of higher radioactivity on the sample surface. The specific tile shown in Figure 57 aligned with autoradiography show a medium level of activity. It appears as though this raster falls on the small portion of this sample which exhibits relatively more radioactivity on the sample surface.

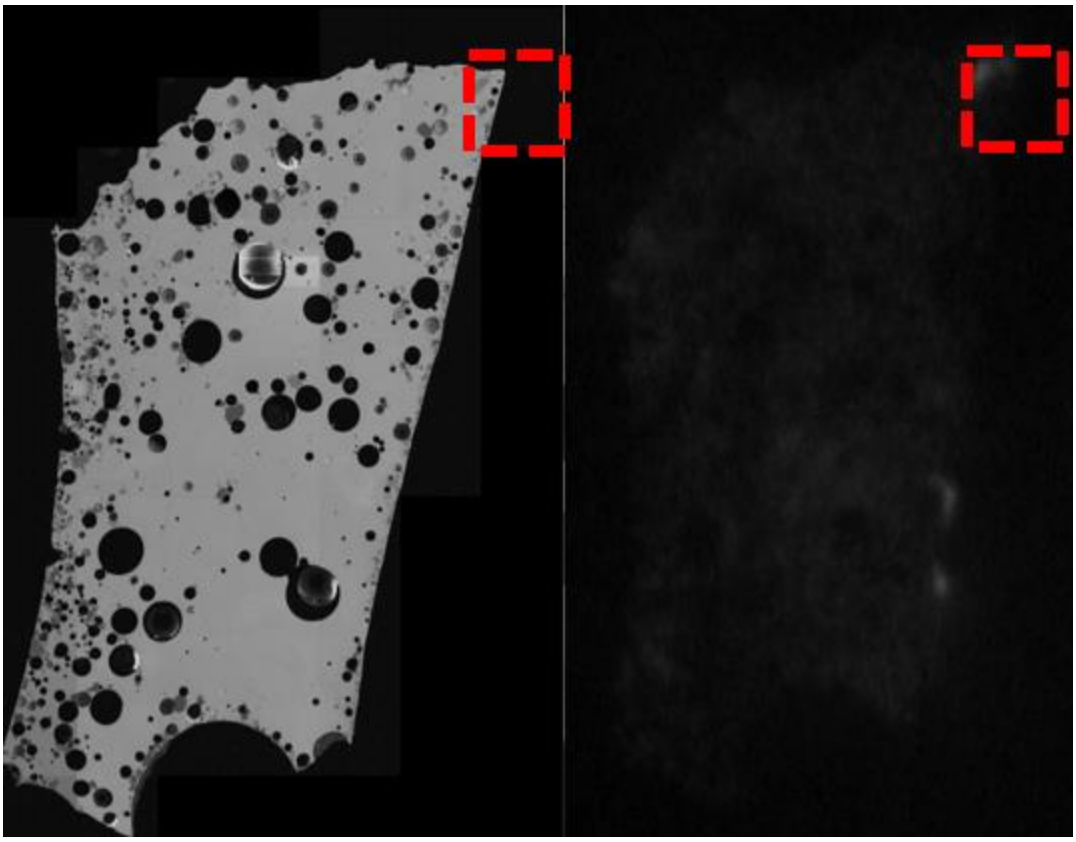

Figure 56. Tile compilation of sample DW-GG-1 with tile highlighted containing feldspar raster (left) and inverted autoradiography of same sample with area highlighted (right).

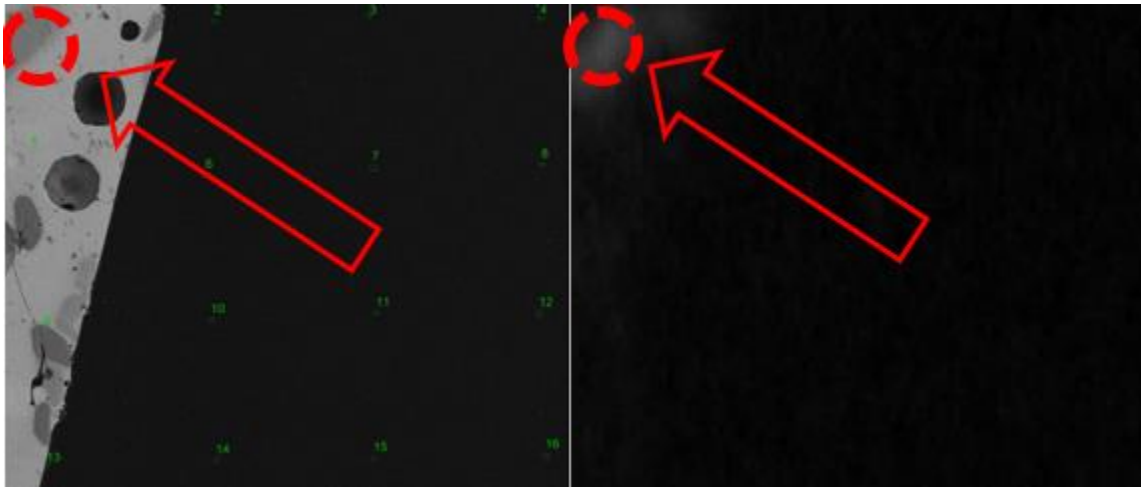

Figure 57. Tile containing feldspar raster (left) and associated inverted autoradiography (right).

The next sample, a half-mm sample, exhibits a uniform degree of radioactivity as shown in Figure 58. This is the the same degree of visual darkness as the second raster.

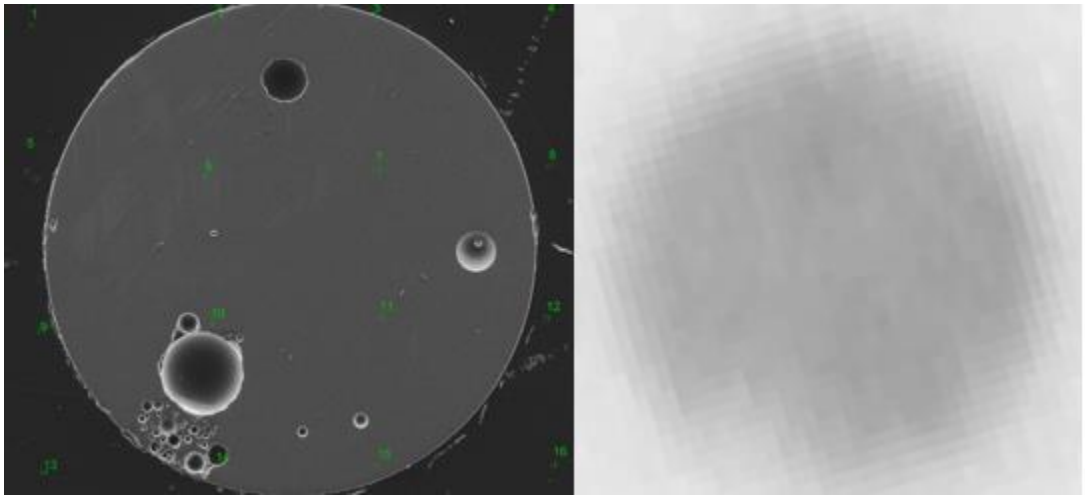

Figure 58. 1-DW-25-37 SEM image (left) and autoradiography (right).

The final two rasters found in the cluster with the feldspar precursor fall on the same sample shown in Figure 59. This is a 3-4 mm spherical sample with denser radioactivity located in the area of the specific rasters. Again, the autoradiography is inverted to better visualize the intensity of the activity on the sample surface.

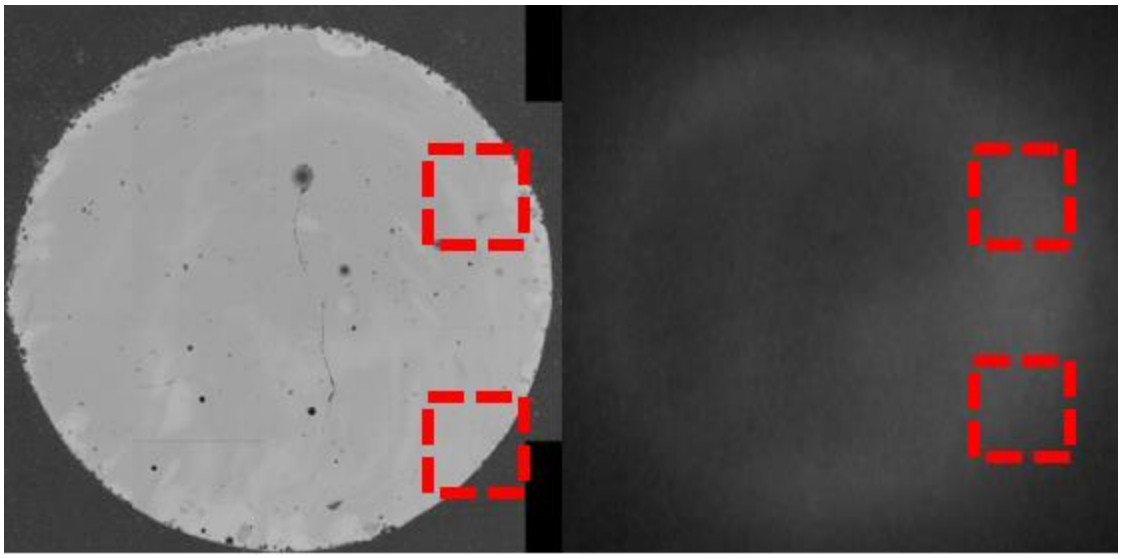

Figure 59. DW-SL-1-10 Tile compilation with highlighted tiles containing feldspar rasters. SEM image (left) with inverted autoradiography (right).

The results for all 5 rasters are tabulated in Table 8. The correspondence to radioactivity seems to have no initial correlation with any specific sample characteristic or sample set. The darkness appears medium for those sample spots which exhibited radioactivity. The darkness was visually selected relative to all samples using the same scale described in Chapter 3: None, Low, Medium, High and Very High. The first raster could possibly be an anomaly as it is located near a crack on the sample surface. This is known to cause possible compositional error. With this in mind, all feldspar locations on smooth surfaces exhibited a medium radioactivity level relative to other samples. The shape, size, or degree of mixing appear to have no relationship with whether radioactivity is co-located with feldspar.

Table 8. Five rasters closest to the feldspar precursor in PC space with associated information for each raster.

Sample Set	Sample #	Tile #	Raster #	Degree of Mixing	Shape	Size	AR Darkness
DW-Irregular	6	7	3	heterogeneous	Irregular	3-4 mm	None
DW-GG	1	58	1	heterogeneous	Ground Glass	4-5 mm	Medium
1-DW-25	37	1	14	homogeneous	Symmetrical	Half mm	Medium
DW-SL-1	10	19	8	homogeneous	Symmetrical	2-3 mm	Medium
DW-SL-1	10	17	12	homogeneous	Symmetrical	2-3 mm	Medium

Precursor 2: Quartz

Quartz, the best matching model estimate, had a significant cluster of rasters in the vicinity of its location, labeled 2 on the PC1 vs PC2 plot in Figure 47. The closest five sample spots were examined in Figures 60 through 66 and rolled up in Table 9. Each quartz raster shows an evident visually dark surface as seen in each SEM image. The radioactivity is minimal or not present for each raster.

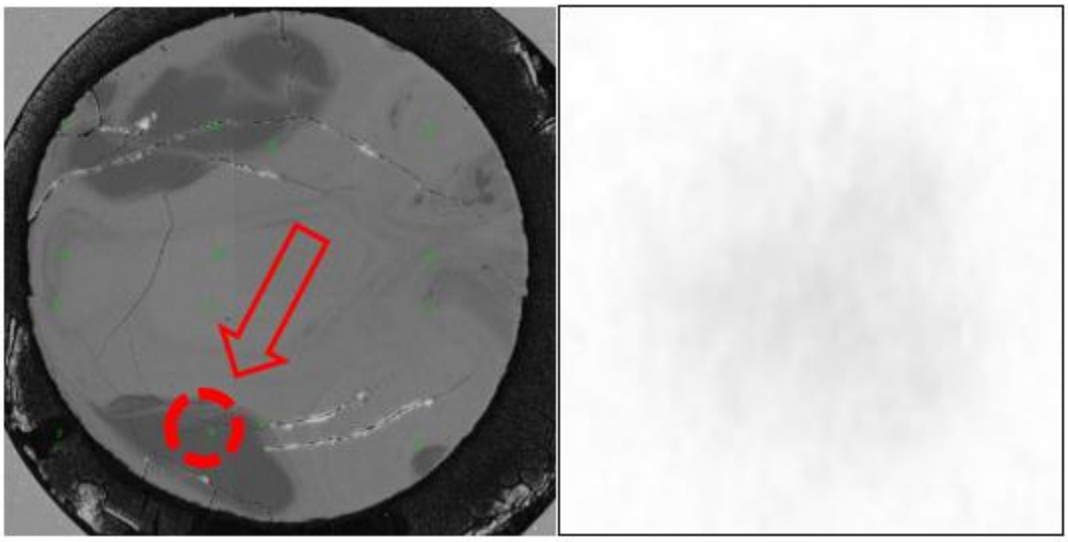

Figure 60. Sample 1-DW-14-M2-4 SEM image (left) and autoradiography (right) with raster circled.

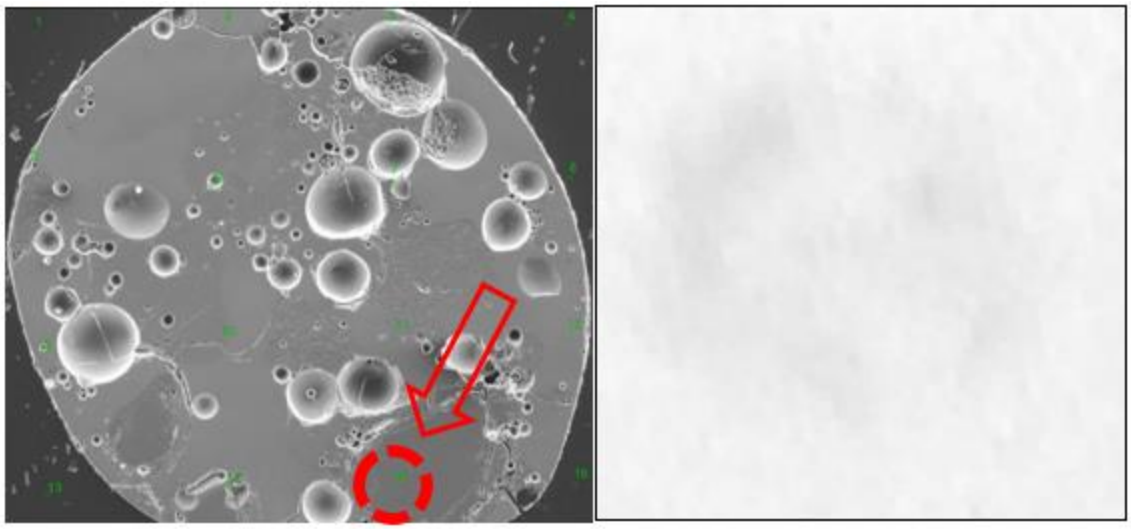

Figure 61. Sample 1-DW-25-5 SEM image (left) and autoradiography (right) with raster circled.

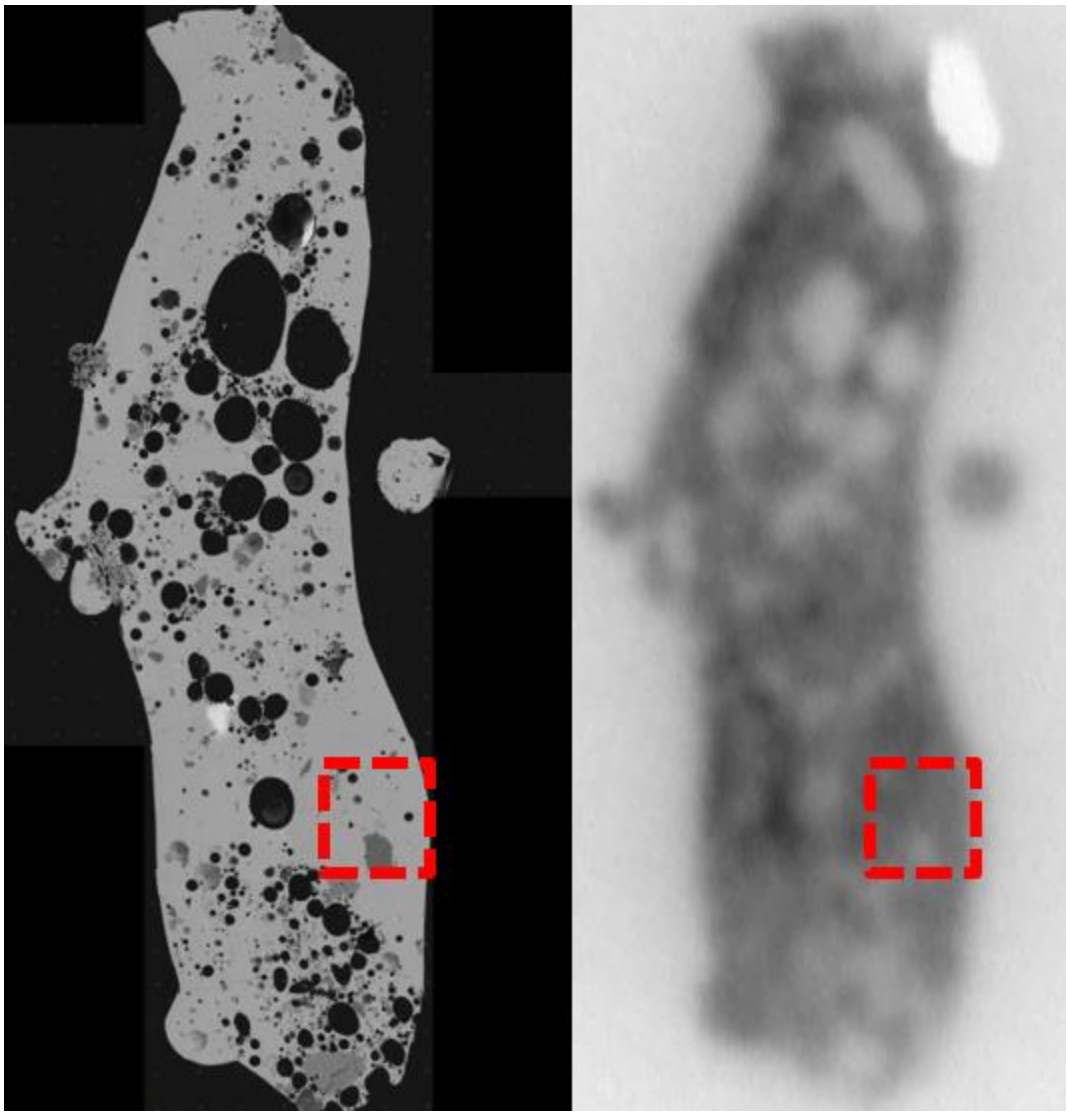

Figure 62. Sample DW-IRR-10 SEM image (left) and autoradiography (right) with tile containing quartz raster indicated.

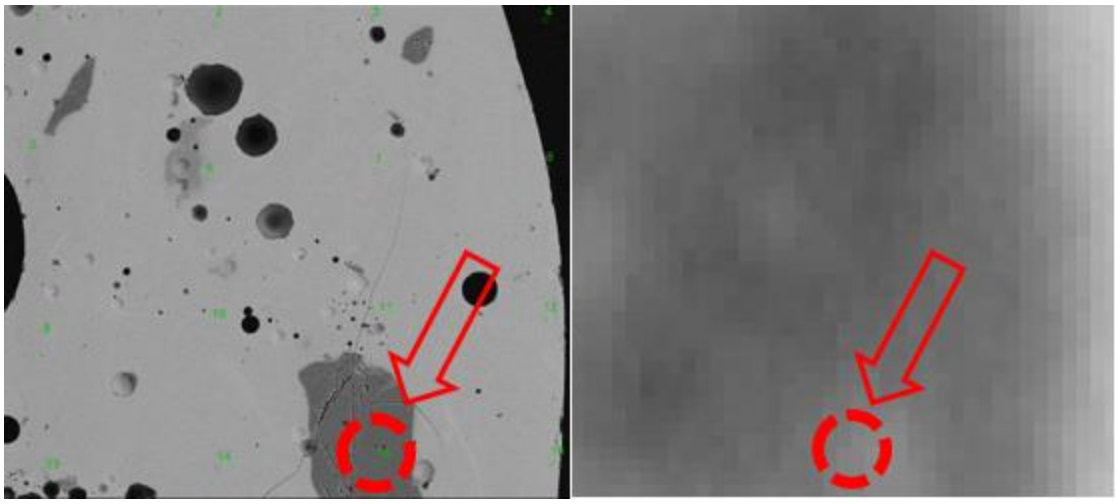

Figure 63. Close-up of tile 17 on Sample DW-IRR-10 SEM image (left) and autoradiography (right) with raster circled.

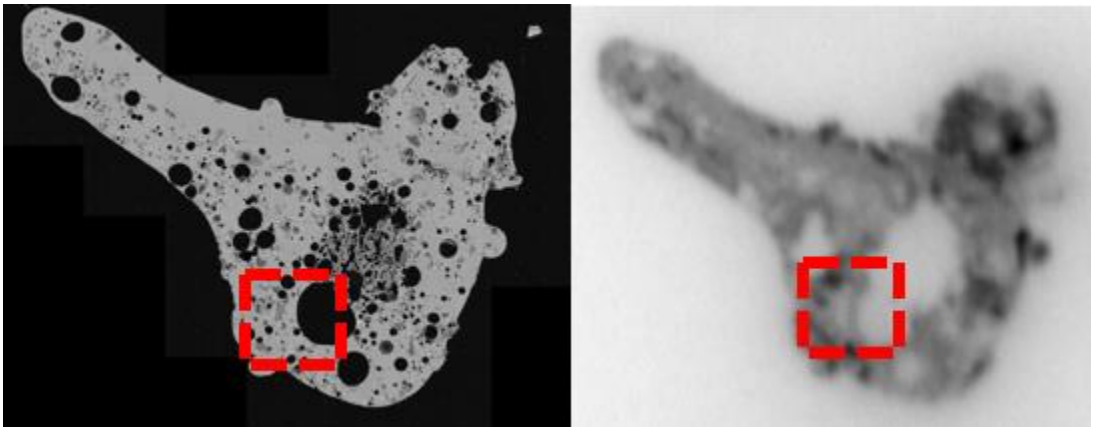

Figure 64. Sample DW-IRR-4 SEM image (left) and autoradiography (right) with tile containing quartz raster indicated.

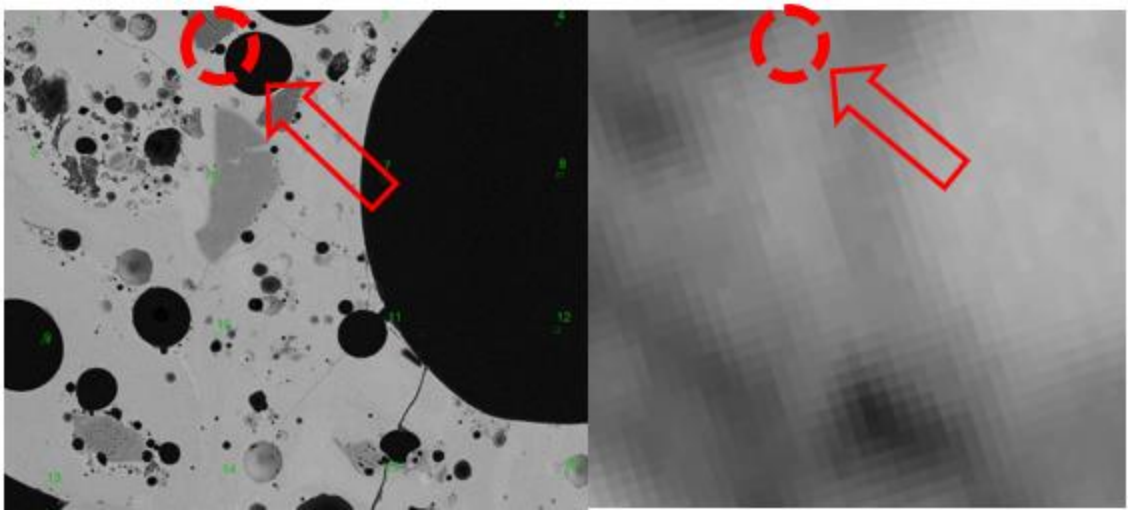

Figure 65. Close-up of tile 6 on Sample DW-IRR-4 SEM image (left) and autoradiography (right) with raster circled.

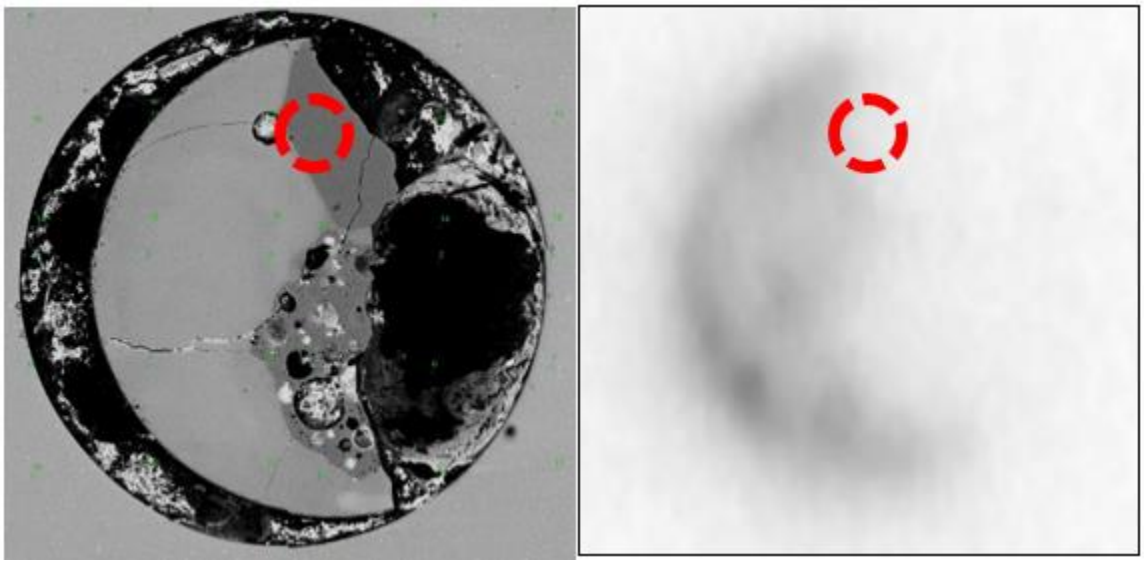

Figure 66. Sample 1-DW-14-M1-14 SEM image (left) and autoradiography (right) with raster circled.

The results of each quartz raster are shown in Table 9. Each location containing quartz seemed to exhibit low or no activity at the location on the sample surface. The size, shape or degree of mixing appear to have no relationship with whether quartz is co-located with radioactivity.

Table 9. Five rasters closest to the quartz precursor in PC space with information for each raster.

Sample Set	Sample #	Tile #	Raster #	Degree of Mixing	Shape	Size	AR Darkness
1-DW-14 M2	4	1	8	homogeneous	symmetrical	1-2 mm	Low
1-DW-25	5	1	15	heterogeneous	symmetrical	Half mm	Low
DW-Irregular	10	17	15	heterogeneous	Irregular	3-4 mm	Low
DW-Irregular	4	6	2	heterogeneous	Irregular	3-4 mm	Low
1-DW-14 M1	14	3	9	heterogeneous	symmetrical	1-2 mm	None

Precursor 3: Calcite

For the calcite precursor, rasters clustered best in PC2 vs. PC3 (Figure 50) and PC3 vs PC4 (Figure 52). Figures 67 through 71 displays the 5 closest rasters on their respective sample surfaces with associated autoradiography for collocating with radioactivity. Calcite appears to be located with low, medium, and high levels of autoradiography, making calcite a less valuable precursor for activity colocation.

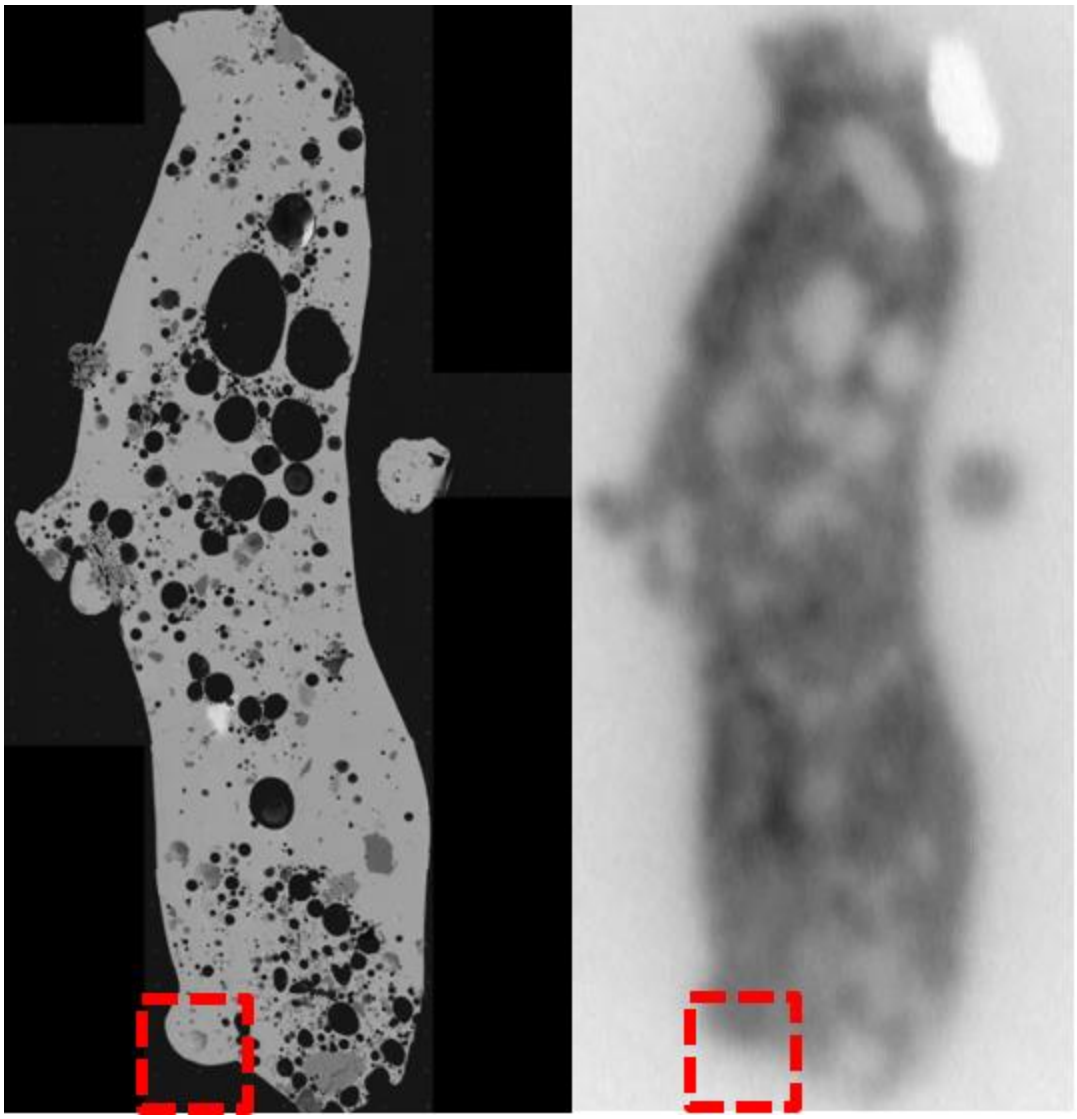

Figure 67. Sample DW-IRR-10 SEM image (left) and autoradiography (right) with tile containing calcite raster indicated.

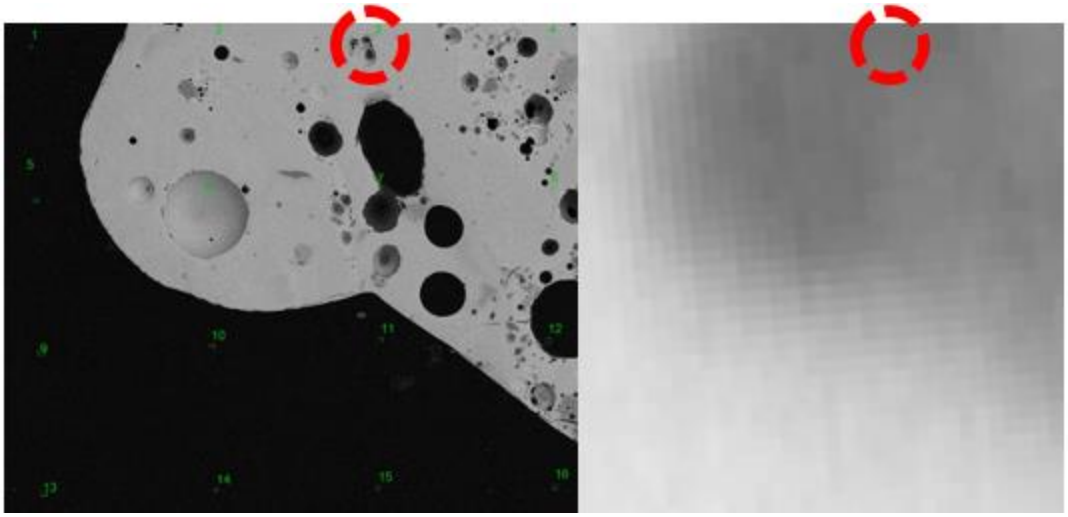

Figure 68. Close-up of tile 14 on Sample DW-IRR-10 SEM image (left) and autoradiography (right) with calcite raster circled.

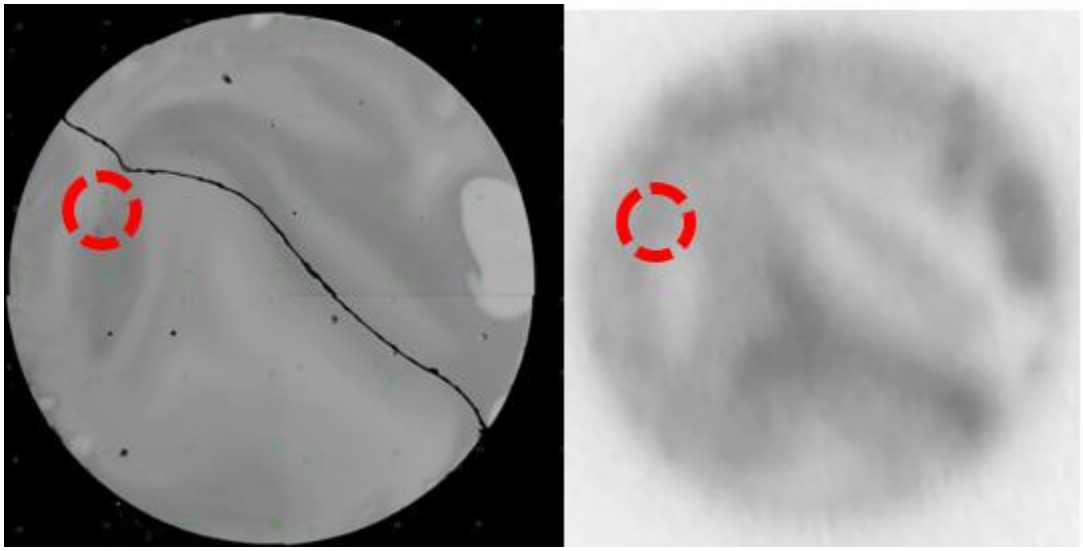

Figure 69. Sample DW-Bullets-7 SEM image (left) and autoradiography (right) with calcite raster circled.

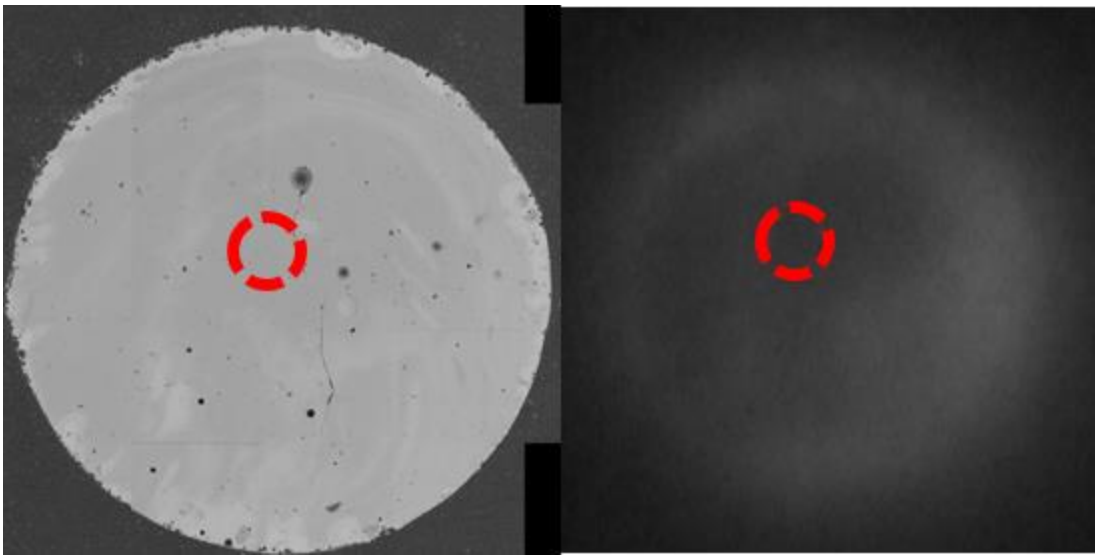

Figure 70. DW-SL-1-10 tile compilation with highlighted calcite raster. SEM image (left) with inverted autoradiography (right).

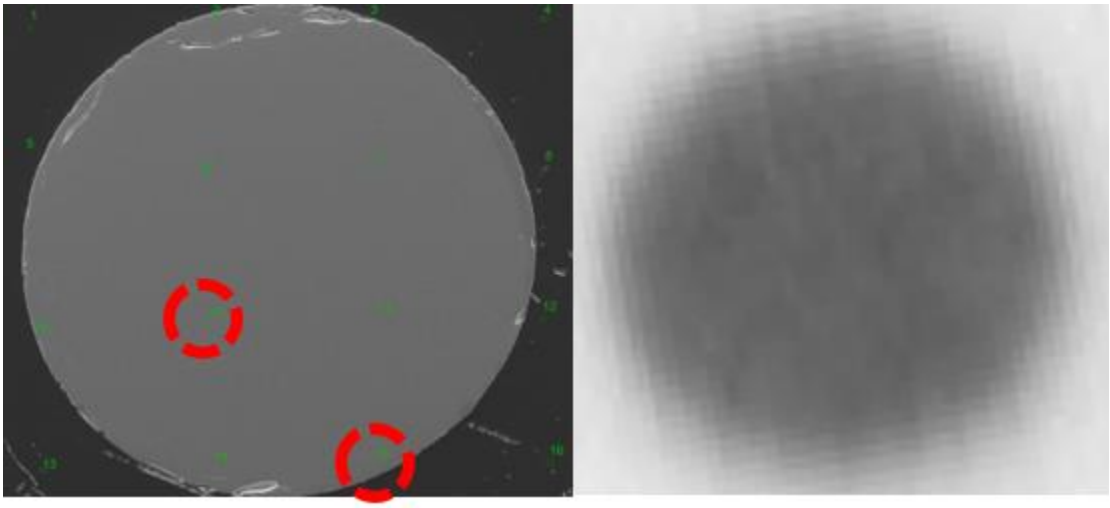

Figure 71. 1-DW-25-22 with highlighted rasters containing calcite composition. SEM image (left) with autoradiography (right).

Table 10 provides the information for each calcite raster analyzed. There appears to be no correlation between this precursor and activity. The sample characteristics associated with each raster also had no relationship with activity.

Table 10. Five rasters closest to the calcite precursor in PC space with information for each raster.

Sample Set	Sample #	Tile #	Raster #	Degree of Mixing	Shape	Size	AR Darkness
DW-Irregular	10	14	3	heterogeneous	Irregular	3-4 mm	Medium
DW-Bullets	7	2	10	homogeneous	Symmretrical	1-2 mm	Medium
DW-SL-1	10	13	1	homogeneous	Symmretrical	2-3 mm	Low
1-DW-25	22	1	10	homogeneous	Symmretrical	Half mm	High
1-DW-25	22	1	15	homogeneous	Symmretrical	Half mm	High

Precursor 4: Amphibole (Actinolite)

Amphibole was matched on PC1 vs. PC2 as shown in Figure 47. The 5 closest rasters are displayed with associated autoradiography in Figure 72 through 76. Amphibole appears to have little correlation with autoradiography, as seen in the images. Like quartz, this precursor may be a particular mineral to avoid when seeking actinides in sample.

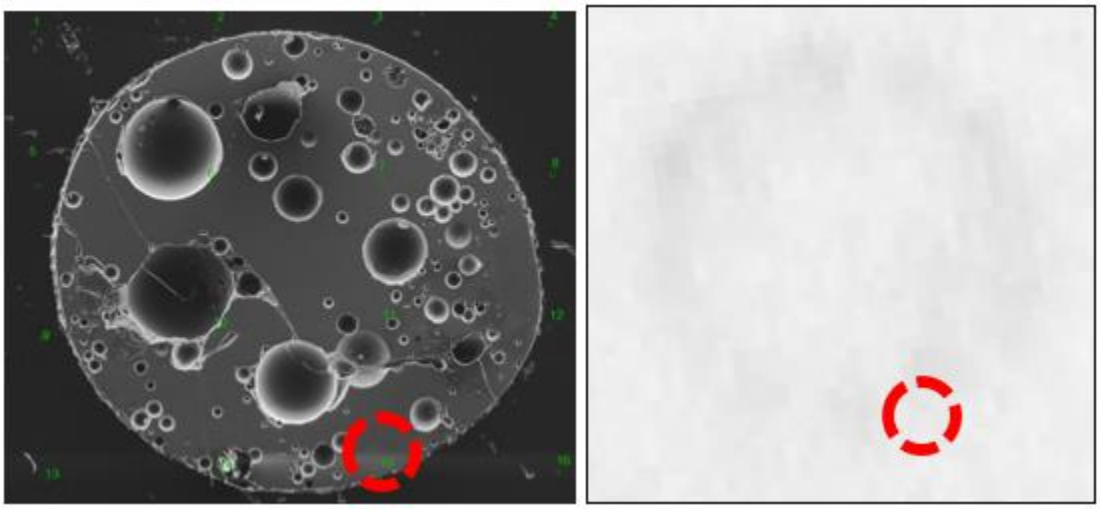

Figure 72. 1-DW-25-42 with highlighted raster containing amphibole composition. SEM image (left) with autoradiography (right).

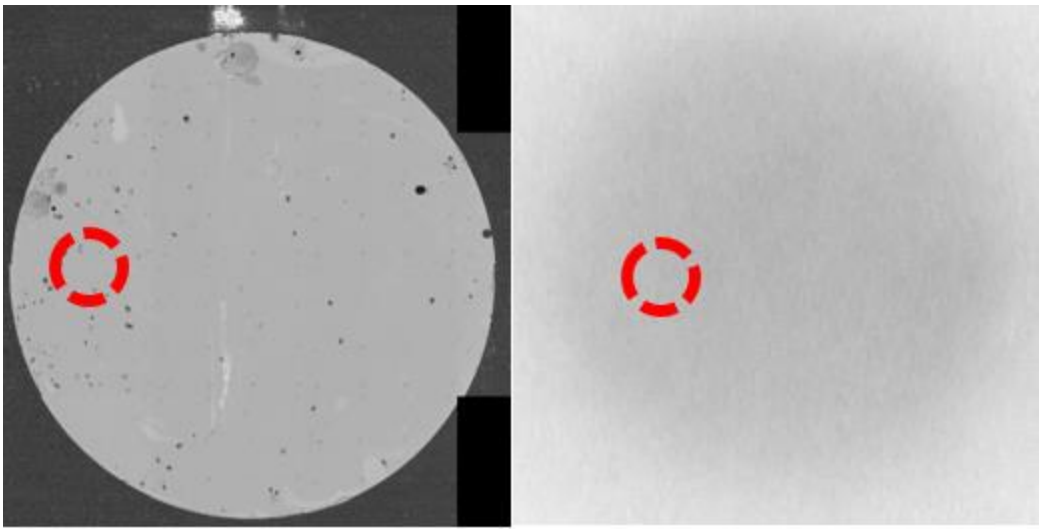

Figure 73. DW-SL-1-5 tile compilation with highlighted raster containing amphibole raster. SEM image (left) with autoradiography (right).

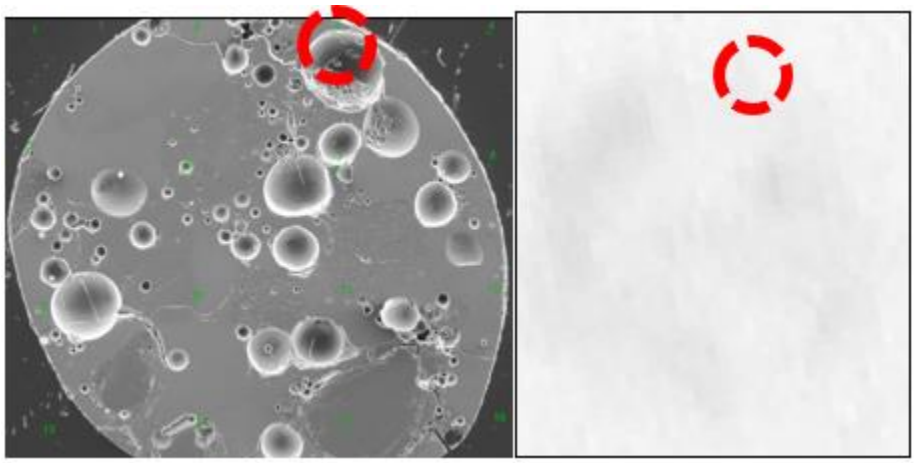

Figure 74. 1-DW-25-5 with highlighted raster containing amphibole composition. SEM image (left) with autoradiography (right).

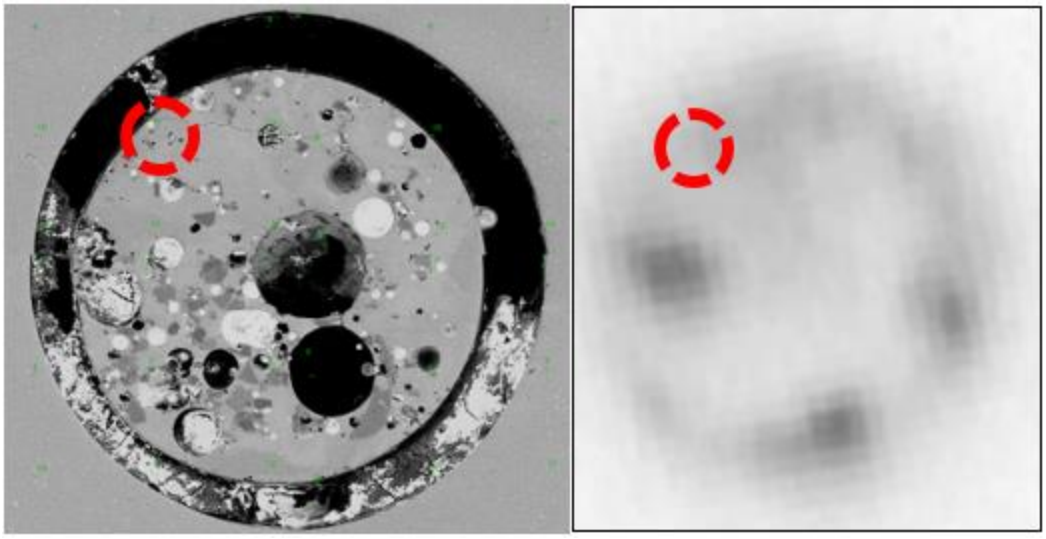

Figure 75. 1-DW-14-M1-20 with highlighted raster containing amphibole composition. SEM image (left) with autoradiography (right).

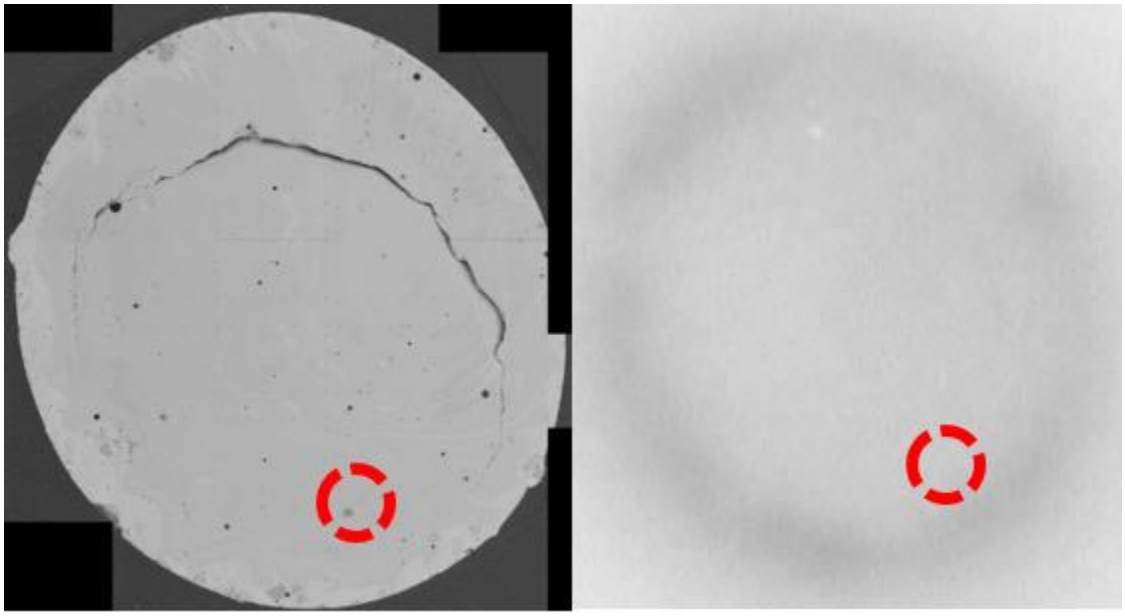

Figure 76. DW-SL-1-11 tile compilation with highlighted amphibole raster. SEM image (left) with inverted autoradiography (right).

Table 11 shows each raster clustered near the amphibole precursor. Each sample was symmetrical in shape, but varied in size and degree of mixing. The half-mm samples showed no apparent radioactivity while the larger, 1-3 mm samples showed a slight or

"low" level of darkness. Perhaps symmetrical samples that are larger than a half-mm could have amphibole co-located with actinides. Further inspection would be needed to verify this. Even so, the radioactivity exhibited is minimal compared to other samples.

Table 11. Five rasters closest to the amphibole precursor in PC space with information for each raster.

Sample Set	Sample #	Tile #	Raster #	Degree of Mixing	Shape	Size	AR Darkness
1-DW-25	42	1	15	heterogeneous	Symmetrical	Half mm	None
DW-SL-1	5	2	14	homogeneous	Symmetrical	2-3 mm	Low
1-DW-25	5	1	3	heterogeneous	Symmetrical	Half mm	None
1-DW-14 M1	20	2	11	heterogeneous	Symmetrical	1-2 mm	Low
DW-SL-1	11	26	11	homogeneous	Symmetrical	2-3 mm	Low

Precursor 5: Monticellite

Monticellite was one of the precursors that matched the data, but not the soil information from previous research. However, this precursor was used as it fit well into the model. Monticellite was best clustered in PC2 vs. PC3 (Figure 50) and PC2 vs. PC4 (Figure 51). In the PC3 vs. PC4 plot it is in a large cluster at the center, but these rasters are not used due to the fact that rasters near the center do not indicate variation from the dataset as a whole captured in these particular principal components. Monticellite was the only precursor which has rasters from porous samples clustered near it in PC space, as shown in Figures 77-80. Porous samples are known to generally have a uniform relative darkness in autoradiography. In future research it would be valuable to specifically analyze more porous samples to determine compositional information on a more detailed level.

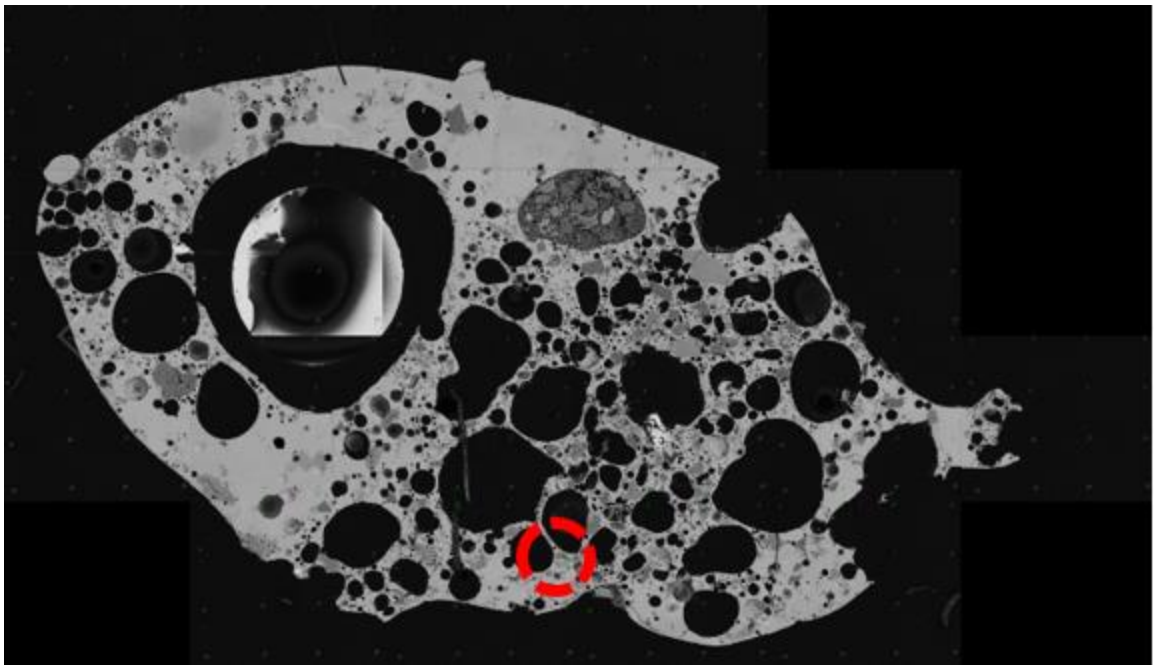

Figure 77. Tile compilation of sample DW-IRR-6 with highlighted area containing monticellite raster.

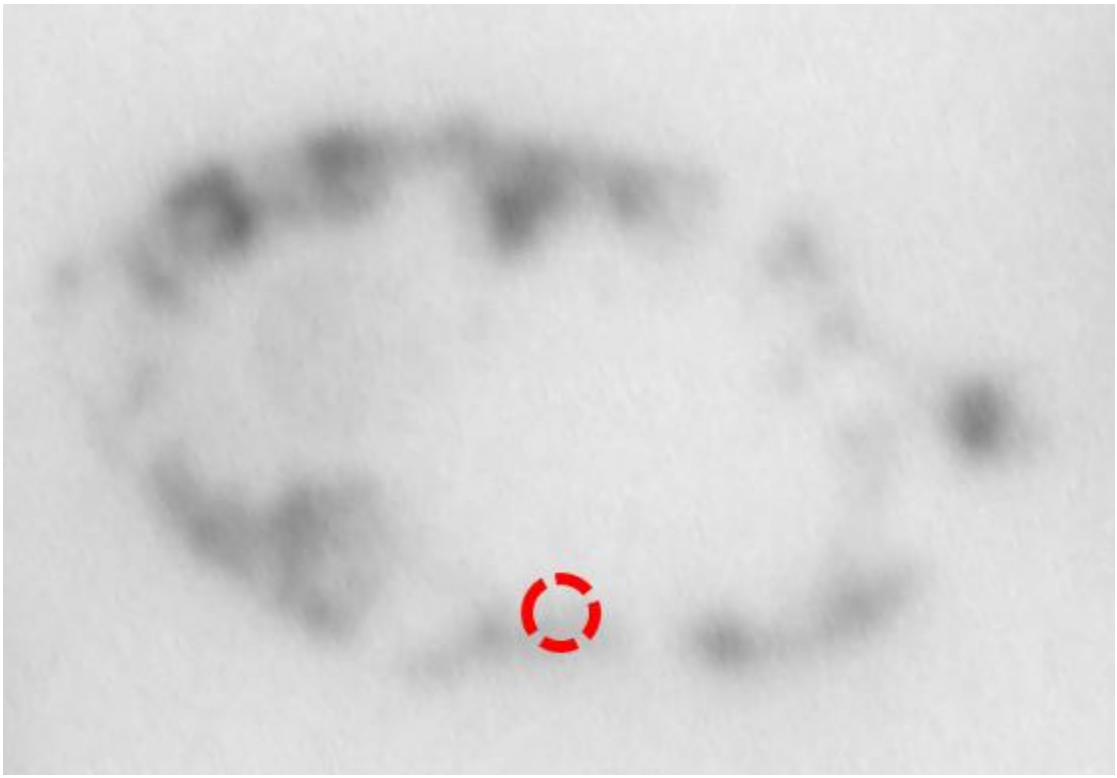

Figure 78. Autoradiography of sample DW-IRR-6 with highlighted area containing monticellite raster.

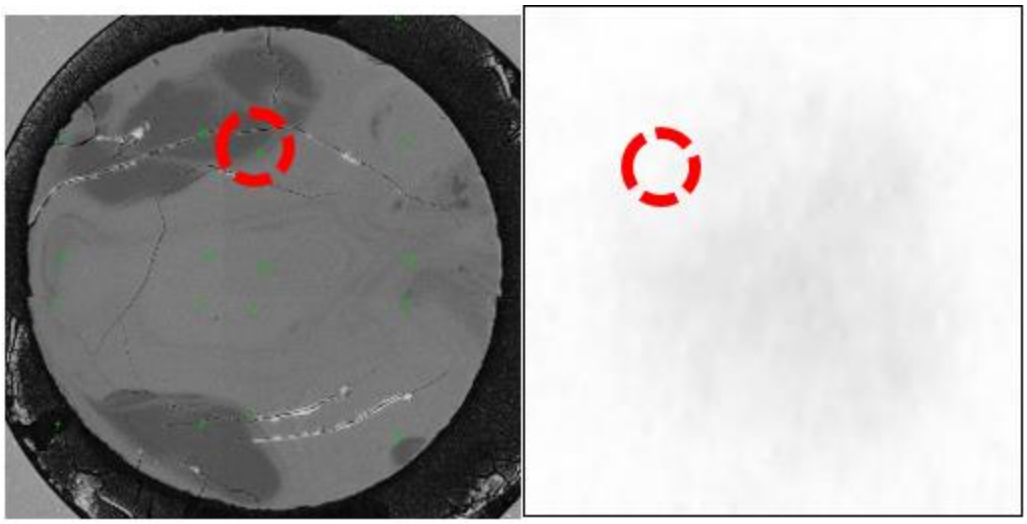

Figure 79. 1-DW-14-M2-4 with highlighted raster containing monticellite composition. SEM image (left) with autoradiography (right).

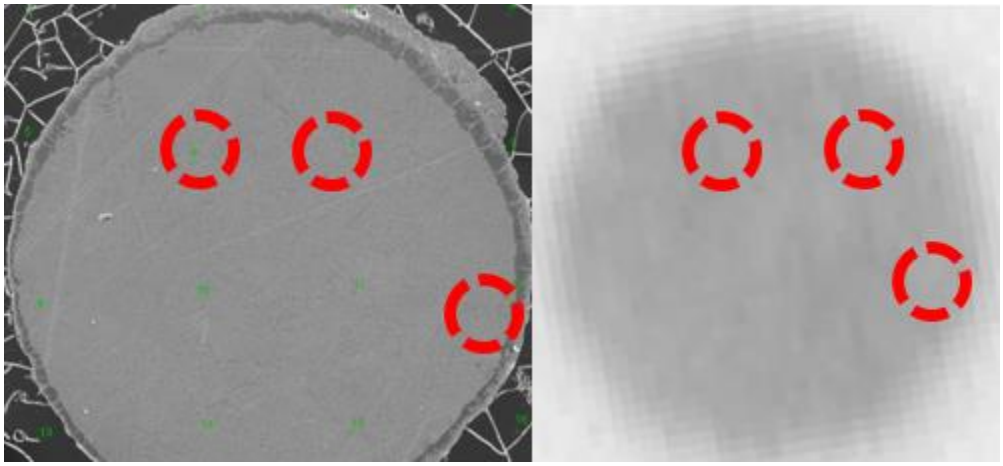

Figure 80. 1-DW-25-3 with highlighted rasters containing monticellite composition. SEM image (left) with autoradiography (right).

Table 12 displays the information for each raster near the monticellite precursor. As stated previously, there is no clear correlation with monticellite and activity, but the porous sample examined in Figure 80 does show a uniform level of radioactivity. Further conclusions when looking at the bulk data in PC space and autoradiography suggests that the porous samples encompass unique compositional variation and also each have a medium level of radioactivity.

Table 12. Five rasters closest to the monticellite precursor in PC space with information for each raster.

Sample Set	Sample #	Tile #	Raster #	Degree of Mixing	Shape	Size	AR Darkness
DW-Irregular	6	2	8	heterogeneous	Irregular	3-4 mm	Low
1-DW-14 M2	4	3	9	homogeneous	Symmetrical	1-2 mm	Low
1-DW-25	3	1	6	porous	Symmetrical	Half mm	Medium
1-DW-25	3	1	7	porous	Symmetrical	Half mm	Medium
1-DW-25	3	1	12	porous	Symmetrical	Half mm	Medium

V. Conclusion

This research was able to determine broad spectrum factors which impact how environmental precursors mix with bomb debris following a nuclear detonation. While precursor estimation with *a priori* knowledge for this sample set resulted in inconsistent findings, the overall examination of the bulk compositional data provided valuable information about how particle morphology, size, and degree of mixing impact compositional variation and possibly actinide concentration. MCR-ALS proved to be a computational asset for un-mixing fallout compositions, but more defined methods are needed in order to initialize precursor estimations. PCA was verified in its power to separate compositionally significant particles. New methods of SEM/EDS collection were used. The following sections discuss in detail some conclusions that were drawn, specifically in reference to the questions posed in the problem statement in Section 1.2.

5.1. Research Conclusions

Three questions were posed in the problem statement and are discussed in the following paragraphs. The results of this research are qualitative in nature resulting from quantitative data statistical methods of analysis, and qualitative observations.

Precursors and actinide concentration

Based on the analysis of the final precursor estimate, there does not appear to be any evidence of strong correlation between the darkness of autoradiography and the precursors. However, observations can be made using the information gathered. As Dierken suggested in his analysis, the feldspar and silicon-rich portions of the samples appear to undergo little diffusion [8]. Based on the findings of this research, feldspar

appears to have a relationship with some level of activity, while quartz was anticorrelated with activity. There exist visual inclusions where the silicon-rich areas are clearly observed in the BSE images in Chapter 4. These areas show a distinct lack of radioactivity. While Holliday and Dierken suggest the lower melting point of mafic glasses attribute to the diffusion of plutonium in the samples, the precursor model appeared to suggest feldspar was more correlated than amphibole [12]. Amphibole (actinolite) is a mafic-like mineral rich in calcium, iron and magnesium. The original highlighted precursor clusters in the first precursor estimation were perhaps too specific. The general compositions did have mafic and feldspar-like compositions. While this research appears to conclude the presence of radioactivity is associated more with feldspathic minerals, the results are not definitive. The other three precursors: calcite, amphibole (actinolite) and monticellite appear to have no evident relationship with actinide concertation based on the autoradiography alignment.

MCR-ALS effectiveness

This method of un-mixing compositional information is extremely valuable for deconvoluting fallout compositions in theory. MCR-ALS has been shown to result in meaningful compositional estimates in previous research [4]. This research results in questions regarding the feasibility of using this method without specific geological information about the mineral environment of the nuclear detonation. Using the method of cluster analysis resulted in a model which seemed to fit the data well, but the results were unrealistic, identifying uncommon mineral compositions which are nonsensical regarding the test location. Using geological assumptions and soil compositions from previous surveys and research, a better estimate was made. However, it is difficult to discern whether the resulting output of the model is real or a result of computational fitting. The resulting

precursor compositions following the deconvolution of compositional data using an initial guess can seem to match the model very well. This does not immediately indicate successful results, but rather that we were able to make some educated guesses about possible minerals mixing in the fallout. Further examination is required to verify geochemical sensibility. For this data set, upon analysis completion, a geological survey was examined to determine if each precursor was present in the test site vicinity [41]. It was determined that all but monticellite were present in the geological survey. However, this method checks for mineral names, rather than compositional matches, so there could be minerals existent in the soil that are similar to monticellite. This is not to say that the mineral does not exist or perhaps a mineral close in composition, but it does demonstrate that without any initial environmental data regarding precursor guesses, the model may converge on mineral compositions which are not present in reality. The user must then discern how to eliminate, add, or modify the precursor initialization to result in the best fit through trial and error. This process yields questionable results in precursor compositions as shown in this research. Therefore, MCR-ALS is a powerful tool for un-mixing fallout compositions, but should be refined with methods of precursor estimation which are clear, quantitative, and analytical. Recommendations for achieving this are in the future research section.

Morphology, Size, and Degree of Mixing

Regarding the different characteristics of samples, broad observations are possible that point to specific attributes which may be correlated with specific compositions as well as actinide concentration. Previous research as discussed in Chapter 2 identify the fact that certain elements and compounds melt and condense with unspent nuclear fuel. For this

research a general goal was to determine if morphology and other sample qualities reflect the chemistry that is unmixed using MCR-ALS. There does not appear to be any systematic difference in the sample qualities in terms of the associating precursors with specific size, shape or degree of mixing of samples. However, it was clear from PCA examination that the porous sample rasters clustered together as shown in Figure 34. These porous clusters displayed significant compositional variation from the bulk data. The uniqueness and relative rarity of these fallout samples make them of interest for further analysis. It was also evident that large, spherical, homogeneous samples encompassed a great deal of variation.

Observations in the overall autoradiography indicate that homogeneous spherical samples have the highest radioactivity and hence contain the most actinides. This information gives insight into how the unspent fuel mixes with the environment throughout the fallout formation process. It would appear that those larger spherical samples reached a higher temperature, and or spent a longer time within the fireball, combining with plutonium in the debris. Porous samples require further examination and should be studied separately, as the unique degree of mixing is easily identifiable under a microscope and these samples have a relatively steady level of radioactivity uniformly across the sample cross-sectional surface. This is apparent in the autoradiography shown in Figure 81. It appears these porous textures only appear in smaller diameters, as only one sample was in the 1-2 mm category while 5 half-millimeter porous samples exist. This however, may be a result of sampling bias. The fact that samples were grouped into sets at different times with different goals in mind, could indicate that porous samples were simply avoided, or not observed for larger samples.

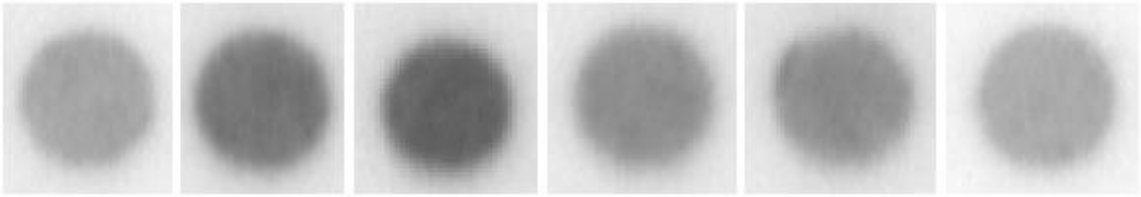

Figure 81. From left to right autoradiography images of samples: 1-DW-25-3,9,18,27,34 and 1-DW-14-M1-23.

The heterogeneous samples were scattered throughout the PCA plots showing varying levels of compositional variation. It is clear that this attribute alone does not contribute to a significant relationship with autoradiography Many of these heterogeneous samples simply did not attain a high enough temperature to fully melt and mix, leaving agglomerated particles and irregular shaped samples as a result.

5.2. Future Research

Continuing research in this area should utilize the same tools used in this study along with more refined methodologies and added quantitative analysis. First, the use of rasters rather than spot data for SEM/EDS should be verified to determine which method is most efficient regarding collection time, and results in the most reliable compositional information. The time for the SEM to gather compositional information across a 10 by 10-micron square vs. a single spot sample significantly changes the time needed to gather data as well as the number of data points gathered on each sample. However, previous research suggests rasters provide better quality compositional data. The issue is the time constraint, and raster density on the sample surfaces.

Further research methods designed to better formulate precursor estimations and alternative methods of autoradiography alignment and raster backtracking would greatly

improve the results and time required to examine clustered rasters. Dierken attempted to refine the alignment process, but due to the lack of autoradiography image sharpness, the error in the alignment or accuracy could not be assessed. The alignment algorithm was therefore discounted for quantitative results [8]. When small half-mm samples are aligned with autoradiography, it is fairly easy to visually adjust the images in order to match a raster location. However, larger samples, when zooming into 1 of perhaps 60 tiles, it is difficult to know the accuracy of the alignment with the fuzzy or cloudy image. A solution to the issue of tracing precursor compositions to specific sample surface locations would be to allot the time needed to acquire full raster elemental maps of the sample surfaces. This allows for a general view of the concentration of elements instead of the need to find a 10 by 10-micron point, therefore the entire surface can be compared to autoradiography.

Analysis of compositional data by one sample group at a time should be considered in the future for different perspectives of compositional variation and precursor estimations within that sample set. An example would be running PCA on only samples with homogeneous surfaces or only samples larger than 2 mm. This analysis may deconvolute or remove compositional information which skews the statistical result. The specific classes of samples could also be looked at alone in the same PCA plot with the rest of the classes, rather than looking at all classes on the same field of view.

Another method is to specifically choose samples which exhibit high relative radioactivity shown in the autoradiography, then examine those compositions specifically. This would require some sort of control composition from a baseline sample or a sample with no radioactivity. The issue is that not enough is known to create a control variable, so

the entire set must be analyzed to observe if more highly radioactive samples have significantly different compositions than relatively lower radioactivity samples.

Another issue which should be addressed in the future is the number of rasters or spots collected on a sample surface. One 3-4 mm ground glass sample may account for nearly 1000 rasters while a half mm sample only accounts for 16. The mass of compositional data from the ground glass included in the PCA may very well skew the PCA weightings and the resulting estimation of mineral precursors. This problem could be solved by examining samples in groups based on size, degree of mixing, or shape as previously mentioned.

With the number of data points varying from sample to sample, the amount of significance given to a cluster which is chosen by visual observation may result in human error. However, the number of data points per unit area is the same across all samples. Even samples with few rasters, such as the porous samples, still stand out if they are compositionally different and cluster together. Issues also lie in that minerals which are similar in composition will cluster near each other, and with large sets of data, machine error will blend clusters together.

Finally, once the precursor estimate model is refined and assessed to be geochemically sensible, with q-residuals reduced to a minimum, more samples should be examined around precursor clusters. Increase in the number of examined rasters will give a better idea of characteristics correlated with high radioactivity and precursors in fallout. Additionally, the Eigenvector software can be utilized following model deconvolution to find samples which match the estimated precursors. The contributions of each precursor modeled in the MCR-ALS can be observed for each raster and how the precursors

contributed to each raster. Using this method instead of plotting precursors in PCA space may prove to yield rasters closer in composition to precursors. However, upon initializing the data in MCR-ALS, the characteristic data attached to each raster point is lost, so a method of back-tracking to a specific sample, tile and raster would need to be devised.

5.3. Summary

The final results of this research indicate that feldspar minerals could be correlated with actinide concentration, and silicon rich minerals (quartz) are anticorrelated. The larger, spherical, homogeneous samples have a higher level of radioactivity as is evident from the autoradiography image, and porous texture samples have a consistently uniform radioactivity. Also, it was demonstrated that the MCR-ALS method of un-mixing is a powerful tool for un-mixing fallout chemical data, but requires additional method refinement for initializing precursor compositions, and determining the viability of model results. Further continuation of this research combined with previous studies could lead to major steps in understanding fallout formation, un-mixing nuclear fallout particle composition and expedite the analytic processes associated with locating actinides or unspent fuel in samples.

Bibliography

[1] P. Leventhal and Y. Alexander, Nuclear Terrorism Defining the Threat, Mclean, VA: Pergamon Press, 1986.

[2] J. McClory and J. Matzel, "MIDAS QPR," AFIT, WPAFB, 2017.

[3] P. H. Donohue, A. Simonetti, E. C. Koeman, S. Mana and P. C. Burns, "Nuclear Forensic Applications Involving High Spatial Resolution Analysis of Trinitite Cross-sections," *Journal of Radioanalytical and Nuclear Chemistry*, vol. 306, pp. 457-467, 2015.

[4] M. Fitzgerald, K. Knight, J. Matzel and K. Czerwinski, *Multivariate Strategies to Modeling Source Compositions in Heterogeneous Melt Glasses*, Livermore, CA, 2017.

[5] J. W. McClory, "Applying Principle Component Anlysis to Fallout Characterization: The link between Actinides and Composition," Defense Threat Reduction Agency, 2017.

[6] E. Mankin, "Principal Components Analysis: A How-To Manual for R," 2010. [Online]. Available: http://people.tamu.edu/~alawing/materials/ESSM689/pca.pdf. [Accessed 15 October 2017].

[7] S. T. Castro, "Nuclear Forensics Applications of Principle Component Analysis on Micro X-ray Flourescence Images," Master's Thesis, Air Force Institute of Technology, 2016.

[8] J. M. Dierken, "Analysis of Fallout Particles Using Image Registration of Autoradiography and Scanning Electron Microsopy," Master's Thesis, Air Force Institute of Technology, 2014.

[9] D. W. Haws, "Using Principal Component Analysis to Improve Fallout Characterization," Master's Thesis, Air Force Institute of Technology, 2017.

[10] LLNL, "Nuclear Science and Security Consortium," Lawrence Livermore National Laboratory, 2017. [Online]. Available: https://st.llnl.gov/partnerships/academia-and-gov/nssc/highlights. [Accessed 12 July 2017].

[11] R. Ehrlich and W. W. Full, "Sorting out geology - Unmixing mixtures," in *Use and abuse of statistical methods in the earth sciences*, New York, Oxford University Press, 1987, pp. 33-46.

[12] K. S. Holliday, J. M. Dierken, M. L. Monroe, M. A. Fitzgerald, N. Marks, R. C. Gostic, K. B. Knight, K. Czerwinski, I. D. Hutcheon and J. W. McClory, "Plutonium Segregation in Glassy Aerodynamic Fallout from a Nuclear Weapon Test," *Dalton Transactions*, vol. 46, no. 6, pp. 1770-1778, 2017.

[13] C. J. Bridgman, Introduction to the Physics of Nuclear Weaopons Effects, Defense Threat Reduction Agency, 2001.

[14] P. J. Glasstone and S. Dolan, The Effects of Nuclear Weapons, United States Department of Defense and Department of Energy, 1977.

[15] G. J. Dilorio, Direct Physical Measurement of Mass Yields in Thermal Fission of Uranium 235, New York: Garland, 1979.

[16] mccord/vandenbout/labrake, "Band of Stability," University of Texas, 2015. [Online]. Available: https://gchem.cm.utexas.edu/nuclear/index.php#radioactivity/band-stability.html. [Accessed 21 December 2017].

[17] C. E. Adams, N. H. Farlow and W. R. Schell, "The Compositions, Structures and Origins of Radioactive Fall-out Particles," *Geochimica et Cosmochimica Acta*, vol. 18, pp. 42-56, 1960.

[18] K. J. Moody, I. D. Hutcheon and P. M. Grant, Nuclear Forensic Analysis, Boca Raton, FL: CRC Press, 2005.

[19] C. Miller, "A Theory of Formation of Fallout From Land-Surface Nuclear Detonations and Decay of Fission Products," U.S. Naval Radiological Defense Laboratory, San Fransisco, CA, 1960.

[20] E. C. Freiling, "Radionuclide Fractionation in Bomb Debris," *Science*, vol. 133, no. 3469, pp. 1991-1998, 1961.

[21] M. L. Monroe, "Forensic Analysis for Elemental Identification in Debris," Master's Thesis, Air Force Institute of Technology, 2013.

[22] W. Hendee, Medical Imaging Physics (4th Ed), New York: John Wiley and Sons, 2002.

[23] A. W. Rogers, Techniques of Autoradiography (3rd ed), New York: Elsevier North Holland, 19979.

[24] N. A., "History of Radiography," [Online]. Available: https://www.nde-ed.org/EducationResources/CommunityCollege/Radiography/Introduction/history.htm. [Accessed 27 9 2016].

[25] G. Crocker, J. O'Conner and E. Freiling, Physical and Radiochemical Properties of Fallout Particles, San Francisco: US Naval Radiological Defense Laboratory, 1966.

[26] M. Zhang, "Image Deconvolution in Digital Autoradiography," 2 2008. [Online]. Available: http://www.ncbi.nlm.nih.gov/pmc/articles/PMC2668928. [Accessed 10 9 2016].

[27] Y. Leng, Materials Characterization: Introduction to Microscopic and Spectroscopic Methods, Singapore, Thailand: John Wiley and Sons, 2008.

[28] J. I. Goldstein, Scanning Electron Miscroscopy and X-ray Microanalysis (2nd Ed), New York: Pelnum Press, 1981.

[29] D. C. Lay, Linear Algebra and its Applications, Boston: Pearson, 2006.

[30] N. Christophersen and R. P. Hooper, "Multivariate Analysis of Stream Water 1352 Chemical Data: The Use of Principal Components Analysis for the End-1353 Member Mixing Problem," *Water Resources Research,* vol. 28, no. 1, pp. 99-107, 1992.

[31] J. Schlens, "A Tutorial on Principle Component Analysis," Systems Neurobiology Laboratory, 10 12 2005. [Online]. Available: http://www.cs.cmu.edu/~elaw/papers/pca.pdf. [Accessed 29 9 2016].

[32] A. T. Miesch, "Scaling variables and interpretation of eigenvalues in 1447 principal component analysis of geologic data," *Journal of the International Association for Mathematical Geology,* vol. 12, no. 6, pp. 523-538, 1980.

[33] S. Wold, "Cross-validatory estimation of the number of components in 1481 factor and principal components models," *Technometrics,* vol. 20, pp. 397-405, 1978.

[34] I. T. Jolliffe, Principal Component Analysis, New York: Springer-Verlag, 2002.

[35] R. M. Renner, "A constrained least-squares subtroutine for adjusting 1462 negative estimated element concentrations to zero," *Computational Geosciences,* vol. 19, pp. 1351-1360, 1993.

[36] J. Dymon, M. Lyle, B. Finney, B. Piper, K. Murphy, R. Conard and N. Pisias, "Ferromanganese nodules from MANOP sites H, S, and R – Control of 1365 mineralogical and chemical composition by multiple accretionary processes.," *Geochim. Cosmochim. Acta,* vol. 48, pp. 931-949, 1984.

[37] NIH.gov, "ImageJ," NIH.gov, [Online]. Available: https://imagej.nih.gov/ij/download.html. [Accessed 16 June 2016].

[38] Eigenvector Research Inc., "Chemometrics 1: Principle Components and Exploratory Data Analysis," 2012. [Online]. Available: http://eigenvector.com/courses/EigenU_Chemo1.html. [Accessed 16 9 2016].

[39] W. A. Deer, R. A. Howie and J. Zussman, An Introduction to the Rock-Forming Minerals, Stevenage, Hertfordshire, UK: Berforts Information Press, 2013.

[40] D. Barthelmy, "Minerology Database," MSAccess, Expressions Web 2, 2014. [Online]. Available: http://webmineral.com/. [Accessed 2017].

[41] J. L. Slate, M. E. Berry, P. D. Rowley, C. J. Fridrich, K. S. Morgan, J. B. Workman, O. D.Young, G. L. Dixon, V. S. Williams, E. H. McKee, D. A. Ponce, T. G. Hildenbrand and e. Swadley, "Digital geologic map of the Nevada Test Site and vicinity, Nye, Lincoln, and Clark Counties, Nevada, and Inyo County, California," U.S. Department of the Interior; U.S. Geological Survey; Nevada Operations Office, 1999.

REPORT DOCUMENTATION PAGE

Form Approved
OMB No. 0704-0188

1. REPORT DATE *(DD-MM-YYYY)*	**2. REPORT TYPE**	**3. DATES COVERED** *(From - To)*
22-03-2018	Master's Thesis	Sept 2016 – March 2018

4. TITLE AND SUBTITLE

Improving Fallout Characterization by Using Multivariate Techniques to Determine Composition

5a. CONTRACT NUMBER

5b. GRANT NUMBER

5c. PROGRAM ELEMENT NUMBER

6. AUTHOR(S)

Pitkins, Christopher R, Capt, USAF

5d. PROJECT NUMBER

5e. TASK NUMBER

5f. WORK UNIT NUMBER

7. PERFORMING ORGANIZATION NAME(S) AND ADDRESS(ES)
Air Force Institute of Technology
Graduate School of Engineering and Management (AFIT/EN)
2950 Hobson Way
Wright-Patterson AFB OH 45433-7765

8. PERFORMING ORGANIZATION REPORT NUMBER

AFIT-ENP-MS-18-M-080

9. SPONSORING / MONITORING AGENCY NAME(S) AND ADDRESS(ES)
Defense Threat Reduction Agency- NTF
Lieutenant Colonel Matthew Zickafoose
8725 John J. Kingman Road
Ft. Belvoir, VA 22060
matthew.s.zickafoose.mil@mail.mil

10. SPONSOR/MONITOR'S ACRONYM(S)
DTRA

11. SPONSOR/MONITOR'S REPORT NUMBER(S)

12. DISTRIBUTION / AVAILABILITY STATEMENT
Distribution Statement A. Approved for public release; Distribution Unlimited

13. SUPPLEMENTARY NOTES
This material is declared work of the U.S. Government and is not subject to copyright protection in the United States.

14. ABSTRACT
Multivariate statistical techniques were applied to un-mix nuclear fallout chemical data. This information is critical to characterization of fallout formation following a nuclear detonation. Understanding the correlation between environmental precursors and actinide concentrations in post-detonation nuclear fallout material aids in the determination of type, source and origin of nuclear fuel. This research examines 123 nuclear fallout samples from a historical nuclear test. Scanning electron microscopy (SEM) and energy dispersive spectroscopy (EDS) are used to collect chemical compositions of the fallout samples. Principal component analysis (PCA) is applied to examine variation in elemental compositions and make estimates of environmental precursor compositions. Estimates are modeled using multivariate curve resolution-alternating least squares (MCR-ALS). The precursors exhibited on sample surfaces were spatially correlated with sample radioactivity using autoradiography imaging of the sample set. Results suggest that feldspar is correlated with a moderate level of radioactivity, samples with porous textures have unique compositions with a uniform surface radioactivity, and quartz is anticorrelated with radioactivity. Additionally, size, shape, and morphology each have a relationship with actinide concentration with large, homogeneous and spherical samples exhibiting the highest relative radioactivity.

15. SUBJECT TERMS
SEM, Principal Component Analysis, Fallout, Multivariate Curve Resolution

16. SECURITY CLASSIFICATION OF:			**17. LIMITATION OF ABSTRACT**	**18. NUMBER OF PAGES**	**19a. NAME OF RESPONSIBLE PERSON**
a. REPORT	**b. ABSTRACT**	**c. THIS PAGE**			Dr. John W. McClory, AFIT/ENP
U	U	U	UU	139	**19b. TELEPHONE NUMBER** (937)255-3636 x.7308; john.mcclory@afit.edu

Standard Form 298 (Rev. 8-98)
Prescribed by ANSI Std. Z39.18